Use of GIS in Radio Frequency Planning and Positioning Applications

Victoria R. Jewell

Thesis submitted to the Faculty of the
Virginia Polytechnic Institute and State University
in partial fulfillment of the requirements for the degree of

Master of Science
in
Electrical Engineering

R. Michael Buehrer, Chair
Peter M. Sforza
Jeffrey H. Reed

July 3, 2014
Blacksburg, Virginia

Keywords: GIS, RF Modeling, Positioning

Use of GIS in Radio Frequency Planning and Positioning Applications

Victoria R. Jewell

(ABSTRACT)

GIS are geoprocessing programs that are commonly used to store and perform calculations on terrain data, maps, and other geospatial data. GIS offer the latest terrain and building data as well as tools to process this data. This thesis considers three applications of GIS data and software: a Large Scale Radio Frequency (RF) Model, a Medium Scale RF Model, and Indoor Positioning. The Large Scale RF Model estimates RF propagation using the latest terrain data supplied in GIS for frequencies ranging from 500 MHz to 5 GHz. The Medium Scale RF Model incorporates GIS building data to model WiFi systems at 2.4 GHz for a range of up to 300m. Both Models can be used by city planners and government officials, who commonly use GIS for other geospatial and geostatistical information, to plan wireless broadband systems using GIS. An Indoor Positioning Experiment is also conducted to see if apriori knowledge of a building size, location, shape, and number of floors can aid in the RF geolocation of a target indoors. The experiment shows that correction of a target to within a building's boundaries reduces the location error of the target, and the vertical error is reduced by nearly half.

Dedication

I would like to dedicate this thesis to my loving parents. My father's electrical engineering background encouraged me to pursue this major, and tales of his own experience through school provided much needed laughter when my motivation was tested by stress and failure. My mother has been my rock throughout my life, always by my side when I need a shoulder to lean on. I'll always love both of you, and I couldn't have completed this thesis without your encouragement and love!

Acknowledgments

I would like to express my appreciation for my committee chair, Dr. R. Michael Buehrer, for your guidance and never failing dedication to all of your students, including myself. I have the highest respect for your knowledge of communications, and your patience with me when your workload is so large. Though we were only able to work together for two and a half years, I will always respect you as a professor, adviser, and person.

I would also like to thank Dr. Jeffrey H. Reed for agreeing to be a part of my committee and for providing much needed information on the properties of RF Cells in practice in your Cellular Radio class.

I cannot thank the staff of the Center for Geospatial Information Technology (CGIT) enough for their guidance and support. I would especially like to thank my committee member, Peter Sforza, for always encouraging me to take my research one step further. The CGIT team, especially Joe Newman and Erica Adams, were always patient with me as I became familiar with ArcGIS and made mistakes along the way. Thank you all!

I would like to thank the rest of Dr. Buehrer's research students for the laughs, encouragement, anecdotes, and assistance throughout my graduate experience. I would especially like to express my appreciation for Javier Schloemann and Reza Vaghefi for their help with the Indoor Geolocation algorithm.

Two federal American Recovery and Reinvestment Act (ARRA) grants issued by the Department of Commerce National Telecommunications Information Administration (NTIA) have supported the Commonwealth's participation in the NTIA's National Broadband Mapping Initiative.

This effort is led by Virginia's Center for Innovative Technology (CIT) in collaboration with the Virginia Geographic Information Network (VGIN) and the Virginia Tech Center for Geospatial Information Technology (CGIT). Peter Sforza, Director of the Center for Geospatial Information Technology is the principle investigator for the Virginia Tech component of the project.

Figures 5.8-6.21 were created by the author, 2014.

Contents

List of Figures

List of Tables

Chapter 1

Introduction

Broadband internet service has shown tremendous growth all around the world over the past few decades, and it continues to grow daily. From large companies to small broadband providers, service providers are struggling to provide internet service to billions of users. Over the last dozen years, broadband users in Northern America have nearly tripled to over 273 million subscribers [1]. These subscribers demand reliable internet services at continually increasing data speeds. However, it is estimated that only 70 percent of the United States has high-speed internet access in their home, which is currently defined by the Federal Communications Commission as 4 Mb/s [2] [3]. Many states, including Virginia, are making a push to provide high speed internet coverage to less densely populated areas using wireless technology. An important aspect of wireless broadband service is the location of the wireless access point. Therefore, it is of utmost importance to use Radio Frequency (RF) Propagation Estimation software to determine the best location to either erect a new tower or place equipment on an existing vertical asset. This will ensure that the costs of

providing service are minimized, and will encourage further broadband growth in these areas.

In a similar situation, a call for growth is heard in highly populated areas where internet service providers are already struggling to meet demand. These areas want higher data rates and more reliable coverage. A similar analogy can be found in wireless telephone systems. In the past, telephone service providers would organize their systems into a series of large cells in which relatively few towers would be spread out. This type of system has become obsolete as each tower can only provide service to a limited quantity of users and fails to exploit spatial reuse. Cells thus began to shrink to increase network capacity [4]. Today, there can be numerous smaller cells within a city, and each cell needs RF Propagation Estimation to determine the best location, power, and coverage. Modeling RF Propagation has become an essential tool in the broadband industry.

There is a need for a new RF estimation algorithm that can use the terrain data within the geoprocessing software, also known as geospatial information systems (GIS). GIS is commonly used by state offices and other geoprocessing companies. GIS serves as a database that contains the latest sets of terrain and digital surface data. This data can be used in an RF estimation algorithm to better reflect terrain obstacles that would attenuate the signal. There are also geoprocessing capabilities within GIS for processing geographic data. A specific type of GIS, known as ArcGIS[1], is used by the National Telecommunications Information Administration (NTIA) to create a nationwide broadband map [5]. In this thesis, the RF models created will aid broadband internet planners on a large scale and on as outdoor WiFi scale of less

[1]ArcGIS is Copyright ©1995 - 2014 Esri. All rights reserved. Published in the United States of America.

than 300 m. The Large Scale RF Model created for this thesis can be used for RF estimation on a 1 km - 20 km scale, and the Medium Scale RF Model can be used to estimate RF coverage in WiFi systems on a $<$ 300 m scale.

GIS is a database that can be filled with geographic and architectural information. This information can include the size, location, and shape of a building, as well as building materials and floor plans. The architectural data can be used to improve accuracy in RF indoor positioning, which frequently has errors of hundreds of meters [6] [7]. Two experiments are conducted within MATLAB: one in which the target is within a lone building, and one in which the target is located within a central building surrounded by other buildings. These experiments show how GIS building data can aid indoor positioning, and the results are presented in Chapter 6.

In this thesis, applications of widely used geoprocessing software, such as ArcGIS, are described. By developing a Large Scale RF Model and a Medium Scale RF Model that work with ArcGIS, the user can easily use the two models with the latest terrain and building data readily within ArcGIS to predict radio coverage. Similarly, as an application of the building data available within GIS, the apriori knowledge of building shape and location is used to reduce the indoor RF positioning error of a target within a building. The applications take advantage of the regular updates to data that are performed at local, state, and national levels, ensuring that the calculations are being performed with the latest data.

Problems with Available Estimation Software

There are numerous types of RF estimation software available today using a multitude of methods and models to estimate coverage. These models take several RF parameters as inputs and then perform calculations to estimate coverage. Most of these services require a large licensing fee to be able to use the software, but there are a few that are available for free. Though most software will give insight into the methodology behind the calculation of their estimates, finding a version that allows the user to see exactly how the code functions was not possible. RF calculation algorithms can vary in accuracy, but without the ability to change or observe the source code, it is difficult to know the algorithm or update the algorithm to improve accuracy.

Most RF estimation software allows for the estimation to be exported into several formats, but most of those formats contain an image file and a .KML file for the user to input into an application like Google Earth. This format cannot be imported directly into most geospatial information system (GIS) software. A few organizations, such as the Virginia Geographic Information Network (VGIN), use a GIS software known as ArcGIS to develop statewide coverage maps [8]. VGIN is creating a broadband map for the state of Virginia, which is submitted to the NTIA to be used in the nationwide broadband map. These coverage maps are used to illustrate the status of broadband coverage in a large area and to determine the locations of dead zones. The maps require that coverage estimates be submitted in a shapefile format, which is a data type of many GIS programs in which the data is packaged for transfer. There are several RF propagation estimators available that output a shapefile format, such as TAP Software, but there are none that are free or open source [9].

Most RF estimation software is not an ideal fit for small broadband providers, who cannot afford the licensing fees. Radio Mobile, which is a free RF estimation software, does not provide an output format that can be converted into an ArcGIS compatible format. Creating an ArcGIS script that will estimate RF coverage and provide a shapefile output is one of the goals for the Large Scale RF Model described in Chapter 4. The completed Python script for the Large Scale RF Model provides an RF coverage estimate with a shapefile output. The script will be available online for free so that others can use it and can change the algorithm for their own purposes. Both models will be available at `https://github.com/vtcgit` upon the completion of CGIT's State Broadband Initiative project.

Empirical Models for Estimating RF Coverage

As the need arose, RF coverage estimation algorithms were developed. These models were either developed empirically using collected data and generalized parameters, developed using known techniques such as ray-tracing, or were developed using some combination of the two. Since ArcGIS does not have the capacity for ray tracing computation with bounces, only empirical models were considered for implementation into an RF model within ArcGIS. We are also looking for a model that can cover a wide range of frequencies in the broadband range, specifically between 900 MHz and 5 GHz.

A popular statistical model is the Okumura model. The Okumura model was developed in the mid 1960s by Okumura Yoshihisa, and was the result of the ten-year large-scale propagation studies conducted within the suburbs around Tokyo [10]. This model was used by Masaharu Hata to develop an empirical formula in

1980 known as the Okumura-Hata model [11]. These models were derived by taking thousands of measurements of signal strength to determine a correlation between distance and signal strength. Generalized formulas were developed to estimate the farthest distance from the transmitter that a receiver would be able to properly receive the signal. Given input parameters such as antenna height and transmission frequency, the Okumura-Hata model can be used to create a circular coverage estimate that represents the median path loss between the transmitter and receiver. The Okumura-Hata model is fairly accurate for frequencies between 200 and 1920 MHz and in rural, suburban, and urban environments. A summary of the experimental Hata formula is shown in Figure 1.1. However, the Okumura-Hata model does not take into account site specific parameters, making it less useful for practical estimation of coverage. For broadband providers who need to know where they have coverage and how they should expand their system, obstacles in terrain need to be noted in the RF coverage estimate's shape. The shape of the RF estimate will tell the broadband planner where there are gaps in their coverage. Since the Okumura-Hata model results in a circular coverage estimate that does not consider site specific information, this makes the model less useful as a practical estimation of coverage. The Okumura-Hata model also does not cover a wide enough frequency range for the desired tool.

The Irregular Terrain Model (ITM), also known as the Longley-Rice model, was developed in the 1960's and is applicable in a wide frequency range of 20 MHz to 20 GHz. The ITM contains two modes of coverage: area prediction and point-to-point. The area prediction mode is similar to the Hata-Okumura model in that it creates a circular coverage estimate that represents the average coverage estimate. Therefore, the ITM's area prediction mode does not take into account site-specific

Table 1.1: Experimental Formula for Propagation Loss shown in Hata's Paper. Hata, M. Empirical Fomula for Propagation Loss in Land Mobile Radio Services. *IEEE Transactions on Vehicular Technology*, VT-29(3):317-325, August 1980. Used with permission of IEEE, 2014.

Urban Area	$L_p =$	$69.55 + 26.26 * \log_{10} f_c - 13.82 * \log_{10} h_b - a(h_m)^*$	
		$+(44.9 - 6.55 * \log_{10} h_b) * \log_{10} R$	(dB)
	$* =$	Correction factor for vehicular station antenna height	
		medium-small city	
		$a(h_m) = (1.1 * \log_{10} f_c - 0.7) * h_m - (1.56 * \log_{10} f_c - 0.8)$	
		large city	
		$a(h_m) = 8.29 * (\log_{10} 1.54 h_m)^2 - 1.1 : f_c \leq 200$ MHz	
		$a(h_m) = 3.2 * (\log_{10} 11.75 h_m)^2 - 4.97 : f_c \geq 200$ MHz	
Suburban Area	$L_p s =$	$L_p(Urban) - 2(\log_{10}(f_c/28)^2 - 5.4$	(dB)
Open Area	$L_p s =$	$L_p(Urban) - 4.78(\log_{10}(f_c)^2 + 18.33 * \log_{10} f_c - 40.94$	(dB)
	where		
	f_c	: frequency (MHz), 150-1500 (MHz)	
	h_b	: base station effective antenna height (m), 30-200 (m)	
	h_m	: vehicular station antenna height (m), 1-10 (m)	
	R	: distance (km), 1-20 (km)	

terrain obstacles, which is desired for the model within ArcGIS. The ArcGIS model is going to be used to estimate the current status of broadband with the intent to fill in coverage gaps. The final model must consider terrain specifics. The point-to-point coverage estimate is used to determine the signal strength at the receiver after the signal has traveled in the direction of the receiver. This type of coverage can be translated to determine the coverage over a wide area, which takes into account the locations of terrain obstacles, like hills and mountains. However, the point-to-point mode of the ITM would take substantial computation time to run within ArcGIS. This is due to performing dozens of calculations for thousands of cells. It would take at least one hour to perform the calculations necessary to use the ITM, so it would not be a practical solution when it comes to estimating RF coverage within ArcGIS.

GIS and Indoor GPS

Today, it is still difficult to locate a person indoors using the global positioning system (GPS) and other forms of location. In an emergency situation, it is important to be able to quickly and accurately locate a victim within a building. A building's inner and outer walls can severely degrade the signal, however, and increase the distance between the calculated location of the target and the actual location of the target [12].

GIS is a versatile geoprocessing program that can potentially aid the positioning problem. GIS in general is capable of storing architectural data such as a structure's shape, materials used for construction, and floor plan [13] [14]. If a target is within a building for which this data is available, this data could reduce the distance error and help locate the target. Chapter 6 outlines the experiments to determine if building

data can aid in positioning, with a focus being on error in the z-plane (i.e., altitude).

Motivation

Being able to model RF Coverage in ArcGIS is not a simple task, but the rewards are great. ArcGIS, and other GIS software, have access to the most recent terrain data, so utilization of this data can provide more accurate coverage estimates. The output coverage estimates are already within ArcGIS, so it is easy for organizations like VGIN to receive the estimates and integrate them into existing broadband maps. The statewide broadband coverage map created by VGIN aims to fill in zones lacking coverage, and accurate RF estimation can help locate these gaps. Figure 1.1 shows VGIN's broadband map of Virginia, with different colors corresponding to different broadband services, such as LTE and 4G [8].

RF estimation can also be used in optimization studies aimed at determining the best available vertical assets to use to cover the largest area. These optimization studies can even include towers that have yet to be built, to see which locations are best suitable for new vertical assets to be placed. This effort is important for the NTIA's FirstNet emergency response system, which aims to provide Long-Term Evolution (LTE) coverage for all public safety services [15].

The FCC's Enhanced 911 (E911) plan has also recently proposed new indoor requirements to better locate victims while indoors [16]. These new positioning requirements state that callers must be located within 50 meters in the x- and y-directions within 2 years, as well as z-axis errors within 3 meters accuracy [17]. The indoor positioning experiment examines the effects of known GIS building data on

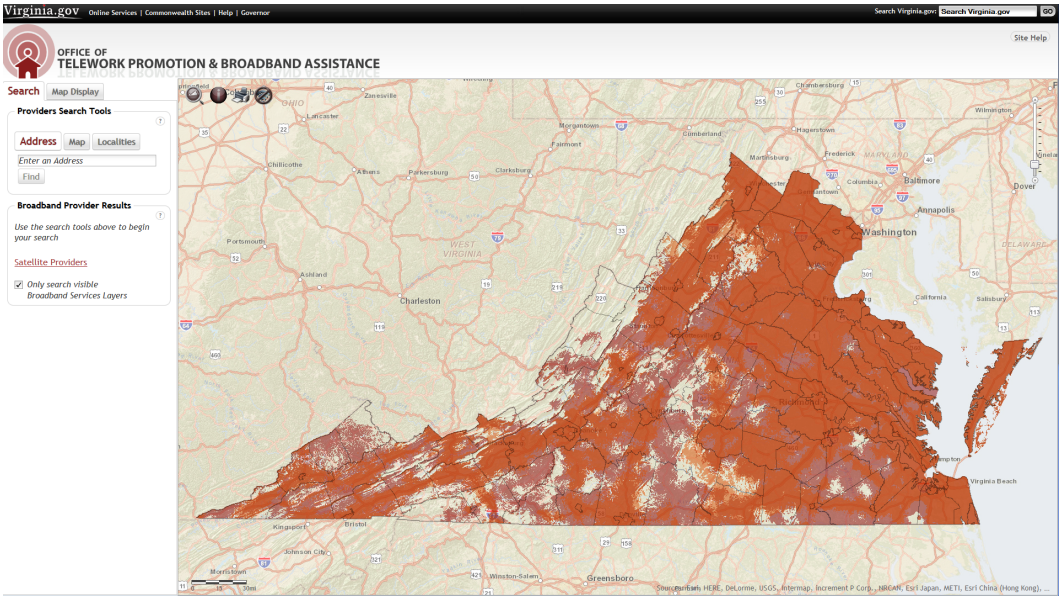

Figure 1.1: Virginia Statewide Broadband Map, Red is LTE Coverage, and Orange is 4G Coverage

positioning error in an attempt to reduce the error and more readily locate victims.

The three applications in this thesis aim to show how GIS can aid public safety.

Outline of Thesis

This thesis describes the development of the RF Propagation Toolset for the Center for Geospatial Information Technology's (CGIT) Vertical Asset Inventory Toolkit (VAIT). This RF Propagation Toolset contains a Large Scale RF Model and a Medium Scale RF Model and will be turned into a web application that is free to use and will be open source so that it can be improved upon.

Chapter 2 contains a literature review of all of the concepts used in this tool, including an overview of propagation prediction methods, currently available propagation prediction software, and in-building propagation research. Chapter 3 of this thesis provides an overview of the features of ArcGIS and its various file formats. This chapter also describes the tools and features of ArcGIS that are relevant to the RF Propagation tool.

Chapter 4 discusses the Large Scale Model, which can be used to estimate coverage over an area of several kilometers. This model will be useful for RF prediction which can be used for planning purposes such as filling coverage gaps either by placing equipment on an existing vertical asset or by building a new tower. Chapter 5 discusses the Medium Scale Model, which uses highly detailed Light Detection an Ranging (LiDAR) data of Blacksburg, VA's surface to provide more detailed coverage estimates on a smaller scale (maximum range of 300 meters). The model also incorporates building data into its algorithm. This Medium Scale Model is developed for use in designing medium cell systems at high capacity and data rate in towns. Both RF estimation models do not consider interference. Because of this limitation, these tools are coverage estimation tools for noise-limited scenarios (e.g. rural broadband or smaller towns).

Chapter 6 contains an exploratory look into ways GIS data can aid in indoor positioning by examining case studies. A MATLAB simulation was performed to determine if "snapping" a target's estimated position into the nearest building will benefit target location. In this simulation, it is assumed that the target is known to be within the building, such as a scenario in which a victim has called an ambulance and told the responder that they are within the building. In Chapter 7, a brief uncertainty analysis is performed to determine sources of uncertainty for the Large

and Medium Scale Models. Chapter 8 contains the conclusion to the thesis and discusses the relevance of the creation of this tool.

These tools will help provide the ability to model RF propagation for free to the public, which will assist in filling in the coverage gaps within the state of Virginia as well as increase capacity within large cities using medium scale modeling. These tools can also be used outside of Virginia to aid in the development of a nationwide broadband map.

Chapter 2

Literature Review

In this thesis, we describe two RF algorithms that were created (the Large Scale Model and the Medium Scale Model) for RF planning in ArcGIS and attempt to determine whether GIS building data can be used to aid in indoor positioning scenarios. This chapter describes the background information to clarify our methodologies when using ArcGIS. First, this chapter specifies why traditional empirical models will not be sufficient for our application. This chapter also defines the complications when using existing RF propagation algorithms within ArcGIS as well as issues with current RF modeling software. The chapter concludes by developing a preliminary model for building penetration to be elaborated on in Chapter 5. Chapter 6 contains the literature review for modeling positioning using ArcGIS data.

2.1 Brief Discussion of Statistical Models

Predicting RF propagation is very similar to predicting the weather: there are countless variables at work preventing exact predictions, but a reasonable estimate is generally sufficient. Electrical engineers worldwide have spent decades developing new ways to improve RF prediction or improving previous ways of estimating RF propagation. There is still debate over the validity of empirical, or statistical, RF estimation models. There is no doubt that statistical models are useful, as they are more computationally efficient and are based upon statistical data often collected over several years. However, in areas outside of electrical engineering, there is a demand for RF estimation models that consider site-specifics of local terrain and don't report a simple regular shape, such as a circle or a hexagon. Section 2.1 is a short section that is designed to explain the difference between empirical and terrain-specific models and clarify why a terrain-specific model is desirable for our application.

The nature of empirical models is that they are based on statistical trends in data collected over a long period of time and in a wide variety of circumstances. The results of an empirical estimation isn't an exact representation of coverage, but is rather something that is defined probabilistically. For example, a model will generate a perfect circle for the coverage prediction, but at the edge of the circle, it is only 50% likely that one can receive a signal. This is due to the circle's edge representing the 50th percentile of the signal's attenuation, or where the coverage is 50% likely. The ITM results in estimates like this. Anywhere within the circle will have a higher probability of coverage. This is intuitive because the likelihood of coverage is higher near the source of the signal, where the signal will be stronger. Within a 50th percentile circular coverage estimate, the user has a 77% chance of

being covered on average [18]. A decibel margin of signal strength above the median (e.g. a 7 dB margin) can increase the probability of coverage to greater than 90% within the smaller circle that is created by increasing the minimum received power threshold (i.e., when the signal is not strong enough to be received properly) by 7 dB [19]. This topic is explored further in Chapter 4.

As an example, let us say that we have a very simple city with only one building in it, illustrated by Figure 2.1. Then, let's suppose there is an empirical model that estimates that there is 95% coverage within that city. Technically, the empirical model is correct, because 5% of the city within the coverage circle is shadowed by the building and is therefore not covered. However, the city's layout is unknown, the 5% of uncovered area could be anywhere, thus making it difficult to locate gaps in coverage. With terrain based modeling, the algorithms are more complex, but it will better indicate where gaps in coverage will be.

For this reason, the state of VA only allows terrain based models into the statewide broadband map [8]. The maps they compile will show gaps in coverage so that wireless internet service providers (WISPs) can fill the holes in coverage. Though a regular empirical model can represent the same probabilistic coverage as is represented a terrain-based model, the locations of the gaps in coverage are a mystery. The National Telecommunications and Information Administration (NTIA) is trying to cover the nation entirely for the nationwide emergency response system, therefore it is important to find areas lacking broadband and focus on filling those areas. Therefore, the NTIA doesn't accept regular shapes because they do not show specific gaps in coverage.

Finding a compromise between accuracy and computation time is also important. We want to make a model that will run fast enough that it can be used as a web

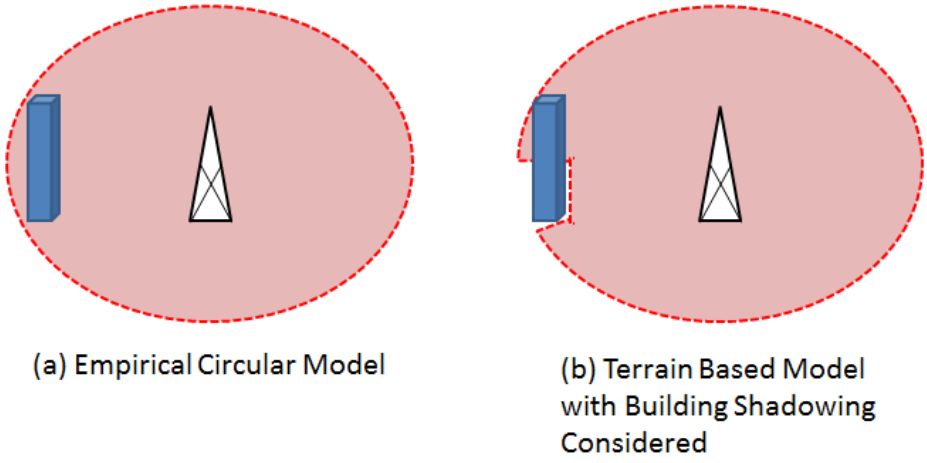

Figure 2.1: Illustration of the Difference Between Empirical (a) and Terrain-Based (b) Model Outputs. The terrain-based model has a small indent in coverage where the building is located. The Empirical model may predict that coverage is 95% likely within its radius, but does not describe where the uncovered 5% would be. Figure by author, 2014.

tool, but complex enough that it takes into account terrain obstacles. Most models currently in existence create regular shapes. Two of these models are covered in the next section.

2.2 RF Estimation Models

Over the past half century, electrical engineers all over the world have worked to develop models to estimate RF propagation. From the ITM developed in the 1960s to the COST 231 model developed at the end of the 20th century, many years of diligent data collection has resulted in dozens of ways to estimate RF coverage. Many of these models were explored for use in the Large Scale Model in this thesis. Unfortunately, most models are not compatible for work within ArcGIS either due to computational tool constraints (since ArcGIS is not designed to model RF) and computational time constraints (ArcGIS runs calculations on thousands of data points). This section will describe a two models considered for the model within ArcGIS: the ITM and the Okumura-Hata model.

Irregular Terrain Model

The Irregular Terrain Model (ITM), also known as the Longley-Rice Model, was developed in the late 1960s by Anita Longley, and Philip Rice [20]. At the time, there weren't any accurate means of estimating RF propagation, and the ITM offered a wide variety of variables to customize the propagation settings. The ITM has two main modes: area prediction and point-to-point (P2P)[21]. The point-to-point mode takes into account a direct link between two antennas, taking terrain-specifics

into account. However, the point-to-point mode is designed for a single antenna-to-antenna link, and is not a practical model to use in the Large Scale Model due to the long computation times of over an hour required for those calculations to be performed over a wide area.

The area prediction mode takes into account the general hills and valleys of the surrounding area, ground parameters, atmospheric parameters, as well as transmission settings to estimate coverage in a circle around the transmission antenna. This model is used as a general purpose model and is designed to predict the additional average attenuation when compared to the Friis free space path loss. The Friis free space path loss is a value that would be obtained if the terminals were to be unobstructed by terrain and unaffected by atmospheric refraction. The ITM calculates the attenuation relative to free space in decibels [22].

The ITM's area prediction mode has a very diverse set of uses, since it's design limits allow for a wide range of RF scenarios. Table 2.1 lists the input parameters of the ITM with their original design limits; Table 2.2 lists the possible values for the terrain irregularity parameter, Δh; and Table 2.3 describes the seven radio climates around the world [22].

Once provided the input parameters, the ITM computes numerous geometric parameters to describe the path of the signal around the Earth's surface [22]. The model uses empirical relations with the terrain irregularity parameter to estimate a few of these parameters that are unknown. The model then computes the reference attenuation, which is a median attenuation relative to free space [22]. This median attenuation is defined piecewise into four regions: free space, line-of-sight, diffraction, and forward scatter. These regions are shown in Figure 2.2. The Free Space region is the region in which the Large Scale RF Model would be ranged. The model uses

Table 2.1: Input Parameters for the ITM with Design Limits

System Parameters:	
Frequency	20 MHz to 20 GHz
Distance	1 km to 2000 km
Antenna Heights	0.5 m to 3000 m
Polarization	Vertical or Horizontal
Environmental Parameters:	
Terrain Irregularity Param. Δh	Default is 90 m
Electrical Ground Constants	Default, $\mu = 15$, $\sigma = 0.005$ S/m
Surface Refractivity	250 to 400 N-units
Climate	One of seven; see Table 2.3
Deployment Parameters:	
Siting Criteria	random, careful, or very careful
Statistical Parameters:	
Reliability and Confidence Level	0.1% to 99.9%

A brief description of the ITM parameters are listed below [22]:

Frequency - The carrier frequency of the signal

Distance - Distance between two terminals

Antenna Heights - The height of the center of radiation above ground

Polarization - The polarization, either horizontal or vertical, of the two antennas (assumed to be the same for both antennas)

Δh - The terrain between two terminals is treated as a random function of the distance away from one of the terminals. The ITM uses Δh to characterize the size of the irregularities. The terrain irregularity parameter represents the interdecile range of terrain elevations, that is, the total range after the highest and lowest 10% have been removed [22]. See Table 2.2 for values.

Electrical Ground Constants - The relative permittivity and conductivity of the ground

Surface Refractivity, N_s - The atmospheric constant represents the normal value of refractivity near ground levels. The atmospheric refractivity must be treated as a random function of position and time.

Climate - In conjunction with the Surface Refractivity, the climate can be used to find N_s. The climate attempts to characterize the atmosphere and its variability in time. See Table 2.3

Siting Criteria - A qualitative description of the care taken to site each terminal on high ground.

Reliability and Confidence Level - A statistical value describing the confidence of the estimate. Generally, these are given in the form of quantiles of attenuation

Table 2.2: Possible Values for the Terrain Irregularity Parameter

Terrain Type	Δh (meters)
Flat (or water)	0
Plains	30
Hills	90
Mountains	200
Rugged Mountains	500

Table 2.3: Possible Values for the Climate Parameter

Climate Type	N_s (N-Units)
Equatorial (Congo)	360
Continental Subtropical (Sudan)	320
Maritime Subtropical (West Coast of Africa)	370
Desert (Sahara)	280
Continental Temperate	301
Maritime Temperate, over land (U.K.)	320
Maritime Temperate, over sea	350

theoretical treatments of atmospheric and terrain parameters to perform calculations and arrive at a statistical result for coverage. The model itself will not be covered in much detail since it is not used in the final Large Scale Model algorithm.

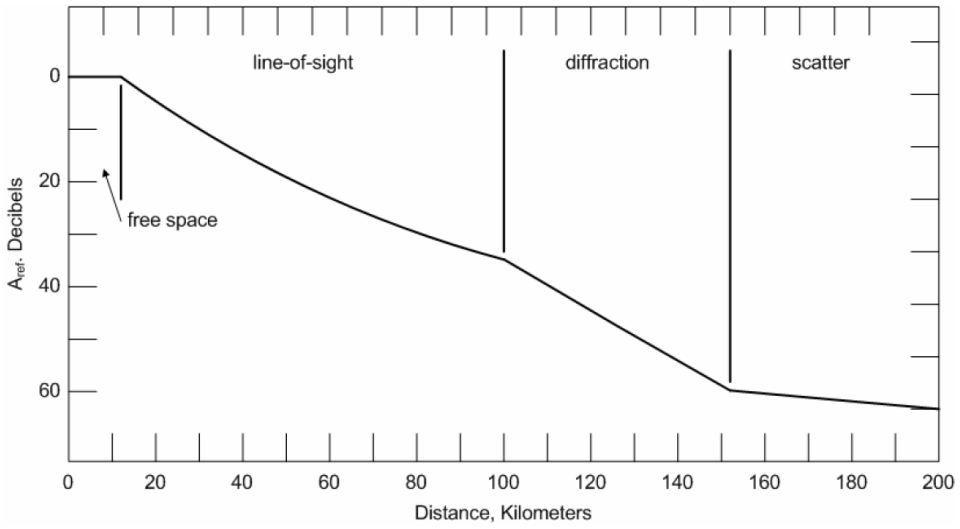

Figure 2.2: Generalized Graph of Reference Attenuation vs. Distance. The three regions beyond 'free space' are outside the range of a typical RF Antenna. The LOS region refers to the region where the general bulge of the earth does not interrupt the direct radio waves. The Diffraction region is the region in which the signal would diffract around the curvature of the Earth. The Scatter region is the distances in which the signal would scatter off of the atmosphere to arrive at a receiver. Hufford, G. A., A. G. Longley and W. A. Kissick. A Guide to the Use of the ITS Irregular Terrain Model in the Area Prediction Mode. Technical Report 82-100, NTIA, April 1982. Used under fair use, 2014.

The area prediction model results in a circular RF estimate, which is not an acceptable shape for the Virginia Broadband Map. A circle is not acceptable for the

Statewide Broadband Map due to the circular coverage estimate not being differentiable from other estimate locations. Due to hills and valleys, there are always going to be areas that will show up as covered within a circle that are not actually covered, therefore it is an unrealistic representation of that tower's actual coverage [8]. The point-to-point model is designed for a single RF estimate between two antennas, and is an inefficient method when trying to take a large area into consideration. However, when the area prediction mode was being considered, a small script was created to calculate the preliminary parameters required for both modes of the ITM. The script takes at least 30 seconds to run, and since the more computationally intense portion of the code is not included in that run time, both modes are too computationally intensive to use in ArcGIS for this project. Many of the parameters can be calculated once, but there are many others that require updating for each tower, such as the terrain profile between the transmitter and receiver. It is estimated that the point-to-point mode would take at least one hour per transmission antenna when the process is repeated for all of the cells in a wide area.

Okumura-Hata Model

The Okumura-Hata Model is a popular empirical and statistical RF estimation model due to its simplicity. In 1968, Okumura published the results of a decade long empirical study of frequencies in the ultra high frequency (UHF) and very high frequency (VHF) bands [10]. Based on measurements collected in the city of Tokyo, Japan, the Okumura model can be used to estimate RF attenuation loss in three generalized scenarios: urban, suburban, and open areas. In 1980, Hata released a paper that altered Okumura's model so that it could be plugged into computers for faster computation time [11]. The basics of the Okumura and the Okumura-Hata

model will be outlined in this section, but neither model was used due to the fact that they do not take into account specific terrain data and have a limited applicable frequency range of 150-1500 MHz.

The following expression was derived from Okumura's work and is listed in Okumura's paper [10]:

$$L = L_{FSL} + A_{\mu} - H_{MG} - H_{BG} - \sigma K_{correction} \tag{2.1}$$

where,

- L = the median path loss [dB]
- $L_{FSL} = 20 \log_{10}\left(\frac{4*\pi*d*f}{c}\right)$ = the Free Space Loss [dB]
  - ➢ $c = 3 * 10^8$ =the speed of light
  - ➢ d = distance [m]
  - ➢ f = frequency [MHz]
- A_{μ} = the median attenuation, extracted from data curve in Okumura paper [10] [dB]
- H_{MG} = the mobile station antenna height gain factor [dB]
- H_{BG} = the base station antenna height gain factor [dB]
- $K_{correction}$ = the correction factor gain (environment, etc.), based on data curves in Okumura paper [10] [dB]

The height gain factors can be calculated using the receiver (RX) heights as

follows:

$$\begin{aligned} H_{MG} =& 20 \log_{10}\left(\frac{h_{RX}}{3}\right) && 3m < h_{RX} < 10m \\ & 10 \log_{10}\left(\frac{h_{RX}}{3}\right) && h_{RX} < 3m \\ H_{BG} =& 20 \log_{10}\left(\frac{h_{TX}}{200}\right) && 30m < h_{TX} < 1000m \\ & 10 \log_{10}\left(\frac{h_{TX}}{200}\right) && h_{TX} < 30m \end{aligned} \tag{2.2}$$

The Okumura model was versatile, since it was a reasonable path loss estimate for frequencies between 150 - 1920 MHz (with an extension to 3 GHz), distances of 1 - 100 km, and base station antenna heights from 30 - 1000m [10]. However, the Okumura model relied heavily on charts and graphs for path loss derivation, which was inconvenient and difficult to use computationally.

In 1980, Hata published a paper in which he took Okumura's propagation prediction method to derive an easy-to-use empirical formula for propagation loss [11]. He recognized that using curves and tables would be cumbersome for wireless system planning. Instead, he opted for an empirical formula that would take the following into consideration:

1. Propagation loss between isotropic antennas
2. Quasi-smooth terrain
3. The urban area propagation loss standard formula (other areas can be supplemented with correction equations)

Hata first examines Okumura's formula for received power:

$$P_r(dBm) = P_u(dBm/m^2) + 10 \log_{10}(A_{eff}) \tag{2.3}$$

where

- $A_{eff} = \lambda^2/4\pi$ = The absorption cross section of an isotropic antenna (m^2)
  - ➢ $\lambda = c/f$ = the wavelength of the signal (m)
- $P_u = E - 10\ \log_{10}(120\pi) - 90$ = the received power density (dBm/m^2)
  - ➢ E = the received field strength of an isotropic antenna ($dB\mu V/m$)

The propagation loss is translated from a derivation of Okumura's model for total path loss:

$$\begin{aligned} L_P(dB) &= P_t - P_r \\ &= P_t(dBW) - E(dB\mu V/m) - 10\ \log_{10}(\lambda^2/4\pi)(dBmeters^2) + 115.8 + 30(dBm) \end{aligned} \tag{2.4}$$

where P_t = The effective isotropic radiated power (EIRP) (dBW), and an additional 30 dB are used to convert between dBm and dBW. Hata then calculates the EIRP of an average antenna, arguing that P_t can be found by finding the effective radiated power per antenna (P_t')and adding the difference value for power gain between isotropic antenna and dipole antenna. The absolute power gain for a dipole antenna is 2.2 dB, therefore

$$P_t(dBWEIRP) = P_t'(dBWERP/dipole) + 2.2(dB) \tag{2.5}$$

For a 1kW EIRP/dipole antenna, P_t = 32.2 dB. By combining equation 2.4 and equation 2.5, we arrive at a formula that can be used to calculate propagation loss using the prediction curves and the wavelength of the signal:

$$L_p(dB) = 178 - 10log_{10}(\lambda^2/4\pi) - E(dB\mu V/m) \tag{2.6}$$

Hata examined Okumura's field strength curves and discovered a pattern emerged over quasi-smooth terrain by using the basic median field strength curves. Hata

found that the field strength, E, can be derived as a function of distance R (km) as follows:

$$E(dB\mu V/m) = \gamma + \beta \log_{10} R \tag{2.7}$$

where γ and β are constants derived from the height of the base station, h_b, and the carrier frequency of the signal, f_c. Therefore, the standard of propagation loss can be translated into a simple form:

$$L_p = A + B \log_{10}(R) \tag{2.8}$$

$$A = 178 - 10 \log_{10}(\lambda^2/4\pi) - \gamma + a(h_m) \tag{2.9}$$

$$B = -\beta \tag{2.10}$$

where A and B are frequency and antenna height functions, and R is the distance. Hata found that A is given by the value of the field strength E, at R = 1km and B is determined by the slope of the field strength curve. Two tables are derived, but are not included in this paper for brevity.

From the table for A, Hata found a formula to describe A using the base station height, h_b, the carrier frequency, f_c, and a correction factor based on the mobile's height $a(h_m)$:

$$\begin{aligned} A &= \alpha - 13.82 \log_{10}(h_b) - a(h_m) \\ \alpha &= 69.55 + 26.16 \log_{10}(f_c) \end{aligned} \tag{2.11}$$

Similarly, Hata derived a formula to describe B, which is only dependent on the height of the base station, h_b:

$$B = 44.9 - 6.55 \log_{10}(h_b) \tag{2.12}$$

By substituting equations 2.11 and 2.12 into equation 2.8, we arrive at a standard formula for propagation loss:

$$\begin{aligned} L_p(dB) = 69.55 + 26.16\ \log_{10}(f_c) - 13.82\ \log_{10}(h_b) \\ -a(h_m) + (44.9 - 6.55\ \log_{10}(h_b))\ \log_{10}(R) \end{aligned} \tag{2.13}$$

where

$$f_c : 150 - 1500MHz, \tag{2.14}$$

$$h_b : 30 - 200m, \tag{2.15}$$

$$R : 1 - 20km, \tag{2.16}$$

and $a(h_m)$ is the correction factor for h_m, and $a = 0$ dB for $h_m = 1.5$ m.

Due to the Okumura-Hata model not being used for the final algorithm, the table for $a(h_m)$ will not be included in this paper and can be found in Hata's paper [11].

The Hata model is a simple-to-use formulation of the Okumura propagation loss algorithm. However, the Hata model, like the Okumura model, does not take into consideration individual obstructions in terrain, such as mountains and hills, that would result in a non-circular propagation estimate. As was mentioned in the section about the ITM, a circle or regular shape will not be accepted into the Virginia broadband map due to the unrealistic nature of a circular propagation estimate. The Okumura-Hata model also is not applicable to all of the frequencies of interest. Therefore, the Okumura-Hata model could not be used in this project to estimate coverage.

Other

There are dozens of other empirical and terrain based RF prediction models. Each is more accurate in certain scenarios than others, but the simplest algorithms are the best for RF estimation in the geoprocessing program, ArcGIS. Most RF prediction algorithms, like the Okumura-Hata model and the ITM, are too computationally intensive to be useful as an ArcGIS script for real-time web-based applications. ArcGIS scripts use ArcGIS tools that take a long time to run due to the hundreds of calculations being performed on detailed terrain data. Therefore, a model that uses the fewest number of ArcGIS tools is the most practical for a web tool.

2.3 Review of Available RF Modeling Software

Estimating RF coverage is becoming increasingly important, and many companies are creating software to capitalize on this need. However, most wireless broadband companies cannot afford to spend the time and capital required to purchase this software and learn how to use it. We set out to create a free ArcGIS script that can be used by VGIN and wireless internet service providers (WISPs) that have access to ArcGIS. This script is easy to use and can be modified for a WISP's individual use. It is important to be familiar with the currently available RF modeling software and the pros and cons therein. Two RF estimation programs are discussed in this chapter: Radio Mobile and TAP.

Radio Mobile

Radio Mobile is a RF propagation prediction program developed by Roger Coudé in 1988 [23][1]. Based on the ITM, Radio Mobile offers both an area prediction model and a point-to-point link, and can be used within a frequency range from 20 MHz to 60 GHz [24]. Radio Mobile allows for elevation maps to be drawn from terrain data downloaded from the United States Geological Survey (USGS), as well as roads and elevation contours. Upon downloading terrain data, Radio Mobile allows for entry of base stations and mobile stations, either manually, or via CSV files. After data entry is complete, Radio Mobile offers several types of propagation analysis based on the ITM. Radio Mobile has multiple output formats, such as image files and KML files that can be opened in Google Earth [23].

Due to the ability to download it for free, this program was used to model coverage for local WISPs who were looking to submit their coverage data to the Statewide Broadband Map during the time in which the model developed for this thesis was being created. Radio Mobile's main window features a large space where a map can be loaded and analysis can be performed. Maps are downloaded from the USGS as needed depending on the location of the desired area and how large the area is. The Unit Properties menus is where tower locations can be added in so that tower locations can be used when generating Maps.

Many features, from antenna pattern to tower height, can be changed in the Network Properties menu. This menu is where all of the frequencies, transmission powers, and environmental conditions can be added for each Unit. Once the Network data has been updated, a polar coverage estimate can be generated on various Picture

[1]Radio Mobile is Copyright ©1988 - 2014 Roger Coudé. All rights reserved.

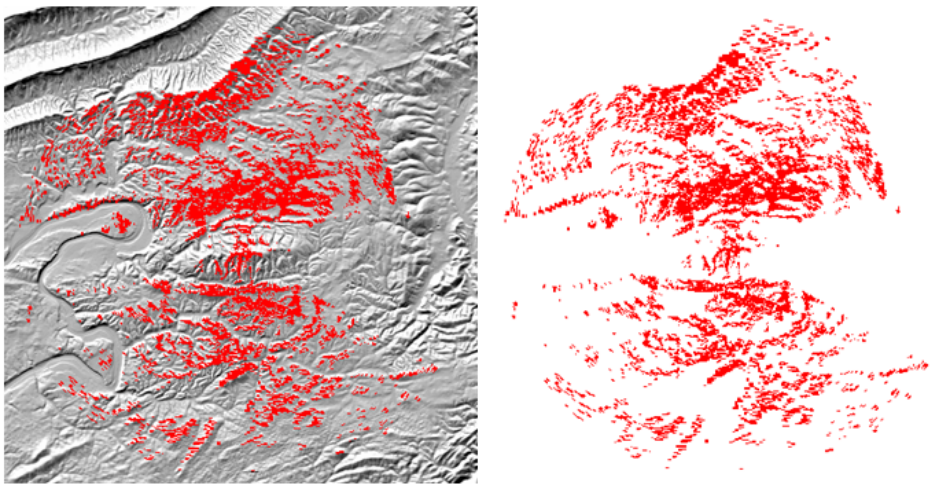

(a) Coverage Over Greyscale Terrain (b) Coverage Over White Terrain

Figure 2.3: Radio Mobile Coverage Plot Results with Greyscale and White Backgrounds. These two outputs are the same coverage plot with different terrain backgrounds. The White Background figure is a Boolean coverage estimate.

backgrounds. Figure 2.3 illustrates the coverage difference (the coverage is in red) between a greyscale terrain background and a plain, white background (which results in a Boolean image).

Using the procedures in Appendix A, RF propagation estimates could be created while the RF propagation model was being developed. Due to the polar coverage estimate being generated on decimal degree wedges, the accuracy of the estimate is lower at the outside of the plot than near the center [25]. The reduced accuracy of the outer edges is indicative of most RF propagation estimates, however, and is therefore an acceptable uncertainty. Radio Mobile provides an estimate that considers terrain obstacles, and will generate estimates that are acceptable for the Statewide Broadband Map. However, like most RF estimation software, the estimate is only as good

as the terrain data it uses, but Radio Mobile is generally considered a good program for this purpose [24]. Radio Mobile is not an ideal program for the FirstNet scenario due to the the output not being in a format that is easily readable by ArcGIS.

TAP Software

Terrain Analysis Package, or TAP, software is a package of software developed by SoftWright and comprised of 27 different software modules [9][2]. Unlike Radio Mobile, TAP Software is not freeware, and offers bundles containing various modules of their software [26]. This software is very expensive, with the total cost of all of the modules surpassing $26,000. Most small WISPs cannot afford to purchase this software to model their broadband system's coverage. For this reason, TAP's tools were not considered. However, as an example software package out of the many available packages, I will cover some of the available features of TAP.

TAP offers a wide variety of modules: general use utilities, propagation modules, path analysis modules, area coverage modules, and interference study modules [9]. The general use utilities deal primarily with mapping terrain and managing antennas and assets. The 3D Display tool exports 3D coverage maps to other programs, like Google Earth and ArcGIS. The Shadow Mapping module can identify areas with line-of-sight and Fresnel zone clearance. The Land Use and Topo Utilities modules import USGS land cover and digital elevation maps, respectively, to be used in propagation estimates. The general use utilities are mostly modules designed to make way for the computational modules.

[2]Terrain Analysis Package is Copyright ©2000 - 2014 SoftWright. All rights reserved. Published in the United States of America.

Though the final three types of modules also offer tools for RF prediction, the eight propagation models offered in the Propagation Module are more relevant to VGIN's statewide broadband map [9]. TAP software's Propagation Modules include ITM, Bullington, Okumura, Rounded Obstacle, Broadcast (FCC Part 73), Carey (FCC Part 22), Hata-Davidson, and Egli. The ITM and Okumura model were discussed previously in this chapter, and out of the other six models, the Broadcast, Carey, Hata-Davidson, and Egli are the most useful for WISPs trying to model their coverage.

Other

There are numerous other types of RF estimation software available, such as EDX Signal Pro or Towercoverages.com. However, many have drawbacks, such as being very costly or not supporting the ArcGIS polygon data type required by VGIN for inclusion into the statewide broadband map. The models described in this paper hope to achieve a balance between being freeware and providing reasonably accurate coverage estimates in the proper format.

2.4 Review of Structure Effects on RF

Electrical Engineers are still studying the effects of building walls on signal strength, and there are many studies that provide detailed algorithms for modeling this. Most studies are empirical and result in an algorithm for a specific set of carrier frequencies or penetration scenarios. These algorithms can vary in complexity, but generally require multiple formulas and building parameters to arrive at a result.

In this thesis, however, we want a model that can simulate building penetration within ArcGIS. We need a simple algorithm to minimize the computational time required for modeling. The algorithm created is the Medium Scale RF Model described in Chapter 5. When creating this model, we examined the following sources for possible algorithms for modeling RF attenuation through buildings. Our focus is on frequencies commonly used in WiFi systems (2.4 GHz and 5 GHz), since the Medium Scale model is designed for use in WiFi systems [27]. The final model uses elements described in these sources that have been modified to reflect data collected in the field. The final model is designed for 2.4 GHz WiFi.

Residential

There aren't many resources available for modeling propagation in residential buildings, since more effort has been made toward determining the characteristics of large buildings. This isn't surprising, since residential buildings are often made of wood which has better transmission characteristics than the steel and cement that are more common with large structures. Also, in emergency situations, it is easier to locate victims in a small home than it is within a large building. For these and other reasons, finding algorithms for signal penetration into houses is difficult.

Though there are limited sources for the desired frequencies, there are enough sources to create a preliminary algorithm to use in the Medium Scale model. Greg Durgin *et al.* explored the effects of residential building penetration at the National Information Infrastructure (NII) band in their papers published in 1998 [28]. Their papers describe their experiments conducted at 5.85-GHz frequencies into three homes and through trees. The experiments had an experimental set up as is illus-

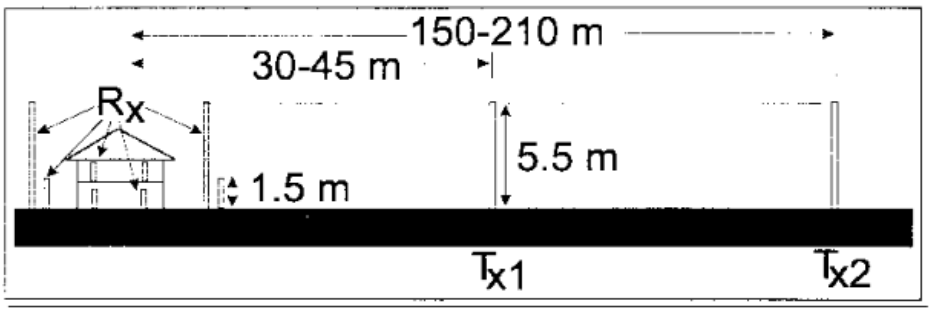

Figure 2.4: Experimental Set Up of the Durgin *et al.* Indoor Propagation Tests. Transmitters 1 and 2 are both 5.5 m tall, and there are several receiver (RX) antenna configurations. In the front of the house are two RX antennas at 5.5 and 1.5 m tall, and this configuration is repeated at the back of the house. Within the house, 1.5 m tall RX antennas are placed on the first and second floors. Durgin, G., T. S. Rappaport and H. Xu. 5.85-GHz Radio Path Loss and Penetration Loss Measurements In and Around Homes and Trees. *IEEE Personal Communications*, 2(3):70-72, March 1998. Used with permission of IEEE, 2014.

trated by Figure 2.4. The first paper, released in March 1998, attempted to come up with an algorithm for home penetration loss, building shadowing loss, and tree shadowing loss. They were able to derive the path loss exponent values described in Table 2.4. Descriptions for Buildings 1, 2, and 3 from Table are in Table 2.5 [29].

As is shown in Table 2.4, an overall path loss exponent of $n = 3.4$ through a home can be expected for a carrier frequency around 5.85-GHz. This path loss exponent can be used to determine the signal's decay as it passes through the building. Though 5.85-GHz is a higher frequency than the 5 GHz frequencies used in some WiFi systems, these path loss exponents can be considered an upper bound for these WiFi systems due to attenuation increasing with frequency.

Table 2.4: Path Loss Exponent Summary for Various T-R Configurations at 5.85 GHz Using 5.5-m Transmitter Height. Durgin, G., T. S. Rappaport and H. Xu. 5.85-GHz Radio Path Loss and Penetration Loss Measurements In and Around Homes and Trees. *IEEE Personal Communications*, 2(3):70-72, March 1998. Used with permission of IEEE, 2014.

T-R Configuration	n	σ [dB]	Num. of Meas. Locations
Indoor			
Overall	3.4	8	96
First Floor RX	3.5	8.3	58
Second Floor RX	3.3	7.3	38
Outdoor			
Overall	2.9	7.9	147
1.5m RX	2.9	9.0	73
5.5m RX	3.0	6.4	74
Building 1			
First Floor RX	3.5	9.7	23
Second Floor RX	3.5	7.4	10
1.5m RX	3.1	10.2	26
5.5m RX	3.0	6.5	27
Building 2			
First Floor RX	3.2	6.2	8
Second Floor RX	3.3	7.7	22
1.5m RX	2.9	8.2	22
5.5m RX	3.1	6.2	20
Building 3			
First Floor RX	3.6	6.9	8
Second Floor RX	3.4	3.1	27
1.5m RX	2.7	6.4	26
5.5m RX	2.8	5.3	26

In the table, n is the path loss exponent, and σ is the standard deviation.

Table 2.5: Test Building Information For the Three Homes Measured. Durgin, G., T. S. Rappaport and H. Xu. Measurements and Models for Radio Path Loss and Penetration Loss In and Around Homes and Trees at 5.85-GHz. *IEEE Transactions on Communications*, 46(11):1484-1496, November 1998. Used with permission of IEEE, 2014.

Parameter	Building 1	Building 2	Building 3
Construction Date	1994	1978	1990
Dimensions	19m x 15m	11.5m x 18m	14.5m x 17m
Num. of Floors	2	2	2
Basement	No	Yes	Yes
Exterior	Brick	Wood	Brick
Insulation Lining	Paper	Paper	Foil

In a similar paper, Sergio Aguirre *et al.* conducted building RF penetration experiments at 912, 1920, and 5990 MHz [30]. Seven residential buildings were tested with various building materials and number of floors. Raw data was collected from four to six rooms in each house and compiled into a cumulative distribution function (CDF) in Figure 2.5 [30]. The median penetration losses for 912, 1920, and 5990 MHz are 7.7, 11.6, and 16.1 dB, respectively. These penetration losses can be considered for residential buildings in the Medium Scale model.

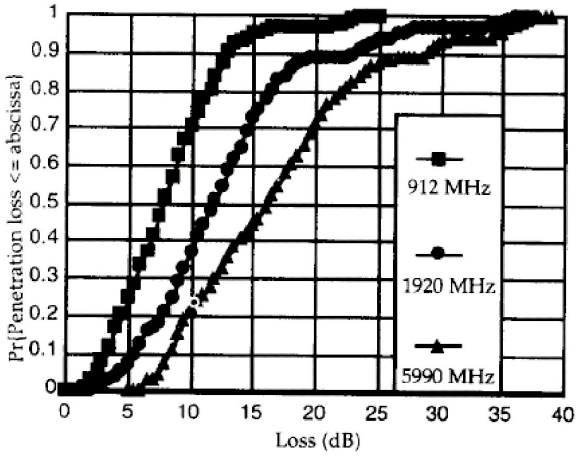

Figure 2.5: CDF of Residential Building Penetration Losses at 912, 1920, and 5990 MHz. The CDF demonstrates that 912 MHz has smaller loss than 1920 and 5990 MHz. The loss increases as frequency increases. Aguirre, S., L. H. Loew and Y. Lo. Radio Propagation Into Buildings at 912, 1920, and 5990 MHz Using Microcells. *Universal Personal Communications*, pages 129-134, September 1994. Used with permission of IEEE, 2014.

Commercial and Large Buildings

Radio frequency penetration losses have been studied more extensively in larger commercial buildings. Since the walls of commercial buildings tend to be made of thicker materials like concrete and stone, the signal degradation is much greater. In buildings made from thick and unevenly cut stone, such as Hokie stone, the exterior walls can create a scenario in which scattering and building materials make penetration challenging. This can make calling for help in an emergency situation dangerously difficult.

In Aguirre's article, they also examine high-rise buildings for frequencies of 912, 1920, and 5990 MHz [30]. Out of the four high-rise buildings tested, one had walls made of glass, one was made from concrete, and two were made of stone. The median penetration losses measured were 12.5, 15.5, and 20 dB for 912, 1920, and 5990 MHz, respectively. It was also noted that the measured losses did not increase nor decrease monotonically as a function of increasing floor level [30]. The stability of the measured losses depending on floor level is significant for our model because GIS building data with floor information may not be available. Therefore, an upper bound for penetration loss for WiFi systems in a high-rise building is 20 dB.

In a similar study conducted in Liverpool, UK, Antonio Fischer de Toledo, *et al.* studied penetration losses into numerous buildings throughout Liverpool [31]. These structures were often made from stone with varying quantities of windows, and at least ten experiments were conducted at each of the transmitter locations. Twenty-three buildings were tested for building penetration at 2300 MHz, which is the lower end of the WiFi spectrum of interest to us. The results from the 'into building' experiments are that the average penetration loss into a building was approximately

15 dB [31]. Experiments 'within buildings' were also conducted, and the average path loss exponents were 5.3, 5.5, and 6.0 for 900, 1800, and 2300 MHz, respectively. These two studies can be combined with the residential building data into a model for building penetration.

Combination of Residential and Commercial Buildings

Due to the computational limitations of ArcGIS, the Medium Scale Model described in Chapter 5 will need to use a simplistic algorithm to estimate RF propagation. As will be mentioned in Chapter 5, there are tools within ArcGIS that allow us to determine the number of times that a signal's path penetrates a building. Using this data, we can come up with an algorithm using the path's total length and the number of times that a path passes through a building to determine the total path loss along the segment. An easy way to do this is to calculate the path loss along the line segment through air, and then modify that result with the distance of the path through structures:

$$\begin{aligned} L_p[dB] &= n_{air} * 10\log_{10}(d_{total}/d_0) + n_{building} * x_{wall} + L_0 \\ L_0[dB] &= 20 * \log_{10}\left(\frac{4 * \pi * d_0}{\lambda}\right) \\ d_0[m] &= 10 \end{aligned} \tag{2.17}$$

where n_{air} is a path loss exponent describing the signal's attenuation through air, $n_{building}$ is the additional attenuation experienced when a signal passes through a building, and x_{wall} is the number of walls the signal passes through. This additional attenuation is a compromise between residential and commercial path attenuation, since the currently available building data within ArcGIS does not distinguish between residential and commercial buildings.

For now, we set $n_{air} = 2.2$, just above the free space path loss exponent of 2. This value takes into account the small attenuation in addition to free space that occurs due to non-ideal free space conditions. To find $n_{building}$, we must find a compromise between residential and commercial path loss.

Durgin *et al.* classify common attenuation values for building materials, and the results are listed in Table 2.6 [28]. In general, a brick house exterior is a good compromise between a residential building and a commercial building. Therefore, in the preliminary model, we chose to have $n_{building} = 14.5$. Our final combination model is:

$$\begin{aligned} L_p &= 2.2 * 10\log_{10}(d_{total}/d_0) + 14.5 * x_{wall} + L_0[dB] \\ L_0 &= 20 * \log_{10}\left(\frac{4 * \pi * d_0}{\lambda}\right)[dB] \end{aligned} \tag{2.18}$$

2.5 Conclusion

This chapter discussed reasons why a new algorithm must be created in order to model RF propagation within ArcGIS. Available terrain data must be used in the algorithm so that terrain features are considered and terrain-based gaps in coverage can be simulated. Existing models are too computationally intensive to be used within ArcGIS, often taking at least 30 seconds just to run the preliminary calculations. Current modeling software is often expensive and difficult to use, and most software does not allow the user to see how the code works. A new model must be created, and residential and commercial building data was examined for use within the Medium Scale Model outlined in Chapter 5. The outputs of these models will be compatible with ArcGIS.

Table 2.6: Generalized Shadowing Attenuation Values in Excess of Free Space. Durgin, G., T. S. Rappaport and H. Xu. 5.85-GHz Radio Path Loss and Penetration Loss Measurements In and Around Homes and Trees. *IEEE Personal Communications*, 2(3):70-72, March 1998. Used with permission of IEEE, 2014.

Shadowing Element	Loss	
Brick House Exterior	14.5	dB
Wood Siding Exterior	8.8	dB
Cinderblock Wall	22	dB
Subterranean Basement Loss	31	dB
Interior Wall	4.7	dB
Close-in House Shadowing (1.5m RX height)	24	dB
Close-in House Shadowing (5.5m RX height)	16	dB

Chapter 3

ArcGIS

Geographical data is most commonly processed using geographical information systems (GIS) software. ArcGIS is a popular GIS software program that has grown rapidly over the past fifteen years since it was first released by Esri in 1999 [32]. The software is versatile and can be used to store data, update and perform calculations on geographic surfaces, and display numerous geographic data types for planning and illustration purposes.

This project focuses on bringing electrical engineering concepts of RF propagation into geoprocessing software. The state of Virginia has developed numerous databases including RF coverage estimates, dead zones, and wired connection broadband availability. In an effort to serve its citizens and broadband providers, this information is available online for customers to find local providers or to report dead zones. This data is collected from broadband providers and processed through ArcGIS before being displayed. However, many small broadband providers do not have access to ArcGIS software or any other RF modeling software. They often neglect to model

their coverage information and report it to the statewide broadband map, which can negatively affect their business. It became important to create a free RF model to estimate coverage efficiently. ArcGIS was chosen as the software platform due to its easy access to terrain data, its hundreds of geoprocessing tools, and for its ability to return data types that are required by the statewide broadband maps.

3.1 Background

Prior to the release of ArcGIS, Esri focused on a set of FORTRAN programs known as ARC/INFO [33]. ARC/INFO was released in 1982, and featured an easy to learn command language that would allow for analytic and graphic geographic products. ARC/INFO's command line computation ability was integrated with Esri's geographical user interface (GUI) products, such as ArcView. ArcView was released in 1991 and offered a view and query capability that ARC/INFO did not provide [34]. Figure 3.1 contains a graphic of the 1991 ArcView interface [35].

ArcGIS was first released as ArcGIS 8.0 in 1999 by Esri [32]. Figure 3.2 shows the ArcMap 8.0 interface with some polygon feature sets in the main window [36]. ArcGIS combined the user friendly interface of ArcView with the power of ARC/INFO. An expanded image of the ArcToolbox containing ARC/INFO's functionality is visible in Figure 3.3 [36]. The combined application was known as ArcMap version 8.0. ArcGIS 8.0 included an additional file management application called ArcCatalog [37]. One of the largest changes was Esri's decision to drop support of application specific languages in favor of Visual Basic for Applications (VBA), Visual Basic, Visual C++ or Delphi [38]. Since ArcGIS's initial release, Esri has released twelve major version upgrades, its most recent being ArcGIS 10.2 in July of 2013.

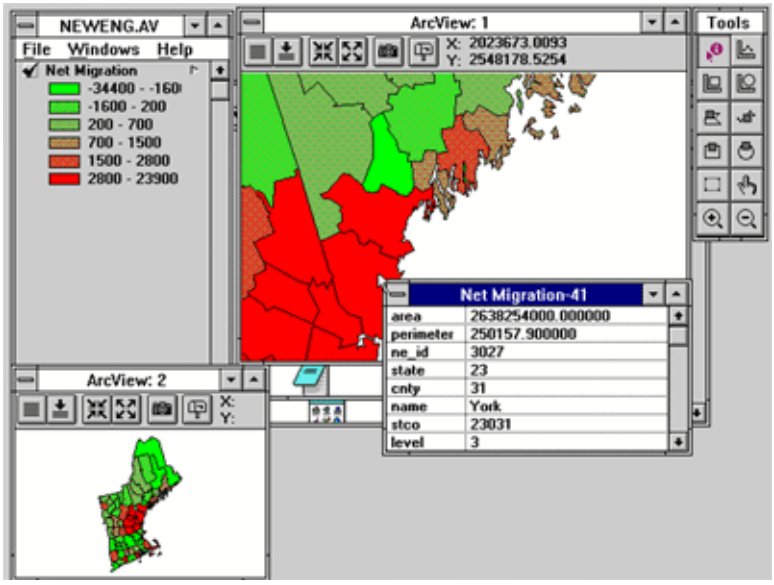

Figure 3.1: MDI Interface of 1991 release of ArcView. This graphical interface has some geographical data of New England.

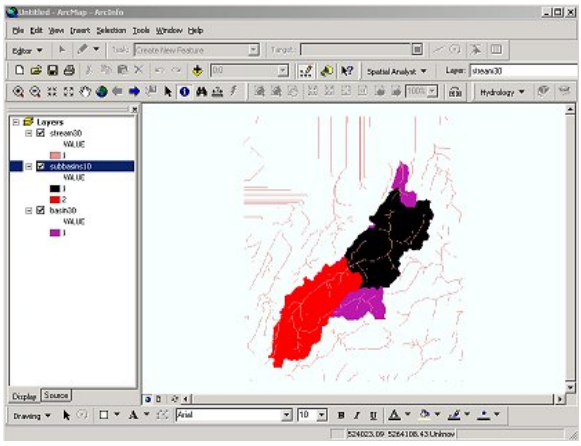

Figure 3.2: ArcMap 8.0 Interface. This graphical interface has some geographical data in the main window, with the available layers in the left-hand panel.

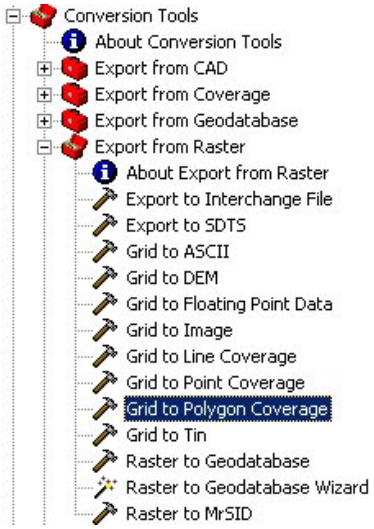

Figure 3.3: ArcToolbox Heirarchy with Export from Raster Toolbox expanded This figure shows som of the available tools in ArcToolbox, such as the Grid to Polygon Coverage tool that is highlighted.

3.2 Using ArcGIS

ArcGIS is a user-friendly tool designed for geographical data analysis, calculation, visualization, and storage. ArcGIS has three major functions : Geodatabase, Geovisualization, and Geoprocessing [14]. The Geodatabase view is a spatial database containing geographic information data in the form of generic GIS data types. Geovisualization is the set of maps and other views that illustrate relationships between features and the earth's surface. The Geoprocessing view is a set of tools to derive new geographic datasets from existing datasets.

Geodatabase

ArcGIS's Geodatabase view comprises a database designed explicitly to contain geographic data in various formats. This data can include collections of vector-based features like roads, raster datasets containing elevation data, points containing tree information, or a polygon of a building layout. This section will describe a few of the data formats most important to the RF estimation algorithm developed for this thesis [39].

Raster

A raster is an array of pixels that represents a continuous layer, such as elevation or terrain data. Each raster is made up of cells, and each cell can contain numerous layers of information. For example, a raster can contain information about terrain elevation, foliage elevation, population density, etc. Rasters are stored in geodatabases, but they can be converted to image files to be stored outside of geodatabases. Figure

3.4 is a raster containing a digital elevation model (DEM) of the state of Virginia and the information contained in one of its cells in the adjacent window.

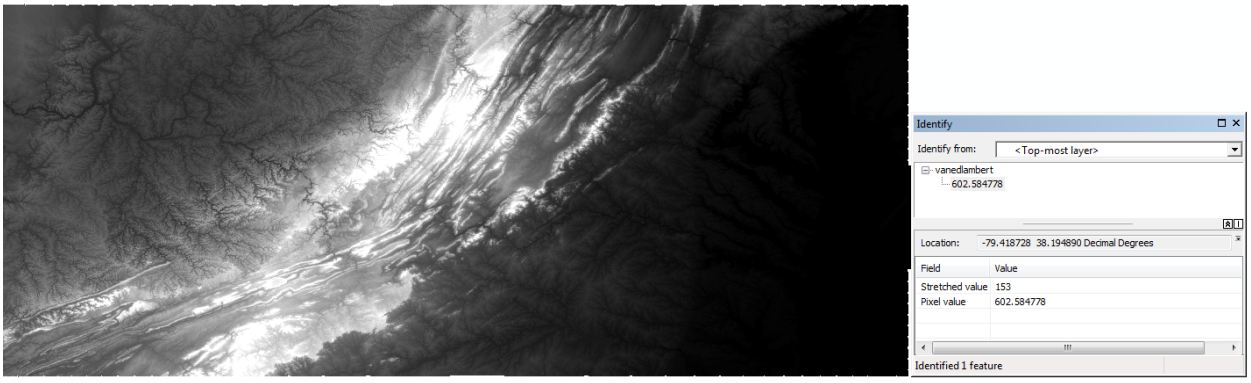

Figure 3.4: Raster DEM with a Pixel's Value of 602.6 m Elevation Selected in the Right Window. This DEM is of the state of Virginia, with the lighter colored pixels representing the mountain ranges in the western portion of the state.

Feature Geometry

Feature Geometry is a diverse geographic data type, since there are five different subtypes: points, lines, polygons, annotations, and 3D multipatch. The RF coverage models described in this thesis use points, lines, polygons, and 3D multipatch feature types in their algorithms. Figure 3.5 contains a picture of the first four feature geometry types, and Figure 3.6 contains an image of multipatch data [39]. The four relevant feature geometry types, points, lines, polygons, and 3D multipatch, are described below.

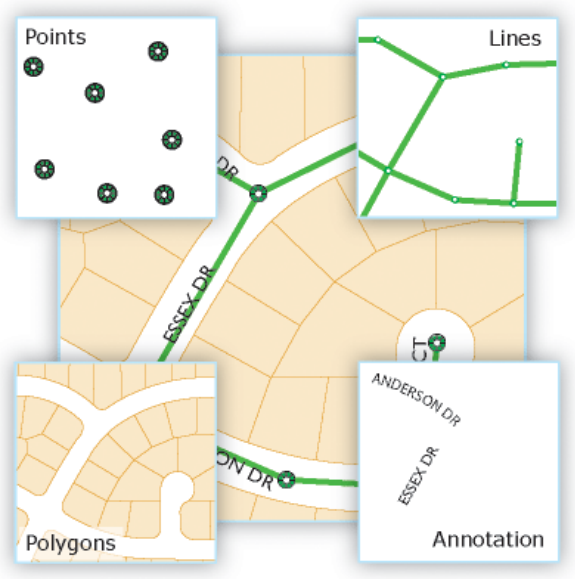

Figure 3.5: Example of Point, Line, Polygon, and Annotation Feature Classes

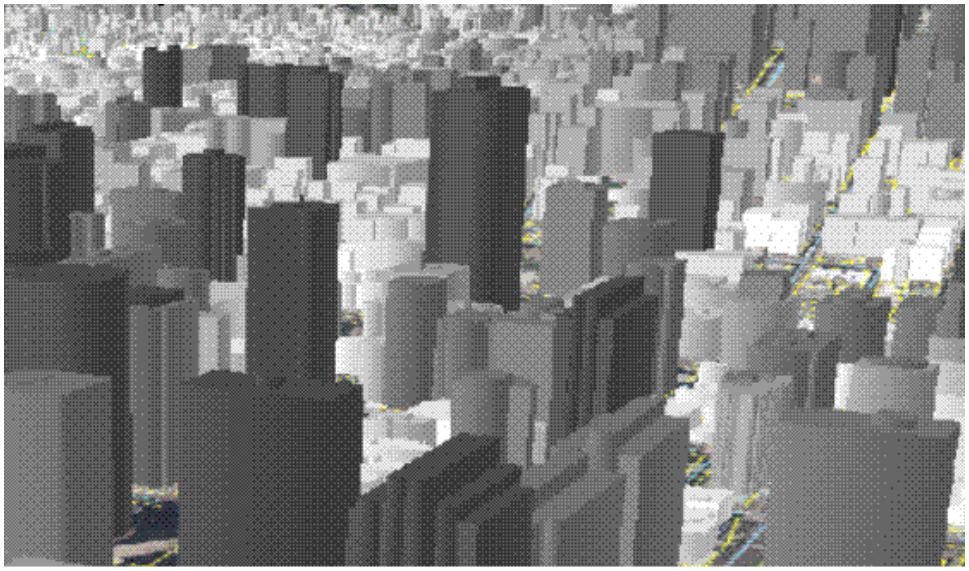

Figure 3.6: Example of 3D Multipatch Data within a City

Points A point feature represents a point of interest at a certain location and generally contains information about the location that can be used in geoprocessing. For the RF estimation algorithm, numerous antennas are represented by points containing information about latitude, longitude, distance above ground level, transmission power, etc.

Lines Line features can be used to illustrate road systems, rivers, paths, and any other similarly shaped geographical feature. Lines are an output of the small cell RF estimation algorithm, with each line representing a segment of the path between the transmitter and the receiver. Each segment contains information about the length and the type of material the signal is trying to pass through.

Polygons Polygons are feature lines that are enclosed to represent an area. Upon creation, information about area and length are included in the object's attributes, and more fields can be added to contain a variety of information. The RF coverage data for the statewide broadband map must be in a polygon format, and the polygon must contain information about the service provider, data speeds, spectrum, and technology type.

3D Multipatch A multipatch feature is a GIS object that uses a collection of 3D data "patches" to represent a 3D object as a single row in a database [13]. These patches can store visualization data such as texture and color, as well as geometric information. Multipatches are often used to represent buildings, trees, and subsurface geological formations. The Medium Scale Model uses 3D Multipatch data to represent the buildings in downtown Blacksburg.

Points, lines, and polygons can all be represented in the form of shapefiles, which can be stored outside of a geodatabase. The RF coverage estimation data in the statewide broadband map is a polygon converted into a shapefile.

Geovisualization

ArcGIS has numerous ways to visualize data, from a 2-dimensional view in programs like ArcMap to an interactive 3-dimensional view in ArcScene. These visualization tools will not be elaborated on, but they are invaluable debugging tools. For example, in Figure 3.7, we can see that there was a problem with our building database that was making the buildings too thin in 3D.

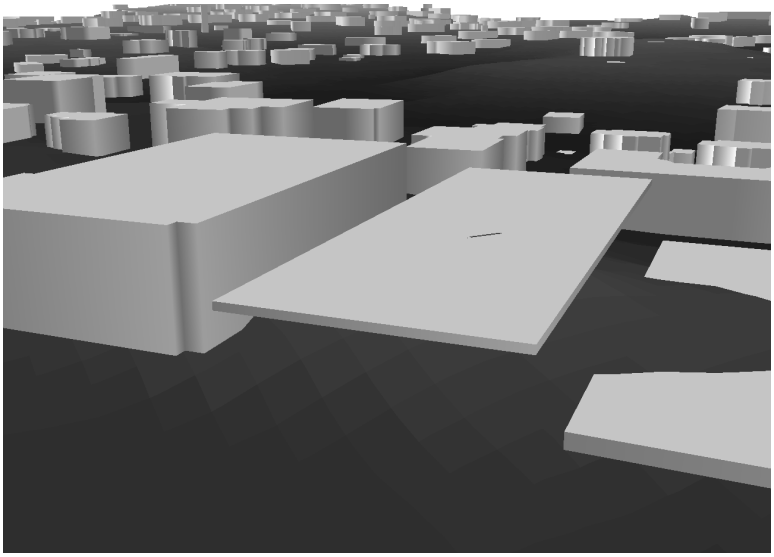

Figure 3.7: Example of Multipatch Data with Incorrect Height Parameter and Thin Geometry. In this graphic from ArcScene's 3D visualization of Building Multipatch data in Blacksburg, it can be see than one of the building's height parameters was incorrectly extracted, resulting in an unrealistically thin building.

Geoprocessing

Geoprocessing is where ArcGIS thrives, with a wide variety of tools and means of programming. As mentioned before, ArcGIS allows for scripting in Visual Basic. ArcGIS also has a built-in programming system called ModelBuilder, as well as the extension into Python called arcpy. All three pull tools from the ArcToolbox to create, change, or use geographic data. Visual Basic was not used in the development of the models, but ModelBuilder and arcpy were used extensively.

ModelBuilder

ModelBuilder is less of a programming languange and more of a programming flowchart. The scripts created are displayed as a flowchart of inputs, tools, and outputs which help illustrate the logical flow of the algorithm. Inputs to the script are represented by blue ovals, yellow rectangles are functions, and the output of every function is a green oval. Figure 3.8 is a quick script that takes a raster input and clips it down to a smaller size.

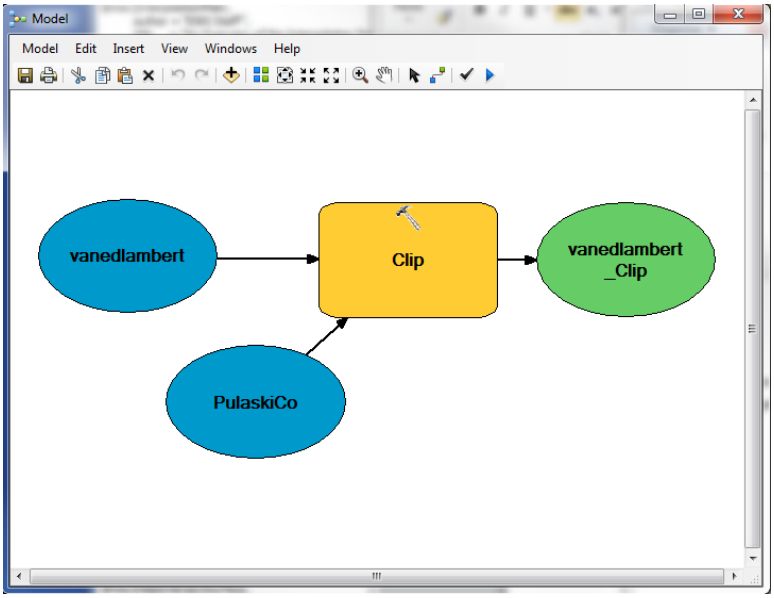

Figure 3.8: Example ModelBuilder Window with Vanedlambert Raster being Clipped by PulaskiCo Polygon

Arcpy

Arcpy is an ArcGIS package that can be used directly within Python scripts for easy coding that is more computationally efficient than ModelBuilder [40]. ArcGIS employs a tool that can automatically convert a ModelBuilder flowchart into a Python script or a Visual Basic script. Within a Python script, it is much easier to carry out calculations that are required for modeling RF propagation. Once a Python script is written for a tool, one simply adds a Python script tool to an ArcGIS toolbox and links the Python script to the Python tool. Then, the Python tool can be run within ArcGIS.

ArcGIS is a powerful geoprocessing software package that can be used for a plethora of tools and calculations. ArcGIS also offers the ability to convert a ModelBuilder script into a Python or Visual Basic script. This feature allows for a visual representation of the script's flow in ModelBuilder to then be converted into a more efficient form in Python.

Conclusion

ArcGIS is a versatile software package that is designed for working with geographic software. For this thesis, the challenge is to model RF propagation analysis in a program that is not designed for electrical engineering. RF propagation analysis lends itself to ArcGIS due to ArcGIS's ability to store and perform calculations on complex terrain data. ArcGIS also contains building data that can be used to aid indoor positioning experiments, as outlined in Chapter 6. The Large Scale Model in Chapter 4 and the Medium Scale Model in Chapter 5 model RF propagation within ArcGIS in acceptable computation time.

Chapter 4

Large Scale RF Coverage Model

Though there has been a push toward smaller cells, there is still a demand for larger broadband cells, especially in rural areas that are currently lacking coverage. These areas are generally underrepresented due to the relatively sparse customer base in which service may not be commercially viable. This is understandable from a business perspective, but as we push to provide coverage everywhere for emergency purposes, this is an obstacle we must overcome. This chapter will describe our efforts to create the Large Scale RF Model. An example RF estimate is shown in Figure 4.1.

In an effort to cover the entire state, the state of Virginia has assembled the Virginia Broadband Map to collect coverage information from various WISPs [8]. Biannually, data is collected and added to the map so that consumers can view the services available in their area and increase the incentive of service providers to provide coverage in that area. In addition to the broadband map, the Federal Communications Commission (FCC) has databases containing currently existing vertical assets and towers. The FCC also supports the Broadband Dead Zone Registry in which households have the opportunity to establish when a home is within a dead zone, or an area is without coverage [41]. This data is not useful for the purposes of this thesis, as many dead zone complaints do not reflect actual dead zones or were filed by customers who are disappointed with available service providers.

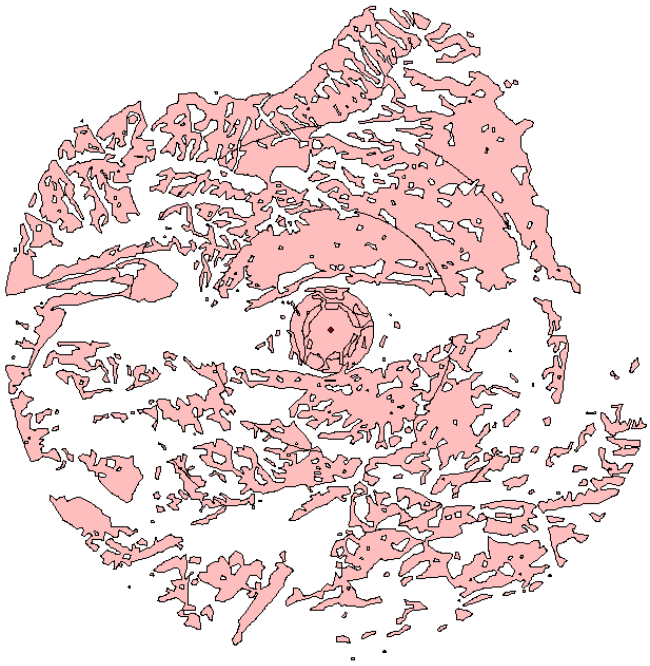

Figure 4.1: Illustration of Large Scale RF Model Output

These efforts help provide wireless broadband coverage to the entirety of Virginia.

A model that can generate coverage estimates from 500 MHz to 5 GHz is needed. The Virginia Broadband Map requires that the coverage estimates be in a shapefile format, commonly used within ArcGIS. The challenge is to find a computationally efficient means of estimating RF coverage using ArcGIS tools designed for use in geospatial applications. The model will also need to run a coverage estimate for a tower in less than one minute in order to be a useful webtool.

Currently existing models were considered first. The Irregular Terrain Model (ITM) was examined for its use of geographical data and its consideration of diffraction and other climate parameters. This model was quickly eliminated due to large computational times of over thirty seconds to run the initial parameter calculations within ArcGIS. The Okumura-Hata model was also considered, but eliminated due to the circle coverage estimate that is an

unacceptable shape for the Statewide Broadband Map. Since most existing models are too computationally intensive to be used in a tool designed for web use, developing a new model that is as simple as possible and yet considers site specific geographic conditions is most desired.

4.1 Approach

Two of the priorities for the model, other than accuracy, were ease of use and fast run time. Since this model is to be turned into a webtool to be used for planning, it needed to be able to provide a result quickly, therefore only the simplest approaches could be considered.

Algorithm

The model is based on Friis' free space path loss equation. In a very generalized sense, RF propagation can be predicted using Friis' free space path loss equation and changing the path loss exponent depending on whether the path is either line-of-sight (LOS) or non-line-of-sight (NLOS). In the Friis free space path loss equation, the path loss exponent determines the rate at which the signal decays. The path loss is measured at a reference distance, d_0, resulting in a reference path loss, L_0. The reference distance, d_0 was chosen to be 100m based on a field test experiment conducted in Europe [42]. The reference path loss is added to the total path loss, L_p in Equation 4.1. Figure 4.2 describes the distances the Friis' path loss equation takes into account the signal's wavelength, λ, the distance between the transmitter and receiver, d, a reference distance, d_0, and the path loss exponent, n:

$$\begin{aligned} L_p[dB] &= (10 * n) * \log_{10}\left(\frac{d}{d_0}\right) + L_0 \\ L_0[dB] &= 20 * \log_{10}\left(\frac{4 * \pi * d_0}{\lambda}\right) \end{aligned} \tag{4.1}$$

In free space, $n = 2$, and in cities, n can range from 3 to 5. For this model, we use a path loss exponent of 2.2 for LOS connections (taking into account small losses from the signal

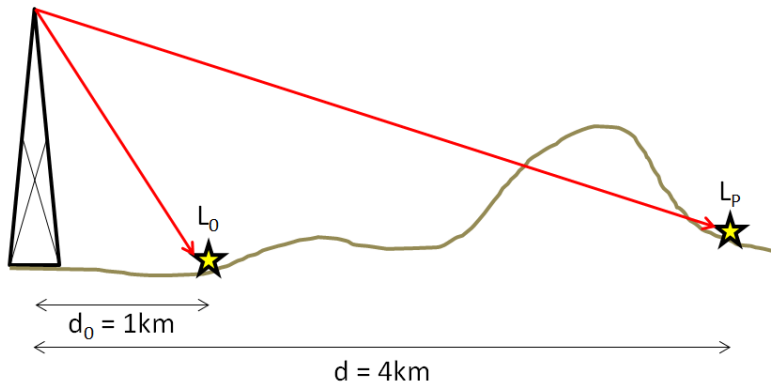

Figure 4.2: Illustration of Friis Free Space Path Loss Equation. Figure by author, 2014.

being non-ideal free space), and 4.2 for NLOS connections. Originally, the Large Scale RF Model used path loss exponents of 2 for LOS (free space), and 4 for NLOS (compromise between 3 and 5), but the values were changed to 2.2 and 4.2 when the resulting coverage estimates matched Radio Mobile more closely with the new values.

This model determines coverage by calculating the power in each cell and then comparing it to a minimum received power threshold. The minimum received power threshold represents the minimum power needed in order to successfully receive the signal at the data rate required. The minimum threshold can be estimated as follows:

$$P_r^{req}[dBm] = \left(\frac{E_b}{N_0}\right)_{req} + 10 * \log_{10}(R_b) + N_0 - G_m \tag{4.2}$$

where $\left(\frac{E_b}{N_0}\right)_{req}$ is the energy per bit to noise power spectral density ratio, or the required signal to noise ratio per bit, R_b is the bit rate, N_0 is the noise power, and G_m is miscellaneous additional gain (i.e. coding or spreading gain). For this model, the noise power is estimated to be $N_0 = k + 10 * log(T) + NF$ [dB] ≈ -195.2 dBW/Hz (assuming an average noise figure $(NF) = 6$ dB, $k = -228.6$ dBW/K/Hz and $T = 293$ K (room temperature)). Once the minimum threshold has been calculated, 30 dB is added to convert the threshold from dBW to dBm; because the transmission power is measured in dBm, the received threshold power must be in dBm in order to get accurate results. If any raster cell's power value is greater than the threshold, the cell has coverage.

Incorporation into ArcGIS

When it comes to modeling RF propagation in ArcGIS, the most difficult part was adapting tools designed for geospatial analysis into a cohesive model that can estimate coverage. ArcGIS has a few tools that can be adapted to model RF propagation, the most notable being the Viewshed algorithm. The Viewshed tool takes a raster input of terrain data and a feature class containing observer point data and returns a raster [43]. The returned raster represents the area with each raster cell representing the number of observers that can see the cell. For example, if there were two observer points being considered, cells that neither tower could see would contain a '0,' cells that can be seen by one tower would contain a '1,' and cells that can be seen by both towers would contain a '2.' However, given only one tower as input, the tool returns a Boolean raster containing LOS data, with ones representing cells with LOS paths to the observer point, and zeros representing NLOS paths [44]. Figure 4.3 shows the raster result of the Viewshed tool with one tower.

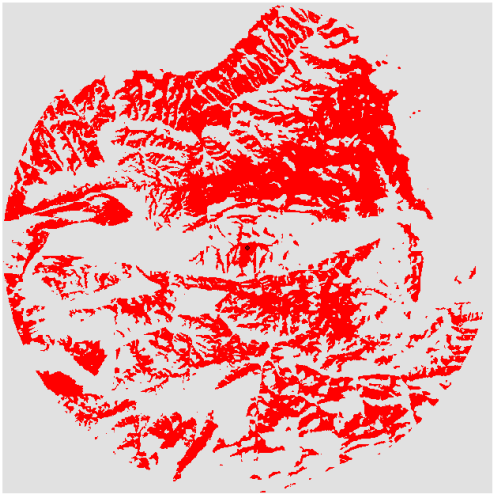

Figure 4.3: Viewshed Tool Output with One Tower. The red represents LOS and the grey represents NLOS.

The Viewshed tool can be further customized by adding fields to the observer point feature

class. Adding fields such as OFFSETA and OFFSETB allows you to customize the transmitter antenna/tower height and receiver antenna/tower height, respectively. The azimuth of the antenna can be changed by adding two new fields, AZIMUTH1 and AZIMUTH2, and formulate them to represent the starting and ending angles, respectively. These fields are added directly to the observer point feature class before the Viewshed algorithm is run [44]. Figure 4.4 shows the Viewshed Algorithm's parameters, and Figure 4.5 displays an Attribute Table within ArcGIS with the Viewshed parameters visible [44].

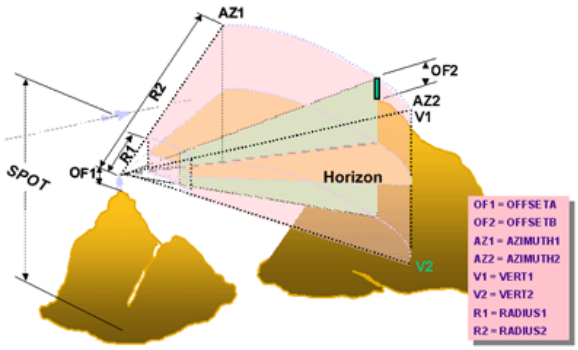

Figure 4.4: Viewshed Tool Parameters Displayed. The OFFSET parameters affect the height of the transmitter and receiver. The AZIMUTH parameters affect the horizontal viewing angle, and the VERT parameters affect the viewing angle above and below the horizon. The RADIUS parameters effect when the analysis begins and ends with respect to the transmitter.

The model runs using a python script, in which the user places a tower with a click of their mouse, sets the desired parameters, and chooses an output type. The script runs for one tower at a time, thus generating a Boolean Viewshed raster for each tower made up of only zeros and ones. The algorithm takes into account several inputs in addition to those listed above. A list of all of the inputs is provided below:

- `'TransPower_dBm'` – Transmission power in dBm
- `'TransGain_dB'` – Transmission antenna gain in dBi

0

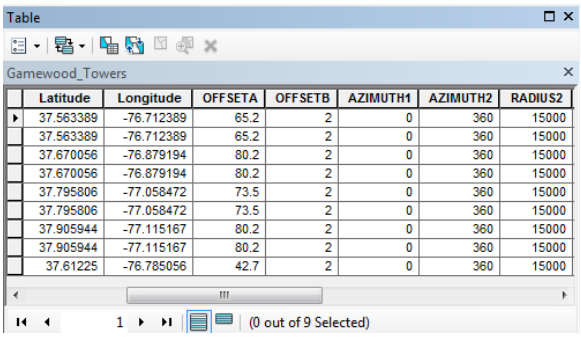

Latitude	Longitude	OFFSETA	OFFSETB	AZIMUTH1	AZIMUTH2	RADIUS2
37.563389	-76.712389	65.2	2	0	360	15000
37.563389	-76.712389	65.2	2	0	360	15000
37.670056	-76.879194	80.2	2	0	360	15000
37.670056	-76.879194	80.2	2	0	360	15000
37.795806	-77.058472	73.5	2	0	360	15000
37.795806	-77.058472	73.5	2	0	360	15000
37.905944	-77.115167	80.2	2	0	360	15000
37.905944	-77.115167	80.2	2	0	360	15000
37.61225	-76.785056	42.7	2	0	360	15000

Figure 4.5: Example Attribute Table with OFFSETA, OFFSETB, and other Viewshed Tool Parameters shown

- `'RecvGain_dB'` – Receiver gain in dBi
- `'Freq_MHz'` – Center Frequency in MHz
- `'Min_Power'` – Minimum required power at the receiver in dBm
- `'Point'` – Tower Feature Set used to get Latitude and Longitude
- `'Antenna_AGL'` – Antenna height above ground level in meters
- `'Receiver_Height'` – Receiver height above ground level in meters
- `'Max_Distance_m'` – Maximum distance considered in meters
- `'Save_Name'` – Name of the final coverage estimate, String
- `'scratch_gdb'` – Geodatabase in which you would like the calculations to be carried out and the final estimate to be located
- `'OutputType'` – Type of output, input as text. Use of the three following inputs:
  - ➢ 'Raster' – will output a raster coverage estimate containing estimated received power in dB
  - ➢ 'Percentages' – will output a polygon containing the coverage estimate divided into an estimate of likelihood of coverage
  - ➢ 'Polygon' – will output a Boolean polygon for the coverage estimate.

Due to the significance of LOS connections on coverage, the Viewshed tool is the backbone

of the large cell model. For this reason, the summarized formula for path loss is:

$$\begin{aligned} P_R[dBm] &= EIRP - (10 * (4.2 - 2 * Viewshed)) * \log_{10}\left(\frac{d}{d_0}\right) - L_0 \\ L_0[dB] &= 20 * \log_{10}\left(\frac{4 * \pi * d_0}{\lambda}\right) \end{aligned} \tag{4.3}$$

where *Viewshed* is the cell value of the Viewshed algorithm and (a 1 or 0 representing LOS or NLOS respectively), *EIRP* is the effective isotropic radiated power (transmitter power, transmitter gain, and receiver gain) in dB, d is the distance between the transmitter and receiver, d_0 is the reference distance of 100m, and λ is the wavelength of the signal [42]. The height of the transmitter and receiver are accounted for in the Viewshed algorithm, as it calculates whether or not there is a LOS connection between the transmitter and receiver at each cell.

Pseudocode

All of the operations of the Large Scale RF Model are performed within a python script calling ArcGIS tools. The script performs the necessary calculations to estimate the RF coverage. There are also several crucial calculations and operations that the script performs to format the resulting estimate properly. An overview of the script's operations is described below:

1. Pulls information from the script's inputs and adds them to the tower's attribute table by using the Add Field and Calculate Field tools.
   (a) This is where the antenna's height is put into the 'OFFSETA' field required for the Viewshed tool, etc.
2. Projects the input tower into a projection known as NAD 1983 Lambert Conformal Conic Meters
   (a) This projection matches that of the digital terrain model (DTM) of the state of Virginia being used by the Viewshed tool. This operation is also essential to

change the default unit of all calculations performed on the tower to match the DTM's default unit of meters.

3. Creates a circular polygon buffer around the tower using the `'Max_Distance_m'` field within the Buffer tool
   (a) This buffer is used to limit the size of the rasters being calculated and thus reduce runtime. This is done by using the buffer as an 'extent' while a tool is being run.
4. Calculates the Euclidean distance from the tower in meters using the buffer as an extent. This operation results in a raster. The Euclidean distance is in meters, and will be used to calculate the distance based path loss at each cell.
5. Copies the DTM using the buffer as an extent
   (a) If the DTM is not reduced in size, then the Viewshed analysis will be performed on the entire DTM of Virginia. The DTM is used in the Viewshed tool to determine whether or not a geographic object is blocking a LOS connection between the transmitter and receiver at the receiver cell.
6. Performs a Viewshed analysis on the copied DTM. This will result in a Boolean raster similar to the raster in Figure 4.3. The raster is Boolean because only one observer is present (the transmitter), so the Viewshed raster cell will be a '1' if seen by the transmitter, and a '0' otherwise.
7. Performs calculations to determine coverage based on Equation 4.1 using a series of arcpy calculations.
   (a) Formula 4.1 takes into account the Viewshed Boolean output in the path loss exponent (the path loss exponent is 2.2 for LOS, and 4.2 for NLOS).
   (b) Within the python script, the value within the log expression for L_0 are as follows:

$$L_0[dB] = \log_{10}\left(\frac{4 * \pi * d_0 * f}{c}\right)$$

   Where f is the frequency in MHz and c is the speed of light (3 x 10^8 m/s) divided by 1000000 (cancels with frequency to convert from Hz to MHz). The constant

numbers are then multiplied together so that we get the final expression:

$$L_0[dB] = \log_{10}(0.041888 * d_0 * f)$$

(c) The received power is calculated as:

$$P_R[dBm] = EIRP - (10 * (4.2 - 2 * Viewshed)) * \log_{10}\left(\frac{d}{d_0}\right) - L_0 \quad (4.4)$$

8. Computes coverage by comparing the calculated received power, P_R, to the minimum power threshold. If the received power at a raster cell is above the threshold, then the cell becomes a Boolean '1' representing a covered cell. If the received power is below the threshold, then the corresponding coverage raster cell will be a '0' representing a lack of coverage.
9. Procedures diverge depending on desired output format given as an input.

Output Types

As mentioned when discussing the inputs of the algorithm, there are three possible output types: Raster, Polygon, and Percentages. These three output types are shown in Figure 4.6. The Raster output will be reclassified into a Boolean raster that represents the coverage estimate. This output is useful if any further calculations must be performed on the coverage model in its raster form, and this output has been used in an optimization study designed to determine the best locations to place antennas.

The Polygon output produces a Boolean coverage polygon to be used in the Statewide Broadband map [8]. Coverage estimates must be in the polygon format to be submitted, containing additional information about the WISP as well as data rates. Polygons can also be merged with other polygons to represent a comprehensive coverage map of a WISP's total coverage.

The final output type is called 'Percentages' and takes the Polygon output one step further. Based on log normal shadowing, which is applicable to the Friis free space path

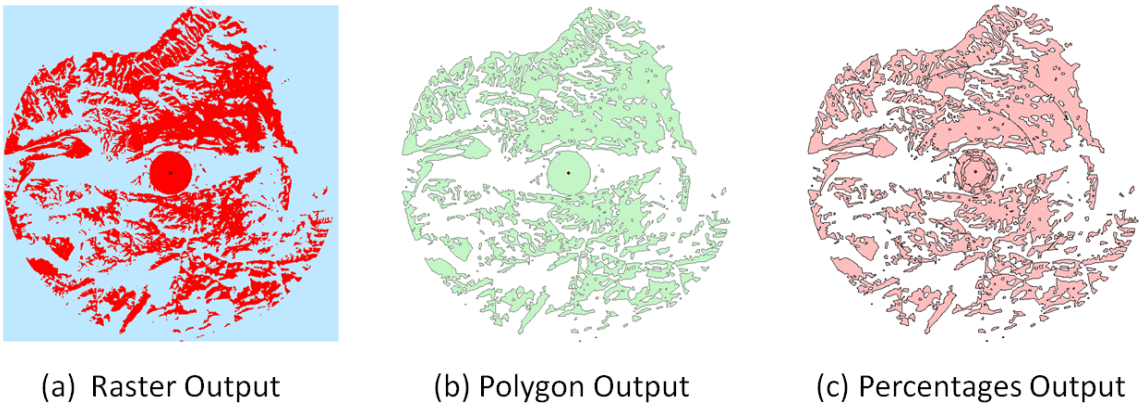

Figure 4.6: Large Scale RF Model Outputs: (a) Raster, (b) Polygon, and (c) Percentages

loss equation, the Percentages output assumes Gaussian noise and calculates probability of coverage based on three fade margins. The coverage probability at the cell edge where the minimum required power threshold is 50% and the coverage probability over the rest of the cell is approximately 77%. However, we can set multiple thresholds corresponding to increases in coverage probability and can represent them in a polygon output. These thresholds are set by increasing the margin over the minimum received (RX) power level in dB. Figure 4.7 demonstrates how a fade margin restricts the total coverage area.

The percent likelihood of coverage at the cell boundary is calculated assuming that power is a Gaussian random variable, X, with mean α and standard deviation σ. In the following equation, b is the value for received power that is some dB margin value above the mean, which is also the minimum power threshold:

$$P(X > b) = Q\left(\frac{b-\alpha}{\sigma}\right) \tag{4.5}$$

where the Q function is defined as:

$$Q(z) = \frac{1}{\sqrt{2\pi}} \int_{z}^{+\infty} \exp\left(-\frac{x^2}{2}\right) dx. \tag{4.6}$$

Once the percent likelihood of coverage is calculated at the cell edge, the overall probability within that cell is determined using Figure 3.18 in Theodore Rappaport's *Wireless*

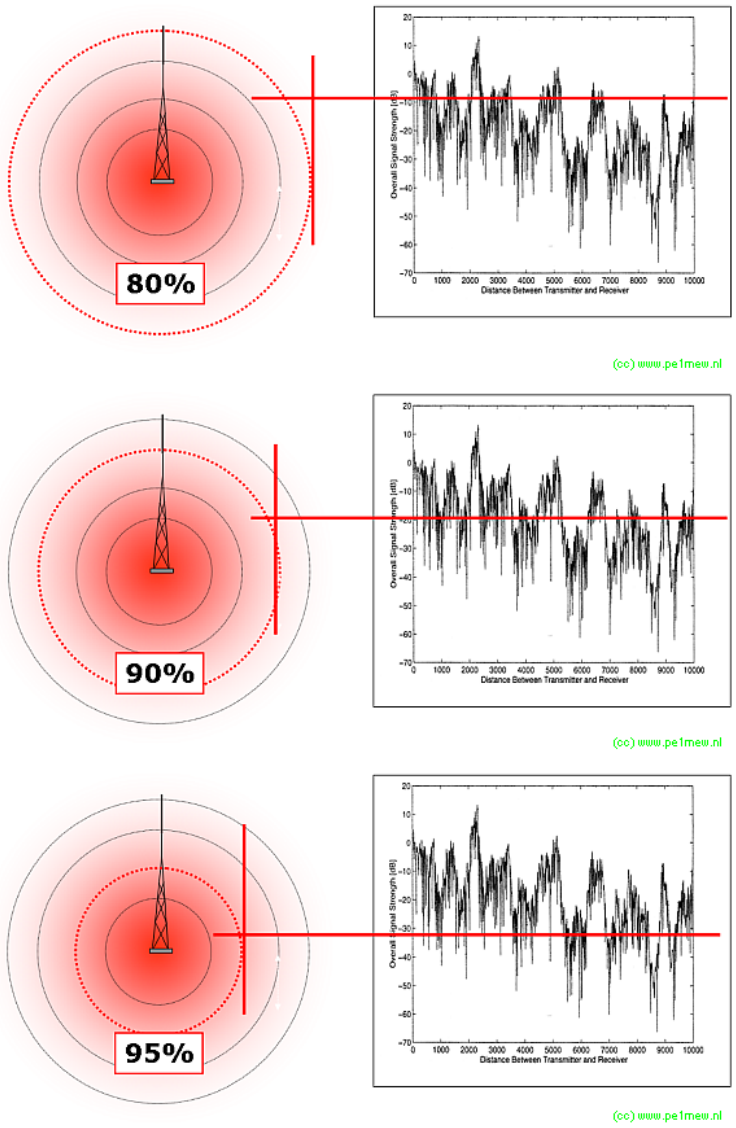

Figure 4.7: Demonstration of How an Increase in a Fade Margin will Reduce the Covered Area at 80%, 90%, and 95%. The fade margin moves the threshold for the overall signal strength (in the graphs on the right) down so that a larger percentage of the signal is above this threshold. PE1MEW. Radio Coverage Probability. Web, Mar 2014. Used under fair use, 2014.

Communications: Principles and Practice book. Using the standard deviation, the path loss exponent of the signal, and the percent likelihood at the cell edge, the overall percent

likelihood of coverage within the cell is found using Figure 4.8 from Dr. Rappaport's book. The finalized coverage probabilities are described in Table 4.1 [4][45].

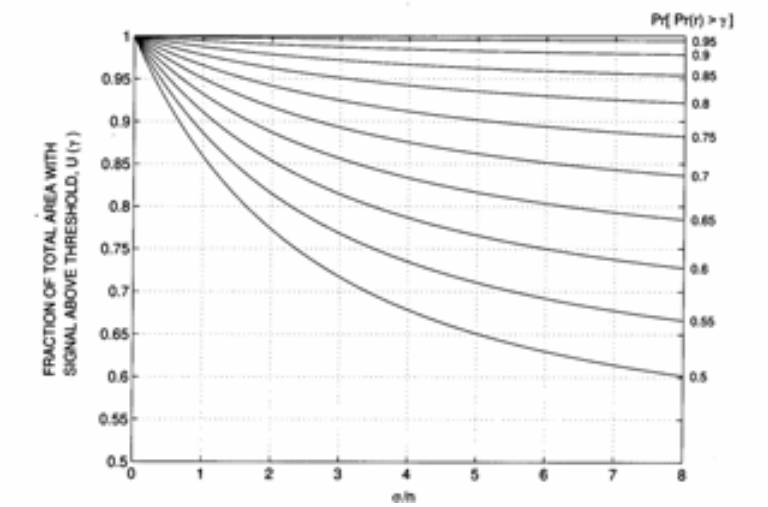

Figure 4.8: Curves relating fraction of total area with signal above threshold as a function of probability of signal above threshold on the cell boundary. Rappaport, T. S. Wireless Communications: Principles and Practice. Prentice Hall, 2 edition, January 2002. Used under fair use, 2014.

The Percentages output returns 3 polygons representing an estimate of the coverage percent likelihood at 77%, 95%, and 99% likelihood, on average. This output is meant to be more demonstrative than the Boolean Raster and Polygon outputs and is based on the Radio Mobile Program Operating Guide's section on fade margins [18]. Fade margins are additional decibel thresholds above the minimum received power threshold that represent an increase in the percent likelihood of coverage. This output will result in three polygons that demonstrate varying quality of service, such as 'Fair,' 'Good,' and 'Best.'

The script reclassifies the raster into three categories,each representing a percent likelihood of coverage based on log normal distributions:

- For 77% likelihood of coverage over the cell, the received power must be above the minimum power threshold.

Table 4.1: RF Coverage Probability Estimate [45][4]

Decibel Margin (dB)	Probability of Coverage at Outer-Edge (%)	Probability of Coverage over Entire Polygon (%)
0	50	77
5	73.4	87.5
7	81	95
9	87	97
12	93.3	99

- for 96% likelihood of coverage over the cell, the received power must be above the minimum power threshold + 7 dB.
- for 99% likelihood of coverage, the received power must be above the minimum power threshold + 12 dB.

After reclassification, the model creates a polygon output and smooths it, resulting in a coverage estimate similar to the estimate in Figure 4.6. This output is useful for graphically representing an empirical interpretation of the coverage estimate.

The user can select which output best suits their computational needs. When it comes to comparing the results of this model and the results of an established model, like Radio Mobile, the Raster output was selected.

4.2 Comparison to Radio Mobile

In an attempt to validate the Large Scale RF Model, a comparison was performed with Radio Mobile. As mentioned in Chapter 2, Radio Mobile is a freeware program based on the Irregular Terrain Model and is generally considered a reasonable RF estimate. Radio Mobile can output its coverage estimate into a raster format, so this is the format considered for

analysis. Two example rasters are shown in Figure 4.9 of the comparison of the Large Scale RF Model and the Radio Mobile output for the same tower. The images in Figure 4.9 may seem horizontally stretched, but this is due to the projection of the rasters in ArcGIS being stretched in the display itself and will not interfere with the correlation analysis.

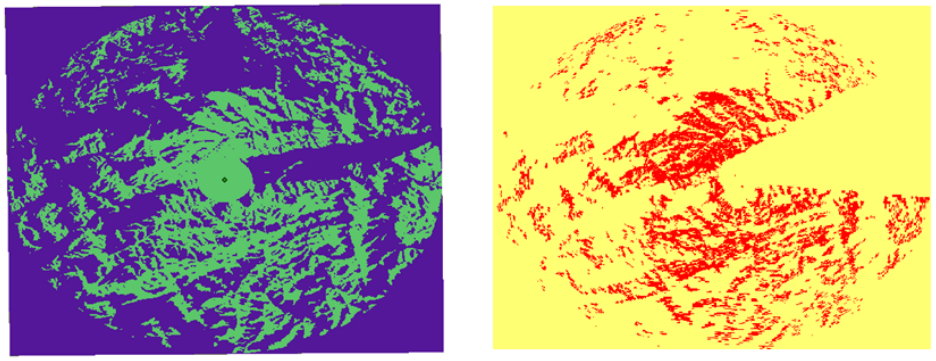

(a) Coverage Using Large Scale RF Model (b) Coverage Using Radio Mobile

Figure 4.9: Large Scale RF Model Output and Radio Mobile Output for Correlation Analysis. The Large Scale RF Model on the left contains a circle of coverage about 0.5 km in diameter. This is due to the signal decaying at two consistant rates, and the border of this circle is when the NLOS cells decay below the minimum power threshold value and are no longer considered covered. The Radio Mobile output does not have this circular coverage in the center. The antennas in Radio Mobile can also be blocked if not placed at the correct latitude and longitude, resulting in an angular chunk appearing to be without coverage

ArcGIS has a raster tool called Band Collection Statistics that can be used to compute the Covariance and the Correlation of two rasters [46]. The covariance between raster 1 and raster 2 is:

$$Cov_{ij} = \frac{\sum_{k=0}^{N}(Z_{ik} - \mu_i)(Z_{jk} - \mu_j)}{N - 1} \tag{4.7}$$

where Z_{ij} is the value of a cell, i and j are the layers of a stack of rasters, μ is the mean of a layer, N is the number of cells, and k denotes a particular cell. The covariance matrix

Table 4.2: Large Scale RF Model and Radio Mobile Correlation Results

Experiment	Correlation
Location 1, 900 MHz	0.53793
Location 1, 1800 MHz	0.36751
Location 1, 2400 MHz	0.30605
Location 2, 900 MHz	0.67513
Location 2, 1800 MHz	0.54184
Location 2, 2400 MHz	0.51404

represents the intersection of the appropriate row and column of the rasters and their variance value, in the rasters' units squared.

The correlation matrix is dependent on the covariance matrix:

$$Corr_{ij} = \frac{Cov_{ij}}{\delta_i \delta_j} \tag{4.8}$$

where δ_i and δ_j are the standard deviations of rasters i and j respectively. The correlation ranges from +1 to -1, and a positive correlation indicates a direct relationship between the two layers. A negative correlation indicates an inverse relationship, and a correlation of zero corresponds to the two layers being independent [46].

Correlation analysis was performed for 3 frequencies (900, 1800, and 2400 MHz) at two tower locations (chosen to be local maxima). Figure 4.9 shows the corresponding rasters at location 2 at a frequency of 900 MHz. Table 4.2 displays the correlation values that result for each experiment. In each case, the Radio Mobile estimate was compared to the Large Scale RF Model estimate at the same frequency and location only.

As can be seen in Table 4.2, the correlation is positive for all six scenarios, indicating a direct relationship. The agreement between the two models is good. However, the correlation decreases with frequency, meaning that the results of the Large Scale RF Model are less correlated with the Radio Mobile result as frequency increases. The correlation results at

Location 2 are stronger than those at Location 1, but this could be due to a misalignment between the rasters. Since the terrain data used in Radio Mobile is not the same as the terrain data used in the Large Scale RF Model, the estimates can be translated slightly when entered into ArcGIS. For the correlation models and analysis in this chapter, the two models were aligned as closely as possible to one another to get the highest correlation possible.

Further analysis was performed to determine whether the Large Scale Model will produce a 1 when Radio Mobile produces a 1 and vice versa. A table describing the results of this analysis is in Figure 4.10. In this figure, it can be noted that the Large Scale RF Model will produce a 1 when Radio Mobile produces a 1 for 89.3% of cells. However, the Large Scale RF Model produces a 1 when Radio Mobile is 0 for 67.3% of cells.

Comparison of Radio Mobile (RM) Results to Large Scale Model (Mod) Results

		RM-1, Mod -1	RM-1, Mod-0	Mod-1, RM-0	Mod-1,RM-1
Location1	900	91.18%	8.82%	63.22%	36.78%
	1800	88.52%	11.48%	72.60%	27.40%
	2400	84.92%	15.08%	72.38%	27.62%
Location2	900	93.55%	6.45%	59.07%	40.93%
	1800	88.62%	11.38%	66.81%	33.19%
	2400	88.88%	11.12%	69.53%	30.47%
	Avg.	89.28%	10.72%	67.27%	32.73%

Figure 4.10: Large Scale RF Model Output and Radio Mobile Output for Correlation Analysis. The comparison graph's columns represent how often the second boolean value occurs given the first boolean value. For example, the first column represents how often the Large Scale RF Model is a 1 when Radio Mobile is a 1. Similarly, the last column represents how often Radio Mobile returns a 1 when the Large Scale RF Model returns a 1. The last two columns demonstrate that the Large Scale RF Model overestimates coverage due to the model resulting in coverage where Radio Mobile does not report coverage 67.27% of the time. The similarities between Radio Mobile and the Large Scale Model decrease as frequency increases.

The comparison to Radio Mobile demonstrates that the Large Scale RF Model overestimates coverage when Radio Mobile is considered the 'truth.' Radio Mobile's coverage is smaller due to its consideration of variables like climate, refractivity, and permittivity and conductivity of the ground. There is still a positive correlation between Radio Mobile and the Large Scale RF Model, so the Large Scale RF Model is still a reasonable estimate for RF propagation.

4.3 Applications

The Large Scale RF Model has numerous applications. It can be implemented into CGIT's VAIT and can be used to estimate the coverage of the vertical assets stored within VAIT. This would be useful for planning purposes and filling in deadzones. A feature can also be added to allow for new towers to be placed, and the Large Scale Model can then be used to estimate the new tower's propagation.

In a similar scenario, the state of Virginia is aiming to have 100% of the state covered for safety purposes. As a part of the nationwide public health and safety system, emergency vehicles and responders need to be able to communicate with hospitals, police stations, and fire departments from anywhere within the state. The Large Scale Model can be implemented within ArcGIS, where the latest terrain data can be used, to generate the most recent coverage estimate for a tower. ArcGIS can also store population and emergency service demographics to locate problem areas. The Large Scale RF Model can then be used to fill in any gaps.

An optimization study was performed using the currently existing vertical assets within the VAIT. Each tower had a coverage estimate performed, resulting in a Boolean raster output. Each raster was converted into a variable within a Linear Program, and an optimization study was performed to cover the largest amount of area with the fewest vertical assets. It was found that only a handful of the towers within a county were necessary to cover the

possible area within the county. Similar experiments could be performed after generating new towers.

4.4 Conclusion

The Large Scale RF Model can provide a coverage estimate for frequencies between 500 MHz and 5 GHz in a very short amount of time. The Large Scale Model can run a coverage estimate for a tower in as little as 30 seconds on a standard computer. Based on the Friis Free Space Path Loss equation, the Large Scale model is simple, but allows room for the algorithm to be expanded upon. The Large Scale Model was also compared to Radio Mobile, and, though the two results are positively correlated, we only learned that the Large Scale RF Model will provide a reasonable estimate like Radio Mobile.

Chapter 5

Medium Scale RF Coverage Model

As the need to increase capacity in urban areas grows, many wireless service providers are pushing to create smaller cells at higher speeds. These smaller cells are generally less than one kilometer in radius and use frequencies in the WiFi band, such as 2.4 GHz or 5 GHz. The Medium Scale RF Model uses 2.4 GHz frequencies to estimate coverage for a range up to 300 m in radius. In smaller cells, interference is typically the limiting factor. This model was designed to determine the best locations for transmission antennas without considering interference. This model does not consider interference due to limited computational ability of ArcGIS tools. It can be used for planning purposes, however. At the time of this thesis' publishing, the Medium Scale Model will only work in downtown Blacksburg, VA due to limited terrain data availability.

As is mentioned at the end of Chapter 2, a suitable algorithm structure would be:

$$L_{total}[dB] = L_{air} + 14.5 * x_{wall} \tag{5.1}$$

where L_{total} is the total path loss along the segment, L_{air} is the path loss of the segment calculated as if the segment is within air, and x_{wall} is the number of walls the signal has passed through. With the Medium Scale RF Model, this algorithm ArcGIS requires new data types (multipatch and polyline features) and new tools. This model is designed for

planning purposes in determining optimum locations for transmission antennas to provide the largest area of coverage. The Medium Scale RF model does not consider the effects of interference between antennas. This chapter will discuss how the Medium Scale Model works, and modifications to the model after field testing was performed.

5.1 Approach

Similar to the Large Scale RF Model, accuracy and efficient runtime are important coding factors. However, the ArcGIS tools used for the Large Scale RF Model will not calculate the number of buildings or other obstructions a path incurs as it travels from the transmitter to a receiver. For a WiFi range system, a signal's path through a building will cause the signal to attenuate, but there may still be coverage on the other side of the building. The Friis' free space path loss equation, as it is used in the large scale model, only considers two scenarios: LOS and NLOS. In the event of a LOS connection, the signal decays at a slower rate over the entire distance to the destination raster cell. On the other hand, in the event of a NLOS connection, it is assumed that there are obstacles such that the overall attenuation is equal to the attenuation induced by a the higher rate of decay. Therefore, with the Large Scale RF Model algorithm, building data contained within a digital surface model (DSM) raster will simply cause shadows in LOS, and the attenuation through the building will not be considered in any context other than as a NLOS connection. When modeling RF on a 300 m scale, incorporating building data in a manner in which the number of times a signal passes through the building is more important. The entire large scale procedure needed to be altered in order to use different ArcGIS tools and bring new data types in.

The most difficult challenge to considering building data in the algorithm is coming up with a way to determine how many walls a signal passes through. Since a simple propagation model is necessary for computationally efficient run time, a formula based on path loss exponent is chosen to determine the attenuation along a path. As was discovered in Chapter

2, the attenuation experienced when a signal enters a building is approximately 14.5 dB per outer wall.

3D Analyst Toolbox

Within the 3D Analyst toolbox in ArcGIS, there are several tools that can be used to model a signal's path through a building: *Construct Sight Lines*, *Intersect 3D Line with Multipatch*, and *Intersect 3D Line with Surface*. *Construct Sight Lines* takes an observer point feature layer and a target feature layer and constructs a polyline feature class representing the LOS paths between the observer and the targets [47]. The resulting polyline feature can be used in the *Intersect 3D Line with Multipatch* tool to create a new feature class containing the sight lines broken into segments based on their intersections with building multipatch features [48]. Similarly, the *Intersect 3D Line with Surface* tool uses the polyline feature and a DSM raster to create a set of line segments broken up where the sight lines intersected with the surface raster [49]. Figures 5.1, 5.2, and 5.3 illustrate the three tools within ArcScene, an ArcGIS program for viewing geographic data in three dimensions. Figure 5.1 shows the resulting sight lines from the *Construct Sight Lines* tool with the observer at the very center of the lines. Figure 5.2 is a closer view of a sight line that has been broken into segments by intersecting a multipatch building using the *Intersect 3D Line with Multipatch* tool. The points of intersection are marked by the large green circles. Figure 5.3 illustrates an intersection between a sight line and the digital surface model, the result of the *Intersect 3D Line with Surface* tool. The points of intersection with the surface are marked by yellow circles.

Data Types

The three tools above use two new data types: multipatch features and polyline features. Multipatch data and polyline features were covered briefly in Chapter 3, but not much was

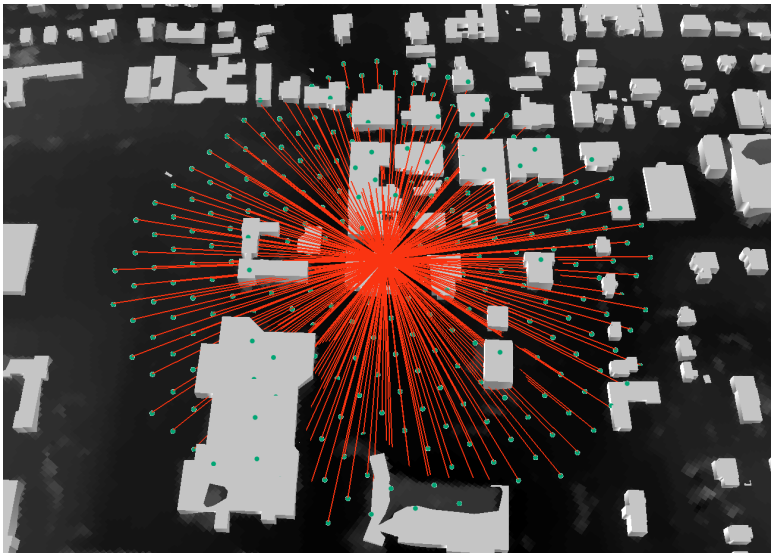

Figure 5.1: *Construct Sight Lines* Tool Output; The Red Lines are the Sight Lines

This graphic shows an example of the output of the *Construct Sight Lines* tool based on a tower on top of Top of the Stairs restaurant in downtown Blacksburg. The large building in the lower left corner is Squires Student Center for perspective.

said about their practical use. Multipatch data is a 3D geometry used to represent the outer surface of features, like buildings or trees [50]. The multipatch data is constructed from planar 3D rings and triangles that are used in combination to model a 3D shell. The multipatch data used in this model was created by taking two-dimensional building data, and converting it to three-dimensional data using a height attribute within the building data. Like other feature class data, multipatch data contains an attribute table that allows for data storage. Each individual building within the feature layer has a row within this table, and columns can store information such as building ID number, size, and building material.

Polyline features are very similar to points and polygons. Lines generally represent shapes that are too narrow to depict as areas, such as roads and streams [39]. Lines can also be used to describe features that have a length but no area, i.e. boundaries. Polyline features can be represented in two- or three-dimensions. In the Medium Scale RF Model, tools from the 3D Analyst toolbox are used, creating line features in three-dimensions. As a feature

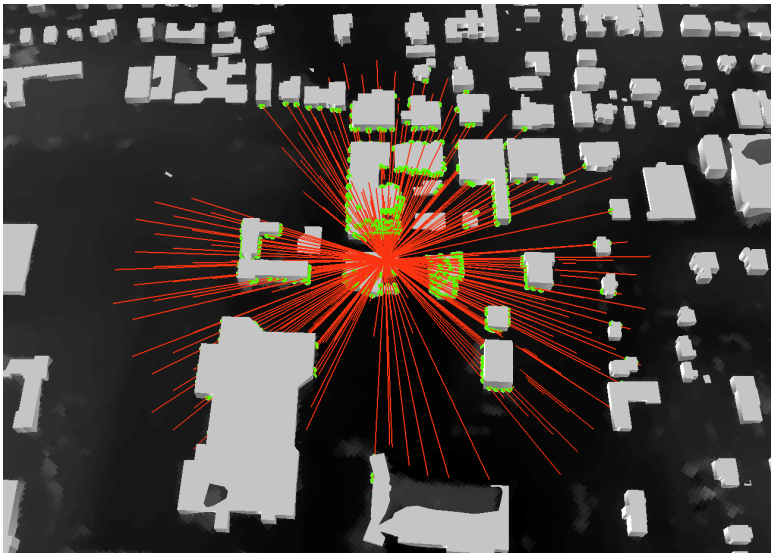

Figure 5.2: *Intersect 3D Line with Multipatch* Tool Output; The Red Lines are the Intersection Lines and the Green Circles are the Points of Intersection. The *Intersect 3D Line with Multipatch* tool is shown above from the same tower on top of Top of the Stairs restaurant. The black 'hills' are the digital surface raster converted to three dimensions.

type dataset similar to points and polygons, line features can also store various data in the attribute table, with each line or line segment occupying one row of the table. Common data included in the attribute table is the line segment's length, object ID, and shape type.

Calculating Path Loss for Intersection with Buildings

Using the above tools and data types, a very simple algorithm was designed. In the algorithm, a location is selected for the observer, or transmitter, and targets are generated around the observer in a grid pattern. Sight lines are created, and an intersection with the multipatch building data is calculated. The Intersection 3D Line with Multipatch operation will only return line segments that intersect with multipatch data. The script iterates through all of the path segments and determines the overall path loss along the total length of the path between observer and target. The path loss is calculated using the attribute table data

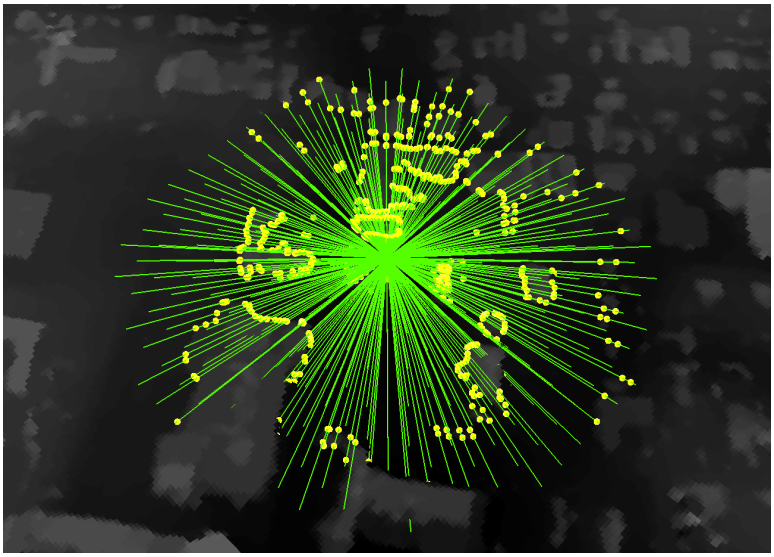

Figure 5.3: *Intersect 3D Line with Surface* Tool Output; The Green Lines are the Intersection Lines and the Yellow Circles are the Points of Intersection. In this graphic, the 3D building multipatch data has been removed so that the digital surface model (black hills) can be seen more clearly. The source of the lines is the top of Top of the Stairs restaurant, and the digital surface data is supposed to represent the terrain an building data in one raster. Due to poor LiDAR data, these buildings are more rounded than they are in actuality.

within the intersection polyline feature. The attribute data contains two columns of note: `'FROM_MP_ID'` and `'TO_MP_ID'`. `'FROM_MP_ID'` represents the ID number of the feature where the line segment begins, and `'TO_MP_ID'` contains the ID number of the feature when the line segment ends. At the observer and target, the ID is always '-1', and each multipatch building has a unique ID that will occupy the corresponding column in the polyline feature table. For all building materials, the decay rate of the signal is assumed to be that of 'air' or $n = 2$. Using these two columns and the attribute column containing the segment's length, the number of walls intersected is calculated as follows:

- If 'from' = -1 and 'to' $\neq$ -1, then the segment is just starting and is assumed to be in 'Air'. A building marker is set to one, signifying that the next segment is starting

within a building. The exterior wall tally is incremented by one.

- If 'from' = 'to' ≠ -1 and the building marker = 1, then the segment is 'within a building' and the building marker is set to zero to signify that the next section will begin in air. The exterior wall tally is incremented by one.
- If 'from' ≠ 'to' ≠ -1, the segment is 'between buildings' and the building marker is set to one since a building is being entered. The exterior wall tally is incremented by one.
- If 'from' ≠ -1 and 'to' = -1, then the segment is ending. The exterior wall tally is incremented by one.
- Note: A scenario in which 'from' = 'to' = 1 is not possible due to the output of the intersecting feature containing only segments in which an intersection with a building occurred.

All of the total path losses for the targets whose segments intersected with a multipatch building are recorded within a separate table called the 'Intersect Table' along with the target's ID number. Their path loss is calculated according to Equation 5.2:

$$\begin{aligned} L_p[dB] &= 2 * 10\log_{10}(d_{total}/d_0) + L_0 + 14.5 * x_{wall} \\ L_0[dB] &= 20 * \log_{10}\left(\frac{4 * \pi * d_0}{\lambda}\right) \end{aligned} \tag{5.2}$$

where x_{wall} is the total number of walls, 14.5 is the attenuation value in dB of a signal passing through a brick wall, and $d_0 = 10$ m [28] [29]. There are, however, some targets who had a LOS connection with the observer. Therefore, after calculating the total path loss along paths that intersected buildings, the script calculates the path loss along all sight lines as LOS connections:

$$\begin{aligned} L_p[dB] &= 2 * 10\log_{10}(d_{total}/d_0) + L_0 \\ L_0[dB] &= 20 * \log_{10}\left(\frac{4 * \pi * d_0}{\lambda}\right) \end{aligned} \tag{5.3}$$

The target point feature class's attribute table is appended with the LOS path loss values. Then, a for-loop is run in which any path loss values form the 'Intersect Table' overwrite the LOS path loss values within the target point feature class's attribute table. This step is

important because the values in the targets' feature class will be used in the interpolation step of the algorithm, in which point data is changed into a heat map of signal strength.

Intersection Analysis with the DSM

The script also performs an intersection analysis for the sight lines with the raster digital surface model, such as the analysis performed in Figure 5.3, but this analysis has not been used in the final calculations due to inadequate digital surface data. As is shown in Figure 5.4, the DSM data is translated from the multipatch data of the same building. It can also be seen that the DSM version of the building is not flat and the edges are rounded. High quality digital surface data obtained through LiDAR is being created, but it was not completed in time to be included in this thesis work. The surface data will include both foliage and building data, and can provide more detail about building shape. A finely detailed DSM can reflect the slanted roofs of buildings that would otherwise have a flat roofed shape in multipatch. Also, the *Intersect 3D Line with Multipatch* tool takes 9.2 times longer to run than the *Intersect 3D Line with Surface* tool. The analysis is present in the script to aid future research as the script will be open source.

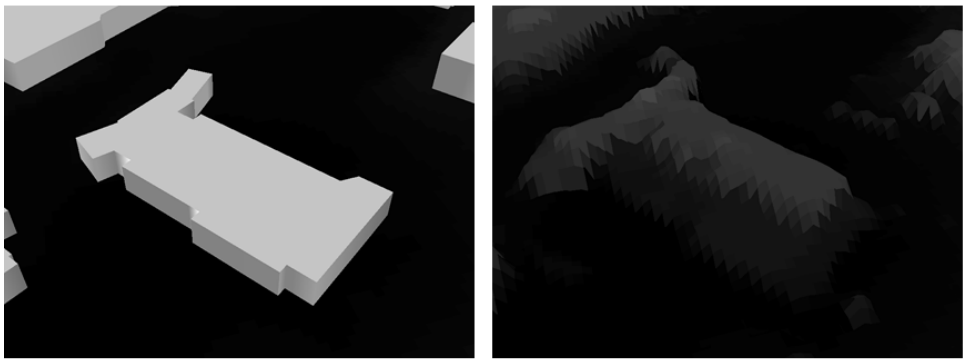

Figure 5.4: Multipatch and DSM Versions of the Same Building

Interpolation

The final step in the algorithm is interpolating the data into a raster containing an RF propagation estimate. ArcGIS's Interpolation toolset contains several tools for interpolating point data into a raster, such as *Natural Neighbor* (finds the closest subset of input samples to a query point and applies weights to them to interpolate a value) and *Kriging* (interpolates assuming that the distance or direction between sample points reflects a spatial correlation) [51][52][53]. The tool chosen for this model is a deterministic interpolation tool known as Inverse Distance Weighting (*IDW*). The *IDW* tool interpolates cell values using a linearly weighted combination of a set of sample points [54]. The tool takes the data from the target points and weighs them as a function of inverse cell distance. Therefore, the variable being mapped decreases in influence with distance from the point location at a rate based on a power parameter input (default is 2) [55]. The resulting raster is a heat map of coverage, and is returned by the script. The script properties contain an ArcGIS Layer file called `'Interpolation.lyr'` that will return the interpolated raster with a specific symbology to visibly show a heat map of coverage. The symbology can be seen in Figure 5.5.

Pseudocode

The medium scale python script has different inputs than the Large Scale RF Model, since the Medium Scale RF Model algorithm does not consider frequency (assumes a wifi frequency range) or EIRP (assumes an EIRP of 28 dBm, which is consistent with WiFi Antennas) [56] [57]. These assumptions are made to make the script easier to use for city planners. However, the Medium Scale RF Model algorithm takes into account several layers of digital geographic data. The inputs for the medium scale model are as follows:

- `'Point_feature_set'` – Point feature set designated by the user that represents the transmitter, or observer
- `'Observer_height'` – Transmission antenna height in feet

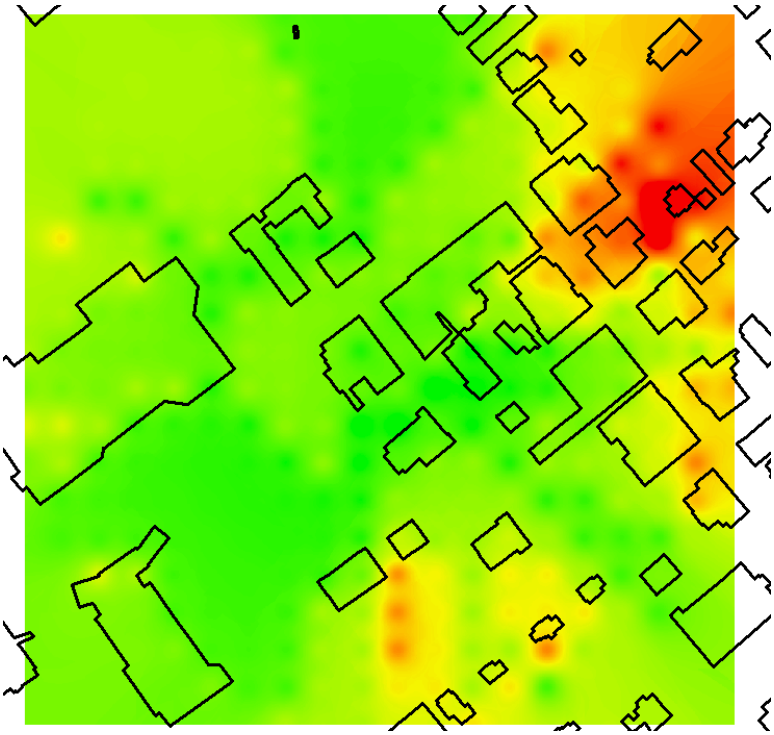

Figure 5.5: Interpolated Result of the Original Medium Scale Algorithm. The green areas show where received signal strength is high, and the red areas indicate where signal strength is lower due to building attenuation.

- `'Target_height'` – Receiver height in feet
- `'Input_multipatch_features'` – Feature layer containing multipatch building data
- `'Input_DSM_raster'` – Raster Layer containing digital surface model (DSM) data
- `'Input_DTM_raster'` – Raster Layer containing digital terrain model (DTM) data
- `'Observed_Radius'` – Maximum distance from the transmitter that is considered

Using the inputs described above, the following steps represent an overview of the Medium Scale RF Model algorithm and script:

1. Reads in the inputs described above, saving them to a temporary location within a variable. A copy of the input observer data is made so that it is saved to a permanent location within the scratch geodatabase for debugging.

2. Enters the user defined 'observer height' into the attribute table of the input observer point feature class.
3. Computes the elevation of the observer point by using the *ExtractMultiValuesToPoints* function, which extracts data from a raster to a point depending on the location of the point on the raster. The operation adds two columns of data to the input observer point feature class: DTMval and DSMval. DTMval and DSMval will contain data extracted directly from the input DTM and DSM. These values are to be used to place the antenna above the DSM by adding the DSMval to the input's 'observer height'
4. Creates a new feature, pointFCobs2925, and calculates the true observer height, AbsElev, by adding together DSMval and the user defined observer height.
5. Removes all additional points from the observer feature class, pointFCobs2925 so that there is only one observer.
6. Creates targets in a grid pattern using the *Fishnet* tool from the Data Management toolbox. The gridded point features that the *Fishnet* tool outputs will be the targets used to create signal paths between observer and target. A grid formation of the targets will provide consistent estimate results.
   (a) The *Fishnet* tool creates a grid of rectangular cells of either a polyline or polygon format. A secondary set of points is created to label the rectangular cells, and this set of points can be used separately as a feature class. The set of points will be used as the targets.
   (b) The script first extracts the latitude and longitude data of the observer point. The user defined observed radius is subtracted from the latitude and longitude to create a point of origin in the bottom left corner of the area of interest. An additional point is created 100 ft. above this point to be used to orient the fishnet by calibrating the y-axis.
   (c) A circular *Buffer* polygon is created around the observer point to restrict the fishnet creation to the extent of the buffer.
   (d) The *Fishnet* is created starting at the origin point and expanding within the

area of the first quadrant. The area between targets is the observed radius value divided by ten, and the *Fishnet* tool creates square polygons within the extent of the buffer. Two features are created: a grid of square polygons and a point feature class where a point is in the center of each square polygon.

(e) The point feature class is reduced in size using the *Clip* tool and the circular buffer, further reducing the number of targets and the overall computation time of the script. The resulting point feature class is saved to a scratchwork geodatabase as a point feature class named pointFCtar2925. The final target feature class can be seen in Figure 5.6, where the targets are green circles, and the observer is a red square.

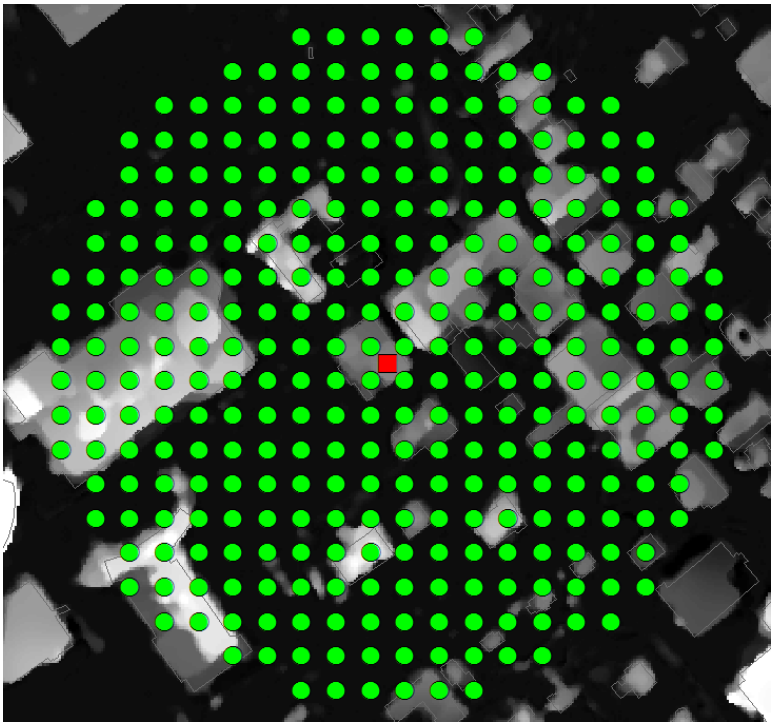

Figure 5.6: Grid Formation of Targets (Green Circles) around the Observer (Red Square)

7. Updates the new target point feature class with the target height specified by the user. The target height will be used in the *Construct Sight Lines* tool.
8. Extracts the DTM and DSM values to the targets in a manner similar to the method

described in Step 6. Similar to Step 6, this will be added to the user defined Target Height.

9. Calculates absolute elevation of each target by adding the DTMval to the user defined target height. The DTM value is used for the targets to simulate a user on the ground.
10. Performs *Construct Sight Lines* operation to create a line feature class containing lines between the observer and targets. This operation creates the feature class called siteline2925, which is used in both of the Intersect tools and is also returned at the end of the script.
11. Performs *Intersect 3D Line with Multipatch* operation, placing the resulting in the feature class labeled intersectFeatFC2925 containing the polyline information. The *Intersect 3D Line with Multipatch* tool also creates a point feature class, with all points representing locations of intersection. The point feature is saved as intersectFeatPtsFC2925 and is returned with intersectFeatFC2925 at the end of the script. Note: This operation is one of the most computationally intensive operations in the script and often takes at least two minutes to run.
12. Calculates the path loss of the intersect line segments as is outlined earlier in the chapter, storing the resulting path loss value in a table called Intersect Table with the target number associated with the path loss. The Intersect Table has data pulled from it to overwrite the LOS path loss data stored in the targets feature class.
13. Updates the intersection point feature class attribute table with path loss information for observation and debugging purposes.
14. Calculates the path loss through air for all targets and updates the target feature class with the LOS path loss. After the LOS data has been added, the intersected building path loss information calculated in Step 12 overwrites the LOS path loss data when a target experienced an intersection with a multipatch building. Therefore, if no NLOS data exists, the LOS path loss data remains, and if NLOS data does exist, it overwrites the LOS data. The data is recorded under a column called TotalLoss, and this is the column of data used in the interpolation step.

15. Performs an *Intersect 3D Line with Surface* operation which can be expanded upon when adequate surface data is available.
16. Interpolates the target point feature class into a raster as described above. The resulting raster, Interpolation, is returned at the end of the script. Figure 5.5 is an example of the final interpolated result.

5.2 Integration of Layers

In the current Medium Scale RF Model, the *Intersect 3D Line with Multipatch* tool allows us to see where a signal's path would intersect with a building. At the time of this thesis' publication, more detailed building data was not available. However, if detailed data were to become available within ArcGIS, such as building material, or floor plans, the polyline feature that results from the intersection with multipatch contains information about which building within the multipatch data is being intersected. The multipatch data, like all feature classes, has a corresponding attribute table, which contains more information about the buildings within the multipatch. This data could contain building materials information which could allow for more specialized building penetration analysis.

The multipatch polyline feature also contains information about a segment's length, which would allow for within building analysis. For example, if we were to use a certain rate of decay while the path is indoors, the total path loss of a segment that barely enters a building versus a segment that spends a significant portion of its length indoors would be vastly different. In Figure 5.7, this idea is illustrated by a simple example in which a building's penetration loss would be affected based on length of the path through a building. With the current model, the building penetration loss would be the same for star 1 and star 2, but if the penetration loss was distance based, the penetration loss for star 1 would be far worse than the loss for star 2.

In addition to building data, if foliage multipatch data existed, foliage effects on a signal's

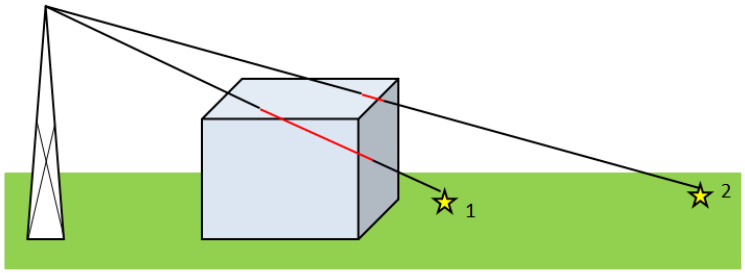

Figure 5.7: Illustration of Building Penetration Distance for Arbitrary Star 1 and Star 2. Photo by author, 2014.

path could also be considered. The *Intersect 3D Line with Multipatch* tool would be run twice: once for the building data and once for the foliage data. There even exists sufficiently detailed foliage data that foliage type could be considered when calculating foliage penetration loss. There is a lot of room for expansion within the Medium Scale RF Model.

5.3 Field Test Comparison

In Blacksburg, there are local contractors who are looking to use this model to plan ideal locations to place new WiFi routers. One such contractor is Bob Summers, of TechPad Blacksburg WiFi Network, who is setting up a free high-speed WiFi system in downtown Blacksburg. He has set up three WiFi antennas on top of restaurants in Blacksburg so far: PK's, Sharkey's and Top of The Stairs (or TotS for short). TotS is located next to a parking lot, and offers a diverse experimental location for propagation through a building as well as in the air. We chose this location to perform our experiment. Figure 5.8 shows the eleven locations where data was collected in experiment 1. Figure 5.9 shows the ten locations where data was collected in experiment 2. Figure 5.10 shows the data collection points for experiment 3. Matej Muza developed a small Android application for CGIT called Wifi Scanner that will observe the signal strength reading for all available wireless internet access points and record the results. Figure 5.11 shows the application window, observing

the Virginia Tech drillfield.

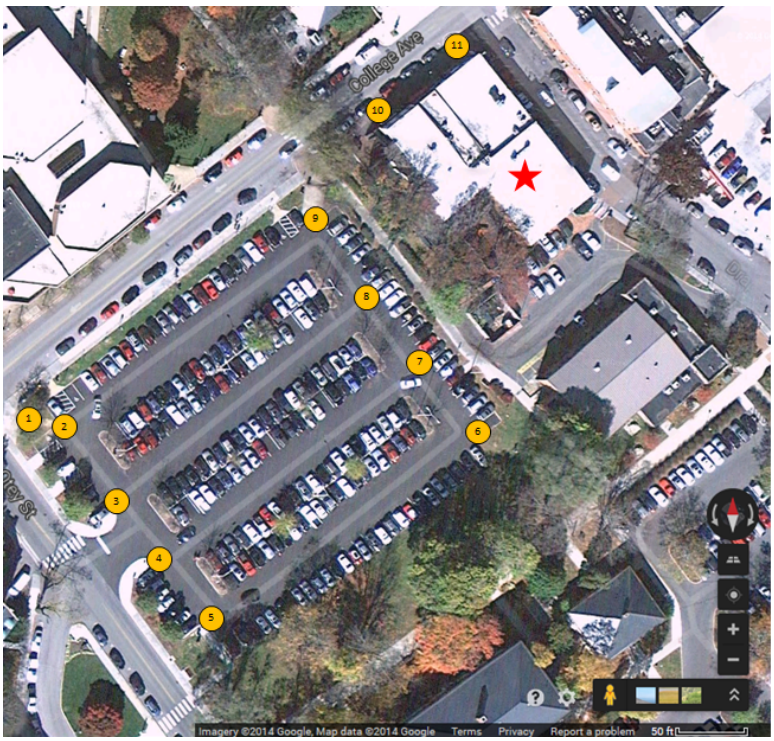

Figure 5.8: WiFi Scanner's Locations around Top of the Stairs Restaurant. The Red Star is the Location of the WiFi Router Being Tested.

- Scan ID
- Scan subID
- Datetime
- XY Location
- MACaddress
- SSID
- Security
- Signal Strength
- Radio Frequency

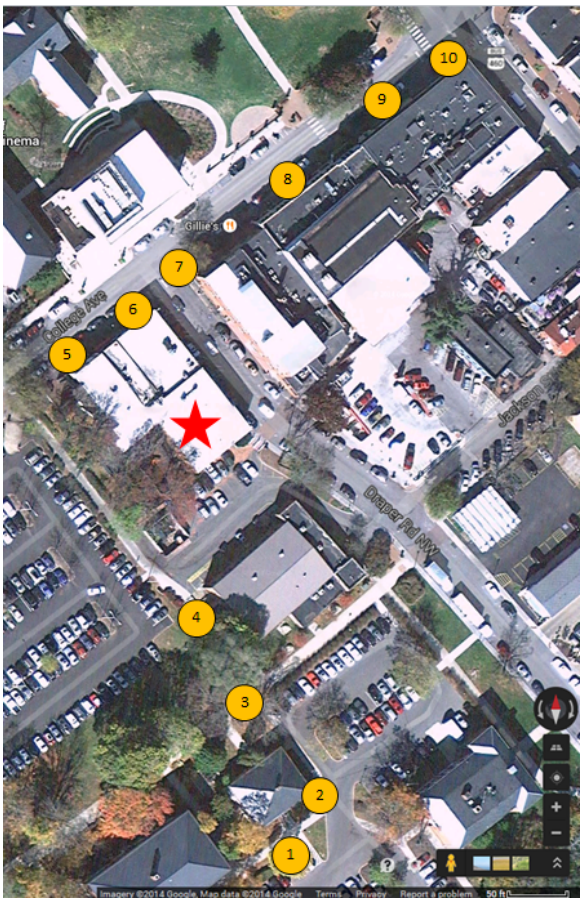

Figure 5.9: WiFi Scanner's Locations around Downtown Blacksburg. The Red Star is the Location of the WiFi Router Being Tested.

The WiFi Scanner app was used at each of the eleven test locations of the first field experiment ten times, and the app was used at each of the ten test locations of the second field experiment eight times. There were times where it did not collect data for the WiFi access point on top of TotS, so not every testing location has ten data entries. It was noted during experiment 2 that the Android's WiFi networks do not refresh quickly and often the measured signal strength would be recorded over the next couple of measurement locations. For example, at measurement location 4 for the second experiment, the recorded signal strength is -77 dB, but at measurement locations 3 and 2, where the signal is farther away and had to penetrate through additional trees, the signal strength was still recorded as -77

Figure 5.10: WiFi Scanner's Locations around Squires Building Parking Lot. The Red Star is the Location of the WiFi Router Being Tested.

dB when the points were measured walking from point 4 to 3 and from point 3 to 2. Similarly, when the signal strength was too low to be recorded at location 1 of experiment two, the measurements at points 2-4 would also be too low, when walking from point 1 to point 2, etc. Extra caution was used in Experiment three to take data slowly, and there was still often data missing from the final output. Each data entry is an average over ten measurements, however, so there was at minimum 50 experimental measurements being averaged. The measurements were taken April 26th - April 28th, 2014 for experiment 1, on May 29th - 30th, 2014 for experiment 2, and on July 3rd, 2014 for experiment 3 in clear weather for all experiments. The parking lot next to TotS was full of cars for all of the measurements. The frequencies of the Blacksburg WiFi router being tested were in the 2.4 GHz range, so there was no field test carried out for the 5 GHz range of WiFi frequencies. Tables 5.1, 5.2, and 5.3 show the field test data collected for Experiments 1 2, and 3, respectively.

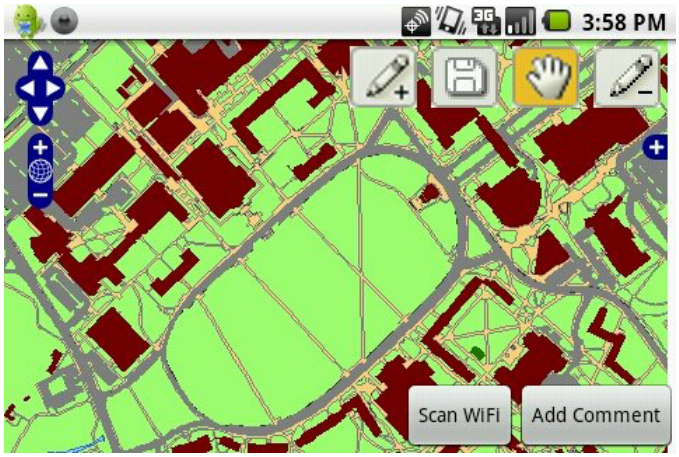

Figure 5.11: WiFi Scanner's Application Window overlooking the Virginia Tech Drillfield. The WiFi Scanner App takes a ten point average of the signal strength and returns the average in dBm. The icon with a pencil and a '+' allows for the introduction of new data points, whereas the pencil icon with the '-' will delete data points. The floppy disk symbol will save the recorded data to a text file containing the following information for each access point

Table 5.1: Field Testing Results of the First Experiment using the WiFi Scanner Application (Received Power in dBm)

Trial\Location	1	2	3	4	5	6	7	8	9	10	11
1	-77	-77	-77	-77	-77	-65	-69	-69	-67	-67	-77
2	-82	-82	-82	-75	-75	-68	-68	-69	-69	-69	-76
3	-77	-77	-79	-73	-73	-66	-68	-66	-66	-66	-66
4	-76	-78	-78			-60	-60				
5	-69	-69					-64	-64	-71	-80	-80
6	-77					-63	-71	-73	-77	-72	
7									-65	-74	-75
8									-68	-66	-75
9	-75	-75	-75	-75	-75	-63	-66	-73	-73	-69	-69
10	-74	-74	-74	-74	-61	-61	-73	-65	-65	-65	-69
Median	-76.5	-77	-77.5	-75	-75	-64	-67	-69	-68	-69	-75

Table 5.2: Field Testing Results of the Second Experiment using the WiFi Scanner Application (Received Power in dBm)

Trial\Loc.	1	2	3	4	5	6	7	8	9	10
1		-78			-69	-81	-70	-67	-67	-67
2				-69	-74	-74	-70	-70		
3		-81	-81	-74	-76	-76	-76	-75		
4			-85		-79					
5					-72	-72	-72	-72	-72	-72
6		-79	-79	-79	-76	-69	-70	-76	-72	-72
7					-74	-70	-67	-78	-78	-78
8		-77	-77	-77	-75	-64	-64	-74	-77	-78
Median		-78.5	-80	-75.5	-74.5	-72	-70	-74	-72	-72

Table 5.3: Field Testing Results of the Third Experiment using the WiFi Scanner Application (Received Power in dBm)

Trial\Loc.	1	2	3	4	5	6	7	8	9	10
1	-83	-85	-80	-85	-83		-84	-83	-88	-78
2		-85	-80	-82	-83		-84	-83	-88	-78
3				-82	-86			-78		-86
4				-84	-87					-86
5					-87					
Median	-83	-85	-80	-83	-86		-84	-83	-88	-82

Results and Changes to Algorithm

The results of the experiment are shown in Tables 5.1, 5.2, and 5.3, with the medians shown at the bottom. Using this data, a linear least squares analysis is performed to determine the best slope and y-intercept for the LOS and NLOS cases. Figures 5.12 and 5.13 show the least squares fit lines for the LOS and NLOS cases, respectively. For the LOS case, or rather, the case in which a building did not attenuate the signal, but foliage may have, it is found to have a slope of -2.72 and a L_0 value of -33.5 dBm. The slope of the LOS case is also the path loss exponent of the signal, and is above the free space value of 2 due to additional attenuation through trees that were not considered to be NLOS due to the signal not passing through a building. The NLOS case has a slope of -1.08 with a L_0 value of -59.4 dBm. The path loss exponent for the NLOS case is lower than expected, because distance is not affecting the path loss output as significantly as the attenuation of the buildings. In the L_0 calculation, the 14.5 dB being subtracted twice is to account for the two layers of walls being penetrated in the NLOS case. The final algorithm for signal's whose path intersects a building is:

$$\begin{aligned} L_p[dB] &= -1.08 * 10 * \log_{10}(d_{total}/d_0) - 14.5 * x_{wall} + L_0 \\ L_0[dB] &= -59.4 + 2 * 14.5 = -30.4 \end{aligned} \tag{5.4}$$

The final algorithm for line of sight signals is:

$$P_R[dBm] = -33.5 - 2.72 * 10 * \log_{10}(d_{total}/d_0) \tag{5.5}$$

The modifications to the algorithm were meant to better fit the experimental data, but were not meant to match it exactly. This is due to the limited scope of our field experiment, which was designed to allow for small changes to the algorithm to better reflect a real environment. For a more drastic change to the algorithm, more extensive field testing must be performed. Tables 5.4 and 5.5 show the difference between the calculated results of the Medium Scale Model at each testing location before and after the modifications were made.

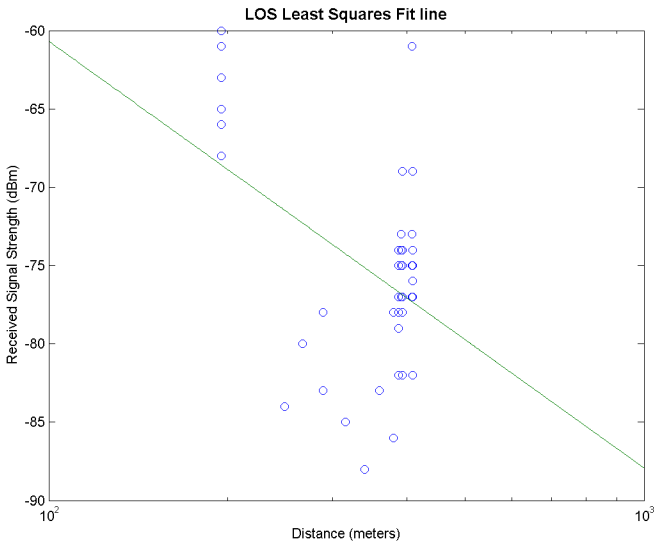

Figure 5.12: Linear Least Squares Fit Line for LOS Field Test Data. The LOS Least fit line has a L_0 value of -33.5 dBm and slope of -2.72

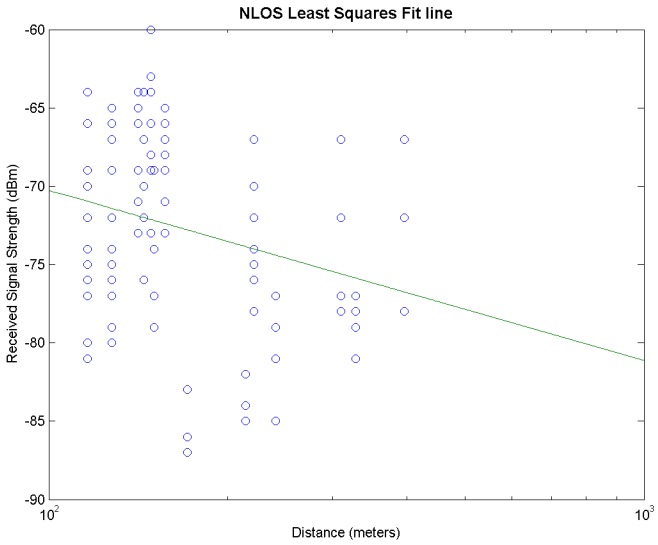

Figure 5.13: Linear Least Squares Fit Line for NLOS Field Test Data. The NLOS Least fit line has a L_0 value of -59.4 dBm and slope of -1.08

A linear comparison of the two algorithms compared to the field test data of the first two experiments is shown in Figure 5.14.

Table 5.4: Comparison to Field Test Data of the Old Algorithm and the New Algorithm - Experiment 1

Data\Loc.	1	2	3	4	5	6	7	8	9	10	11
Median Field Test	-76.5	-77	-77.5	-75	-75	-64	-67	-69	-68	-69	-75
Orig. Model	-60.6	-59.5	-59.6	-59.5	-60.1	-53	-71.5	-75.6	-71.8	-70.6	
New Model	-77.7	-76.8	-76.9	-76.8	-77.2	-68	-68.7	-71.5	-72.2	-70.3	-70.3

Table 5.5: Comparison to Field Test Data of the Old Algorithm and the New Algorithm - Experiment 2

Data\Location	1	2	3	4	5	6	7	8	9	10
Median Field Test	-	-78.5	-80	-75.5	-74.5	-72	-70	-74	-72	-72
Orig. Model	-105.9	-85.-4	-79.2	-56.5	-71.6	-70.6	-68.8	-72.3	-76.7	-88.7
New Model	-98.6	-76.1	-74	-65.5	-70.3	-70.3	-67.1	-66.9	-67.1	-77.4

The final algorithm's results can be seen in Figure 5.15. The simulated signal strength varies from -42 dB to -195 dB, with most LOS connections to the tower (the small blue dot) are green to represent a strong connection. In the upper right hand corner, the signal has had to pass through multiple buildings, and the signal strength was very low.

Table 5.6: Comparison to Field Test Data of the Old Algorithm and the New Algorithm - Experiment 3

Data\Location	1	2	3	4	5	6	7	8	9	10
Median Field Test	-83	-85	-80	-83	-86		-84	-83	-88	-82
Orig. Model	-52.7	-51.9	-56.6	-72.8	-71.5	-53.2	-52.9	-58.5	-53.8	-54.8
New Model	-75.8	-73.9	-73.3	-73	-71.8	-76.4	-75	-74.4	-72.3	-70.2

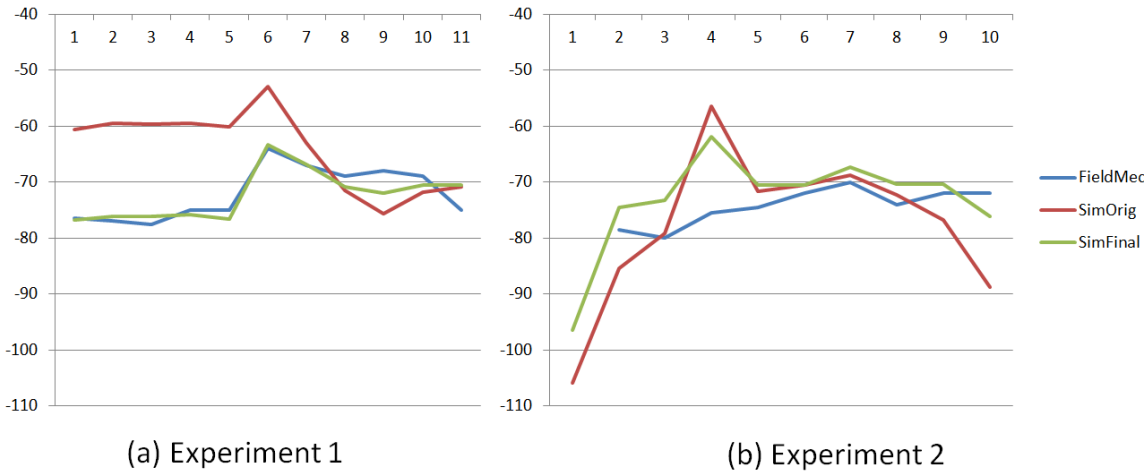

Figure 5.14: Comparison of Field Test Data, Original Simulation Estimates, and Final Simulated Estimates for Experiment 1 (a) and 2 (b). For experiment 1, the final simulation data follows the experimental data much more closely, especially for points 1-6 which are LOS connections. Experiment 2 shows that the final simulation follows the field test data more closely, but there is still a large portion of error.

5.4 Conclusion

The Medium Scale RF Model can be used for WiFi system planning with in ArcGIS. It has a longer runtime than the Large Scale RF Model taking around four minutes to run an

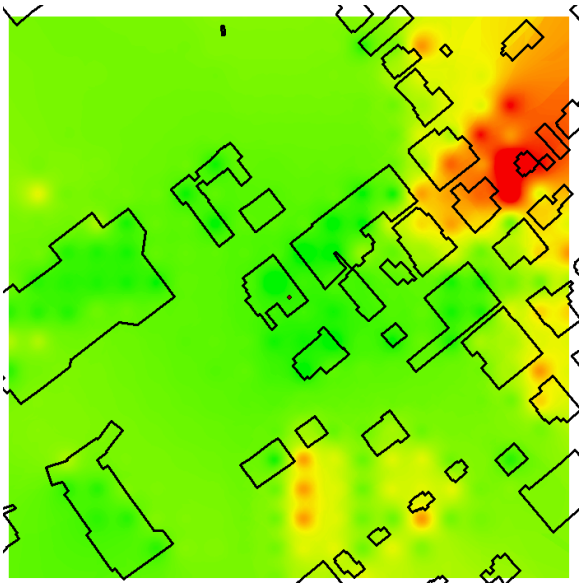

Figure 5.15: Final Algorithm Simulated Result from Top of the Stairs Antenna. Though this interpolated raster is very similar to the original simulation in terms of color, the values of the cells more closely match the field test values.

estimate for one access point. This is largely due to the *Intersect 3D Line with Multipatch* tool, which takes over two minutes to run. The Medium Scale RF Model also has many areas where it can be expanded and improved upon, making it a very diverse model that can be shaped to the user's needs.

Chapter 6

GIS and Indoor GPS

In an emergency, it is important to be able to locate a victim within a building. The FCC's E911 has just had new regulations proposed in which the location error of indoor cellular phone location must be reduced to 50 meters in the x- and y-directions, and 3 meters in the vertical, or z-direction [17]. WiFi positioning is one of the most promising indoor positioning forms available, but this method requires a large amount of data to be viable. RF time difference of arrival (TDOA) estimates are widely available in mobile devices such as cell phones and PDAs. However, there are still situations where accurate geolocation is challenging for current implementations of cellular phones, especially indoors.

GIS contains a wide variety of building information, such as building shape, size, and location, which can potentially be used to aid RF TDOA positioning. GIS can also contain data about a building's materials, locations of windows and number of floors. This chapter explores one of the many ways that GIS can potentially aid RF TDOA positioning: the correction of the estimated position to within the building's boundaries. A special interest is taken in the error in the z-coordinate if the target's position estimate is corrected to within the building's boundaries. The z-coordinate is the most difficult to estimate correctly in practice.

This chapter discusses an initial attempt to use building information within a GIS program like ArcGIS to improve TDOA-based geolocation. In these simulations, it is assumed that the target is known to be within the building, and the simulation will therefore place them into the building even if the estimation is close to ground level. These experiments, in combination with the Medium and Large Scale RF Models, show how GIS can help improve public safety.

6.1 Approach

To find out if GIS building data can aid in emergency victim location, an experiment was designed in which a target is located inside of a building in which size, location, shape, and number of floors is known. Two major experiments are performed: one in which the building is by itself, called the 'single building experiment', and one in which the building is surrounded by other buildings of known size, location, shape, and number of floors, called the 'multiple building experiment.' In each scenario, the building arrangement is surrounded by five fixed RF towers of known position that will serve as location anchors. In each scenario, the following steps were performed:

1. The target is generated within the central building with random x and y coordinates and placed on a random floor for its z coordinate.
2. The distance between the target and each of the tower anchors is calculated.
3. Noise (normal distribution) and bias (exponential distribution) are added to the calculated distances to simulate the additional time delay induced as the signal enters the building and the corruption in the measurement due to thermal noise.
4. The location of the target is estimated using a TDOA algorithm described later in this section. Five towers are the minimum required by this algorithm to accurately model the target's estimated z-coordinate.
5. The estimated target location will be corrected to within the known building bound-

aries, and distance between the estimated location and the true location are calculated for the corrected and uncorrected target locations. The distance is stored as error.

This section describes how GIS data can be used to improve target location indoors, discusses the TDOA algorithm used in the experiments, and the reasons why MATLAB was chosen for this analysis over GIS.[1]

Motivation

In an emergency situation, the location of a potential victim indoors can be extremely difficult in large buildings. There are indoor geolocation algorithms that use WiFi signals and known WiFi access points within the building to estimate the users position based on received signal strength (RSS) measurements. However, these methods require a large database of known information, such as an RF signal strength map or the known locations of the WiFi access points [59][60]. Promising research has been performed in ultra-wide band (UWB) frequencies, but these experiments still require extensive measurement campaigns [61]. Most systems described above require new hardware other than the user's cell phone, and often dedicated frequency bands are required for the system to function.

In this model, the ability for positioning accuracy to be improved if a building's boundaries are known is being tested. It is assumed that the target is within a building and is communicating with tower locations surrounding the building. RF signals propagate to the target, and TDOA distances can be calculated and the estimated target position can be prepared. Localization systems with this form of TDOA calculation can have large errors in position. A recent FCC study reports accuracy 67th and 90th percentiles ranged from 48.5m/210.1m (rural) to 226.8m/449.3m (urban) [62]. Due to the error being so large, it is important to reduce the error to meet the new standards for the FCC's E911 system. The goal of this experiment is to see if the known building boundaries will aid this form of geolocation.

[1]MATLAB is Copyright ©1984 - 2014 Mathworks. All rights reserved.

Time Difference of Arrival (TDOA)

TDOA algorithm chosen to estimate the target's position is the 'estimator for hyperbolic location' developed by Y. T. Chan and K. C. Ho in 1994 [63]. In their paper, Chan and Ho argue that most methods for hyperbolic location estimation that have been proposed are not optimum or require an iterative approach, which is computationally intensive and is not guaranteed to converge [63]. Their solution for hyperbolic location estimation is closed-form, and can estimate the position of the target given the location of TDOA sensors (such as the tower anchors), and the TDOA measurements for each sensor.

The TDOA measurements are time difference measurements that estimate the differences in times taken to travel to two towers. These are converted to distance using the following formula:

$$r_i = t_i * c[m] \tag{6.1}$$

where r_i is the TDOA measurement that has been converted to meters for tower i, t_i is the TDOA difference measurement in seconds, and c is the signal propagation speed and is generally the speed of light, $c = 3 * 10^8 \frac{m}{s}$. Assuming that a two dimensional target is located at $[x, y]$ and tower i out of M towers is located at $[x_i, y_i]$, then r_i can be calculated as follows:

$$\begin{aligned} r_i^2 &= (x_i - x)^2 + (y_i - y)^2 \\ &= K_i - 2x_i x - 2y_i y + x^2 + y^2, i = 1, 2, ..., M \end{aligned} \tag{6.2}$$

where

$$K_i = x_i^2 + y_i^2 \tag{6.3}$$

Another important relationship to note is that of the distance between tower i and tower 1:

$$r_{i,1} = r_i - r_1 \tag{6.4}$$

By expanding Equation 6.2, using the equation $r_i^2 = (r_{i,1} + r_1)^2$, we find:

$$r_{i,1}^2 + 2r_{i,1}r_1 + r_1^2 = K_i - 2x_i x - 2y_i y + x^2 + y^2 \tag{6.5}$$

By substituting Equation 6.3 where $i = 1$ into the above equation, we come up with an equation for the error vector, $r_{i,1}r_1$:

$$r_{i,1}r_1 = -x_i x - y_i y + x^2 + y^2 + 0.5(K_i - K_1 - r_{i,1}^2) \tag{6.6}$$

In our experimental set up, there are five towers providing measurements to find $[x, y, z, r_1]$, where r_1 is the distance between the target and tower 1, which is the closest tower to the target. When the number of measurements is greater than the number of unknowns, the system can be used to derive $z_a = [z_p^T, r1]^T$, where $z_p = [x, y, z]^T$. The error vector derived from Equation 6.6 is

$$\psi = \mathbf{h} - \mathbf{G}_a \mathbf{z}_a \tag{6.7}$$

where

$$\mathbf{h} = \frac{1}{2}\begin{bmatrix} r_{2,1}^2 - K_2 + K_1 \\ r_{3,1}^2 - K_3 + K_1 \\ . \\ r_{M,1}^2 - K_M + K_1 \end{bmatrix}$$

$$\mathbf{G}_a = -\begin{bmatrix} x_{2,1} & y_{2,1} & z_{2,1} & r_{2,1} \\ x_{3,1} & y_{3,1} & z_{3,1} & r_{3,1} \\ . & . & . & . \\ x_{M,1} & y_{M,1} & z_{M,1} & r_{M,1} \end{bmatrix}$$

After some matrix manipulation, an initial estimate of z_a is found to be

$$\mathbf{z}_a = (\mathbf{G}_a^T I \mathbf{G}_a)^{-1} \mathbf{G}_a^T I \mathbf{h} \tag{6.8}$$

This estimate is used to find the covariance matrix of $\mathbf{z}_a$. The covariance is computed by the perturbation approach. In the presence of noise, $\mathbf{G}_a$ and $\mathbf{h}$ can be expressed as $\mathbf{G}_a = \mathbf{G}_a^0 + \Delta\mathbf{G}_a$ and $\mathbf{h} = \mathbf{h}^0 + \Delta\mathbf{h}$ [63] where $\mathbf{G}_a^0$ and $\mathbf{h}^0$ are the components of $\mathbf{G}_a$ and $\mathbf{h}$ without noise. Since $\mathbf{G}_a^0 \mathbf{z}_a^0 = h^0$, we arrive at the following error vector equation:

$$\psi = \Delta\mathbf{h} - \Delta\mathbf{G}_a \mathbf{z}_a^0 \tag{6.9}$$

The covariance of the error vector is calculated by

$$\Psi = \mathbf{E}[\psi\psi^T] \tag{6.10}$$

where $\mathbf{E}[x]$ is the expected value of x. This implies that the covariance of z_a is

$$cov(z_a) = (\mathbf{G}_a^{0T}\Psi^{-1}\mathbf{G}_a^0)^{-1} \tag{6.11}$$

Using the covariance matrix, Ψ, we can also derive a new estimate for z_a:

$$\mathbf{z}_a = (\mathbf{G}_a^{0T}\Psi^{-1}\mathbf{G}_a^0)^{-1}\mathbf{G}_a^{0T}\Psi^{-1}\Delta\mathbf{h} \tag{6.12}$$

The final estimate of position is calculated by determining how the location of closest tower, tower 1, relates to the final estimate. This is found by first calculating a vector denoting inaccuracies in z_a. In the inaccuracy vector, the elements of z_a can be expressed as $z_{a,1} = x^0 + e_1$ where e_1 is an estimation error of z_a in the x component. The inaccuracy vector is calculated as follows:

$$\psi' = \mathbf{h}' - \mathbf{z'}_a\mathbf{z'}_a^0 \tag{6.13}$$

where

$$\mathbf{h}' = \begin{bmatrix} (z_{a,1} - x_1)^2 \\ (z_{a,2} - y_1)^2 \\ (z_{a,3} - z_1)^2 \\ z_{a,4}^2 \end{bmatrix}$$

$$\mathbf{G'}_a = \begin{bmatrix} 1 & 0 \\ 0 & 1 \\ 1 & 1 \end{bmatrix}$$

$$\mathbf{z'}_a = \begin{bmatrix} (x - x_1)^2 \\ (y - y_1)^2 \\ (z - z_1)^2 \end{bmatrix}$$

The desired position estimate is within $\mathbf{z}'_a$ as the x, y, and z coordinates. The covariance of ψ' can be computed as follows:

$$\begin{aligned} \Psi' &= 4\mathbf{B}'\text{cov}(z_a)\mathbf{B}' \\ \mathbf{B}' &= \text{diag}\{x^0 - x_1, y^0 - y_1, z^0 - z_1, r_1^0\} \end{aligned} \tag{6.14}$$

Since ψ is Gaussian, then ψ' must also be Gaussian. The maximum likelihood estimate of z'_a is

$$\mathbf{z'}_a = (\mathbf{G'}_a^T \Psi'^{-1} \mathbf{G'}_a)^{-1} \mathbf{G'}_a^T \Psi'^{-1} \Delta\mathbf{h}' \tag{6.15}$$

The final position estimate is obtained by

$$\mathbf{z}_p = \mathbf{S} * \sqrt{\mathbf{z}'_a} + [x_1, y_1, z_1]^T \tag{6.16}$$

where $\mathbf{S}$ is a matrix of signs:

$$\mathbf{S} = \begin{bmatrix} 1 & 1 & 1 \\ -1 & 1 & 1 \\ 1 & -1 & 1 \\ -1 & -1 & 1 \\ 1 & 1 & -1 \\ -1 & 1 & -1 \\ 1 & -1 & -1 \\ -1 & -1 & -1 \end{bmatrix}$$

The true location $\mathbf{z}_p$ is the location in which the signs matrix is multiplied with $\sqrt{\mathbf{z}'_a}$ such that the distance between $\mathbf{z}_p$ and $\Delta\mathbf{z}_a$ is minimized.

This algorithm for the estimator provides a quick and accurate position estimate for the target and is used in the MATLAB simulations to estimate the target's position.

MATLAB

For this analysis, MATLAB was chosen to perform the simulations. This is due to MATLAB's computational power, large number of engineering toolsets, and ability to display simulation results. ArcGIS does not have the engineering tools necessary to simulate a target location experiment, since it is designed to work with geographic data. Instead of using GIS building data, the experiments were performed in MATLAB using rectangular buildings of known location and size. The experiments were performed for two cases: single building target location, and target location when there are multiple buildings in the area.

6.2 Location Analysis in a Single Building

The goal of the simulation is to determine if knowledge of a building's floor plan and floor location, provided by GIS data, would aid in the location of a person indoors in an emergency. The first experiment is a simulation of a target within a single building of known size, location, and number of floors. In the experiment, the target is placed randomly within the building, and the MATLAB code simulates the location of the target within the building.

Experimental Setup

For the single building experiment, a 30 m x 30 m x 50 m building was placed in a 3D coordinate plane with its lowest left corner placed at the origin. The building has ten floors, each floor being 5m tall. This is the building where the target will be positioned randomly. The z-component of the target is translated to 1 m above a floor; this is done under the assumption that the target is standing up with the receiver at hip height of about 1 m. Five stationary towers are placed around the building at (-250,0,75), (0, 250, 30), (100, 0, 50), (0, -500, 100), and (-250, -250, 25). This is found to be a good geometry for the towers. Figure 6.1 illustrates the experimental set up.

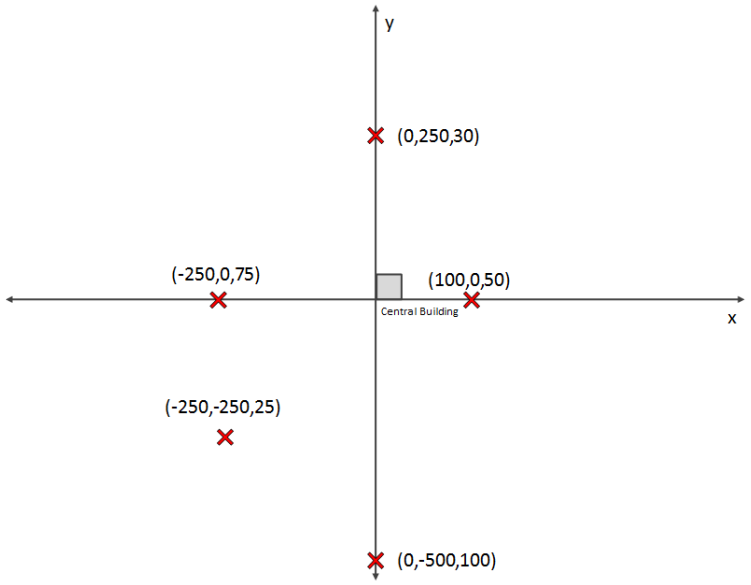

Figure 6.1: Single Building Experiment Set Up. The red 'X's represent the towers, and the coordinates of the tower (x,y,z) are next to the target it corresponds to. The square in the center of the figure is the Central Building where the target is located.

The distance between the top of each of the towers and the target is calculated, representing the time difference between when the signal leaves the tower and is received by the target. Error is introduced into the system according to the following formula:

$$r_i = d_i + b_i + n_i \tag{6.17}$$

where r_i is the measured distance between the target and tower i, d_i is the true distance between the target and tower i, b_i is as exponentially distributed bias introduced to account for the additional path length of the signal as it travels within the building before reaching the target due to NLOS propagation (maximum 2 m), and n_i is normally distributed Gaussian noise with zero mean and variance = σ^2. The variance of the noise is tested at σ^2 = [0,5,10,15,20] m^2, and the bias varies from 0 to 2 m for all variances to simulate additional path length within the building.

The position of the target is estimated using the TDOA formulation described in section

6.1. The estimated position, s_{est}, has three sets of analysis performed: uncorrected analysis, corrected analysis, and floor corrected analysis. The uncorrected analysis calculates the distance between s_{est} and the target and this value is recorded as the error. The corrected analysis translates s_{est} so that it is within the building to create $s_{corrected}$. Translation is performed by observing the x,y, and z coordinates and snapping them within the constraints of the building manually. For example, if a targets estimated x coordinate is -5 m (outside of the building boundary), then the x coordinate is manually changed to 1 m, just inside the building's walls. This change is made through a series of if-statements after the target's position has been estimated. The distance between $s_{corrected}$ and the target are calculated and stored as error. The floor correction analysis takes the corrected analysis further by translating the z coordinate to the nearest floor. This is to simulate apriori knowledge of the building's floor plan provided by geoprocessing software like ArcGIS. The floor correction creates s_{floor}, and the distance between s_{floor} and the target is calculated as the error.

The error values in the z-direction are examined specifically. The z-direction is the most difficult direction to correctly place in practice. A study was performed to see if the floor corrected analysis reduces the z-error when compared to the corrected analysis. The error in z-value was recorded and compared for all three sets of analysis. Two dimensional analysis of the target's estimated error was also performed.

Results

The average z-error of the three forms of analysis are calculated and compared. The additional translation of the floor correction analysis reduced the z-error of the target's estimated location by less than two meters. The improvement in the floor corrected z-error increases as noise increases. The average z-error as a function of noise variance is shown in Figure 6.2. The correction of the target's estimated location to within the building drastically reduced the average z-error, often by more than half of the z-error of s_{est}. The floor correction further reduces the average z-error, demonstrating that knowledge of a building's floor plan provided

by GIS could potentially aid in a target's z-coordinate estimate. The z-error is high due to the high vertical dilution of precision. Due to the low variance of the vertical values of the towers surrounding the central building, the errors in the z-direction are much larger than those of the x- and y-directions.

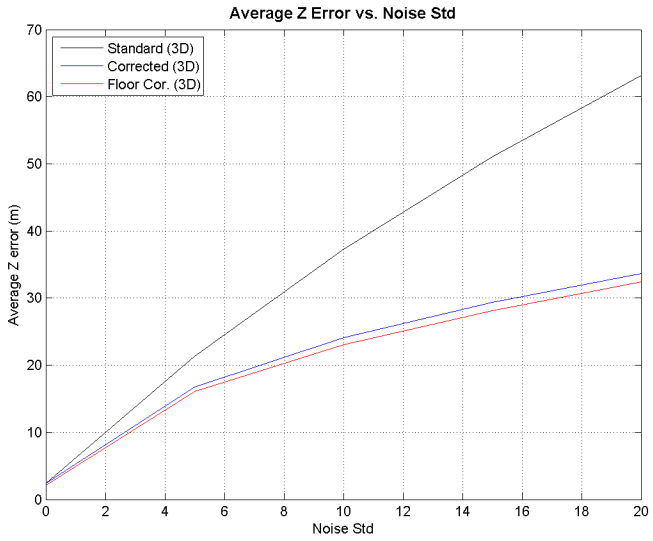

Figure 6.2: Average Z-error vs. Noise Variance. The black line represents the uncorrected z-error and the blue and red lines are the z-error after a correction has been made to place the target within the building and to place the target on the nearest floor, respectively. Both forms of corrected z-error show an improvement over the uncorrected.

A CDF analysis was performed to determine the probability of z-error given a noise variance. The CDFs for the three types of z-error calculation can be seen in Figures 1-3 in Appendix B. As can be seen in Figure 6.3, both the corrected and floor corrected CDFs show a reduction in error when compared to the uncorrected z-error. This can bee seen by the corrected curves being further to the left on the CDF graph.

The root-mean squared error (RMSE) represents a sample view of the differences between predicted values and observed values. It is calculated for each experimental type of error

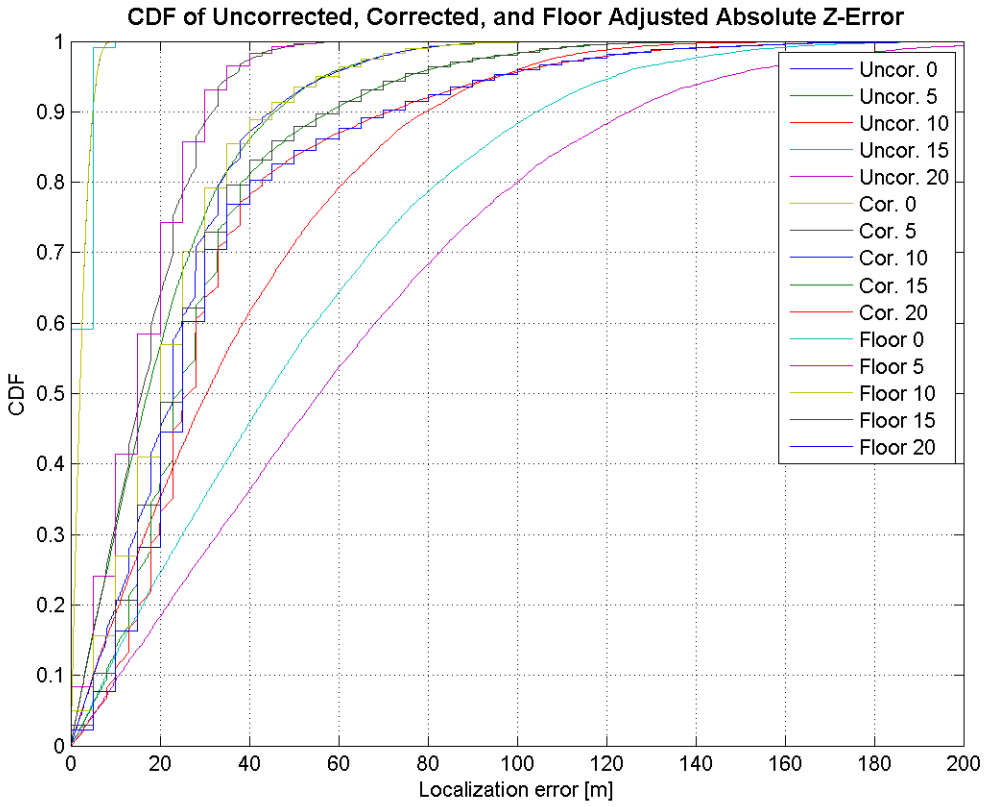

Figure 6.3: CDFs of Z-Error Analyses Together. The overall z-error CDF improves (moves to the left) with correction and floor correction when compared to the uncorrected CDF. In the legend, the type of analysis is the abbreviated word, and the number represents the noise value in m^2.

according to Equation 6.18:

$$RMSE = \sqrt{\frac{1}{N}\sum_{i=1}^{N}(error_i)^2} \tag{6.18}$$

where N is the total number of error entries and $error_i$ is the error at entry i. The position error for each type of analysis is compared for each noise variance in Figure 6.4. Three-dimensional and two-dimensional (for x- and y-components) RMSE calculations are performed. The corrected and floor corrected analysis greatly improve the RMSE when

compared to the uncorrected 3D RMSE. Correction to within the building also improves the RMSE for the 2D analysis, which is expected. It should also be noted that the uncorrected RMSE for the 3D analysis is three times as large as the uncorrected RMSE for the 2D analysis, showing the influence that the z-component has on the target's error.

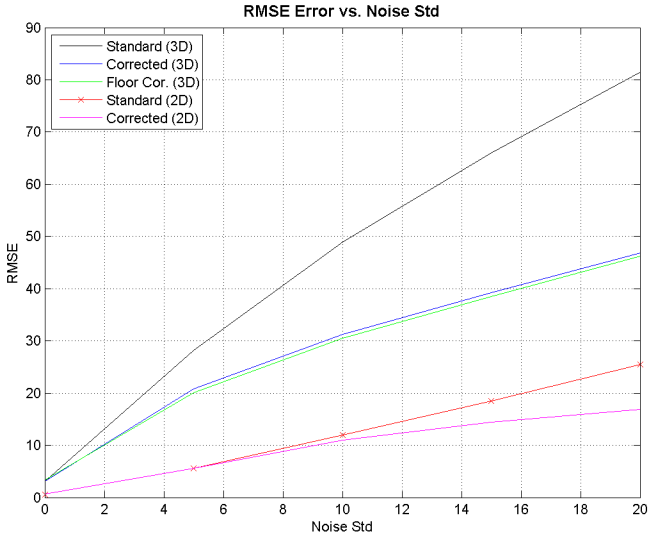

Figure 6.4: RMSE Analysis in 2D and 3D for Single Building Experiment. Correction improves the RMSE for both the 3D and the 2D cases. This is expected, because the target is being moved closer to the building in the corrected cases, and thus closer to the target's actual position. The influence of the z-component on error is noticeable, with the 3D RMSE of the uncorrected (Standard) error being nearly three times as large as the 2D RMSE of the uncorrected error.

Cumulative distributive function analysis was also performed for the three-dimensional cases for the total position error. The CDF results can be seen in Appendix B. The CDF of the corrected and floor corrected analysis are not completely smooth, but this is due to the corrections to the z-error causing error values that are multiples of 5. Both the corrected and floor corrected CDFs show an improvement over the uncorrected, as can be seen in Figure 6.5 where the CDFs have been laid over top of one another.

Figure 6.7 describes the gains of the single building experiment in the overall error at the median, 67^{th} percentile, and 90^{th} percentile. The gains are included for 5, 10, 15, and 20 m^2 thermal noise standard deviations. Figure 6.6 describes the gains at the median, 67^{th} percentile, and 90^{th} percentile for the absolute Z-error. The gains of the z-error nearly match the overall gains of the experiment. This shows that the largest source of error is the z-error, and that the incorporation of GIS data greatly reduced the value of error.

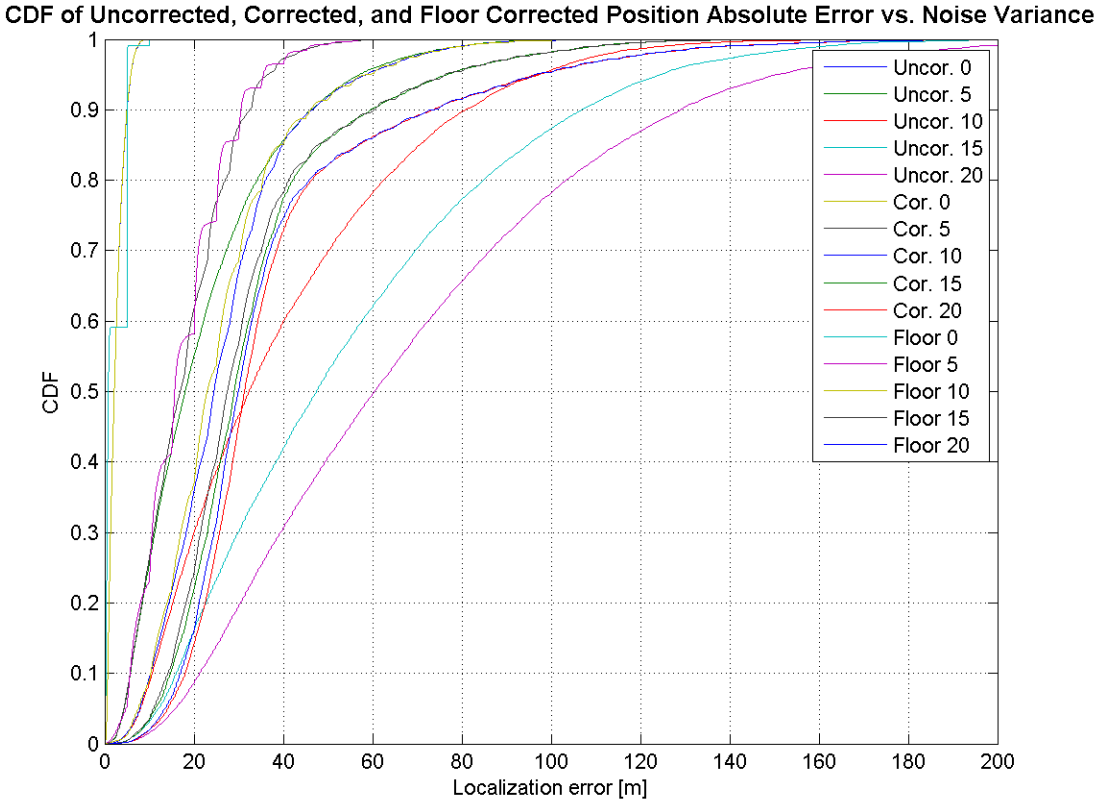

Figure 6.5: Median, 67th percentile, and 90th percentile gains. The floor corrected gains are often larger than the corrected gains, due to the large z-error gain increases at larger noise standard deviation values.

Noise Var.	Absolute Z-Error		
	Median	67th	90th
	Corrected		
5	1.4	3.08	14.39
10	7.1	17.51	34.65
15	19.82	30.83	46.81
20	29.38	45.2	53.59
	Floor Corrected		
5	2.3	4.81	16.14
10	10.1	20.51	34.86
15	19.04	33.83	44.2
20	30.61	48.2	55.2

Figure 6.6: Median, 67th percentile, and 90th percentile gains for the Z-error. The floor corrected gains are larger than the corrected gains frequently. These values for gain are very close to the overall error gains, demonstrating the large effect of Z-error in positioning problems.

Conclusion

The correction to within a building with a single building improves the overall error in position location. The scenario in which only one building is considered is unrealistic, however. In the next section, another experiment is conducted in which multiple buildings surround the central building where the target is located.

Noise Var.	Overall Error		
	Median	67th	90th
	Corrected		
5	0.95	2.97	13.65
10	7.84	17.07	34.93
15	18.34	31.22	46.81
20	29.12	44.73	55.7
	Floor Corrected		
5	2.2	4.87	15.9
10	9.32	18.7	35.31
15	19.87	32.95	46.8
20	30.53	46.13	54.9

Figure 6.7: CDFs of 3D Error Analyses Together. The overall error CDF improves with correction and floor correction when compared to the uncorrected CDF. This can be seen in the five sets of curves that are further to the left and aren't smooth. In the legend, the type of analysis is the abbreviated word, and the number represents the noise value in m^2.

6.3 Location Analysis in Multiple Buildings

In a more realistic scenario, this experiment places other buildings around the central building where the target is located. This is to simulate when the location algorithm contains the locations, shapes, and number of floors of surrounding buildings and must choose the building into which the target will be corrected. Four additional buildings are placed one building length away from the central building in the x and y direction. These buildings will have varying heights. This scenario will give insight into the usefulness of using GIS building information in practice.

Experimental Setup

The Multiple Building Experiment is arranged similarly to the Single Building Experiment. There is a central building that is 30 m x 30 m x 50 m in size where the target will be located. In this experiment, there are four additional buildings that are decoys placed around the central building. The decoy buildings all have a 30 m x 30 m base and a z-component that varies from 20 to 50 m. The decoys are placed around the building along the x- and y-axes 30 m away from the central building, as is shown in Figure 6.8. This arrangement of buildings along the x- and y-axis was chosen due to these 4 buildings representing the shortest distance to the central building given a 3 x 3 building arrangement. The buildings in the corner of the 3 x 3 building arrangement were removed from consideration for simplicity. The penetration of the decoy buildings is not considered in the estimated distance calculation between the target and the towers. The purpose of the decoy buildings is to see whether the target will be translated into the wrong building and introduce more error overall than the uncorrected analysis.

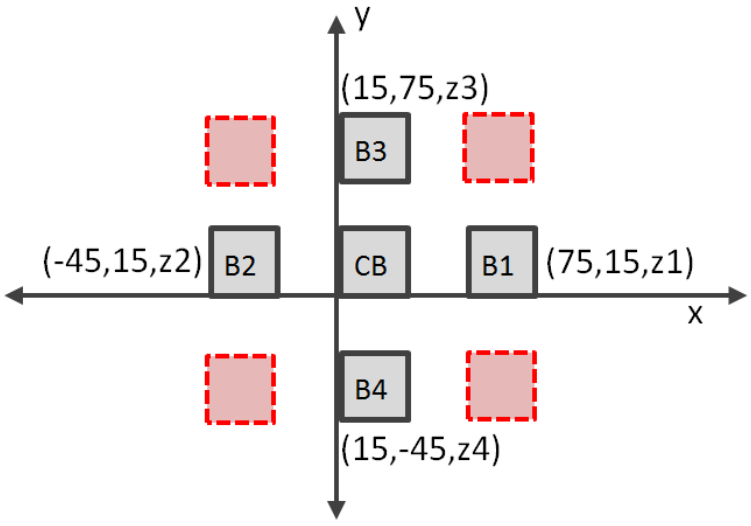

Figure 6.8: Multiple Building Experiment Set Up[2]

[2]The experimental set up has 4 buildings (B1-B4) near the central building (CB). The coordinates next to the additional buildings are the coordinate for the central point in that building. The z value of the

The distance between the tower and the target is calculated in the same manner as the single building experiment. The same noise variances and bias is used in the multiple building experiment, and the estimated position is calculated using the TDOA algorithm described in Section 6.1. In this experiment, the algorithm can translate the target into the wrong building. The building that the target is placed in is chosen by the minimum distance between the centers of all of the buildings and the target. In this way, the target's height relative to building heights is taken into account since each building's z-coordinate will vary based on how tall the building is. The distance between the estimated target's position and the center of each of the surrounding buildings is calculated. The target is placed in the building where this distance is minimum. Corrected analysis places the target just within the building, and the floor corrected analysis translates the target to the nearest floor.

Results

Similar to the single building experiment, the additional translation of the floor correction analysis reduces the z-error of the target's estimated location. The error is reduced by the exact same amount as the single building experiment, as can be seen in Figure 6.9. The z-error in the floor corrected analysis decreases as noise increases. Despite the error induced by placing the target in an incorrect building, the correction of the target's estimated z-location remains the same as it was in the single building experiment. This is due to the z-location still being corrected to within a building's boundaries and to a building's floor in the same manner even when the target is translated to an incorrect building on flat ground.

CDF analysis is performed to determine the probability of z-error given a noise variance. The CDFs for the three types of z-error calculation individually can be seen in Appendix C.

additional buildings, $z1$, $z2$, $z3$, and $z4$, represent half of the building's total height, and varies from 10 m to 25 m. These central coordinates are used to calculate the minimum distance between the estimated target location and all five buildings; the target will be corrected to the building with the minimum distance. There is a 30 m space between all buildings. The red, dotted line squares are the buildings that were removed from the 3 x 3 building arrangement for simplicity.

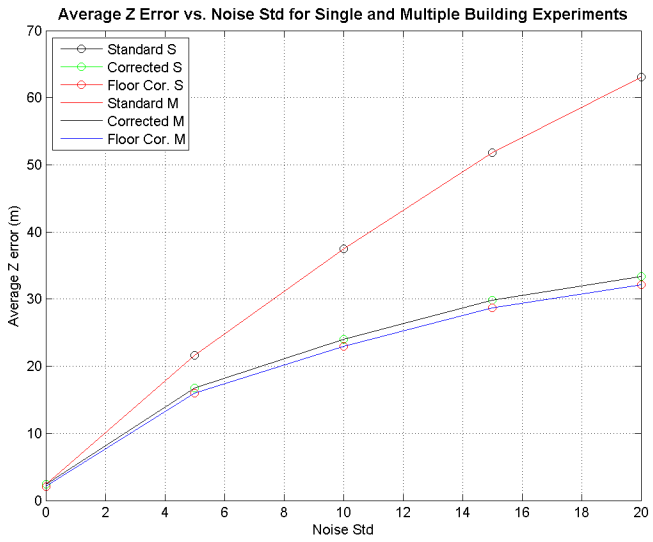

Figure 6.9: Average Z-error vs. Noise Variance. The comparison between single and multiple buildings shows that the average z-error is the same for both experiments. This is due to the central building and the surrounding buildings being on flat ground, and the z-error being corrected in the same manner whether the target remains in the central building or is translated to a nearby building.

As can be seen in Figure 6.10, both the corrected and floor corrected CDFs show a reduction in error when compared to the uncorrected z-error.

A comparison is performed between the single and multiple building experiments for the corrected and floor corrected analysis, and the results can be seen in Figures 6.11 and 6.12. The multiple building experiments show a slight reduction in performance compared to the single building experiments, but the multiple building experiment shows an improvement in z-error performance overall.

RMSE is also calculated for the multiple building experiments and compared to the single building experiments. The three dimensional RMSE is compared in Figure 6.13, and the two dimensional RMSE is compared in Figure 6.14. It can be seen in Figure 6.13 that the RMSE in the single building experiment is lower than the RMSE in the multiple building

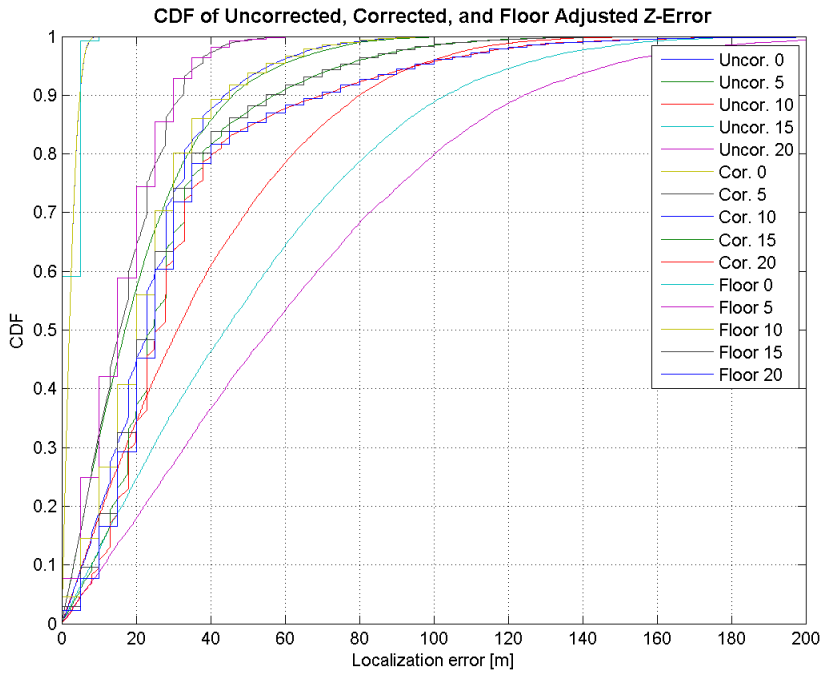

Figure 6.10: CDFs of Z-Error Analyses Together. The comparison between single and multiple buildings shows that the average z-error is the same for both experiments. In the legend, the type of analysis is the abbreviated word, and the number represents the noise value in m^2.

experiment. The RMSE of the multiple building experiment is still reduced drastically from the uncorrected analysis. In Figure 6.14, the 2D RMSE is larger for the multiple building analysis. This is expected, due to the possibility that the target is placed within the wrong building, which will increase error in the x and y direction.

Cumulative distributive function analysis is also performed for the three-dimensional cases for the total position error. The CDF results can be seen individually in Appendix C. Both the corrected and floor corrected CDFs show an improvement over the uncorrected, as can be seen in Figure 6.15 where the CDFs have been cascaded.

A comparison is performed of the corrected error CDFs for the single and multiple building

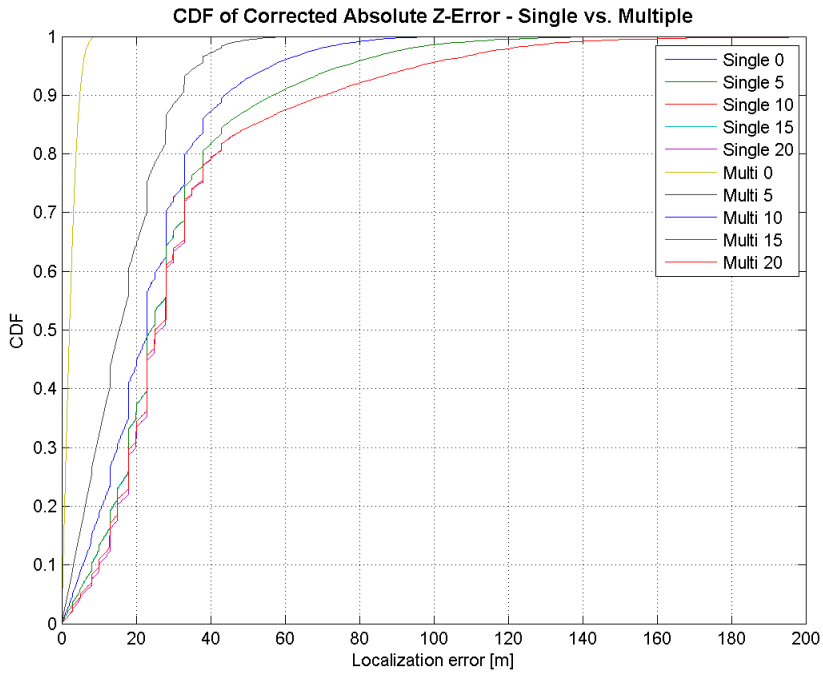

Figure 6.11: CDF of the Single and Multiple Building Experiments for Corrected Analysis. The comparison between single and multiple building analysis shows a small degradation in performance in the multiple building experiments. This degradation does not drastically change the reduction in error for correcting the position of the target to within a building.

experiments, and the results are seen in Figures 6.16 and 6.17. Figure 6.16 shows that the error results of the single and multiple building experiments begin to deviate significantly as the noise variance increases above 10 m^2. A similar result is noted in Figure 6.17, and both results are expected due to the increase in error in the x and y coordinates.

A comparison is also performed for the multiple building experiments at the median, 67^{th}, and 90^{th} percentiles, as is shown in Figures 6.18 and 6.19. The experiment shows that there is still a large reduction in the overall error and z-error in the multiple building experiments.

A comparison at the median, 67^{th}, and 90^{th} percentiles are performed comparing the single building experiment gains and the multiple building experiment gains. The comparison

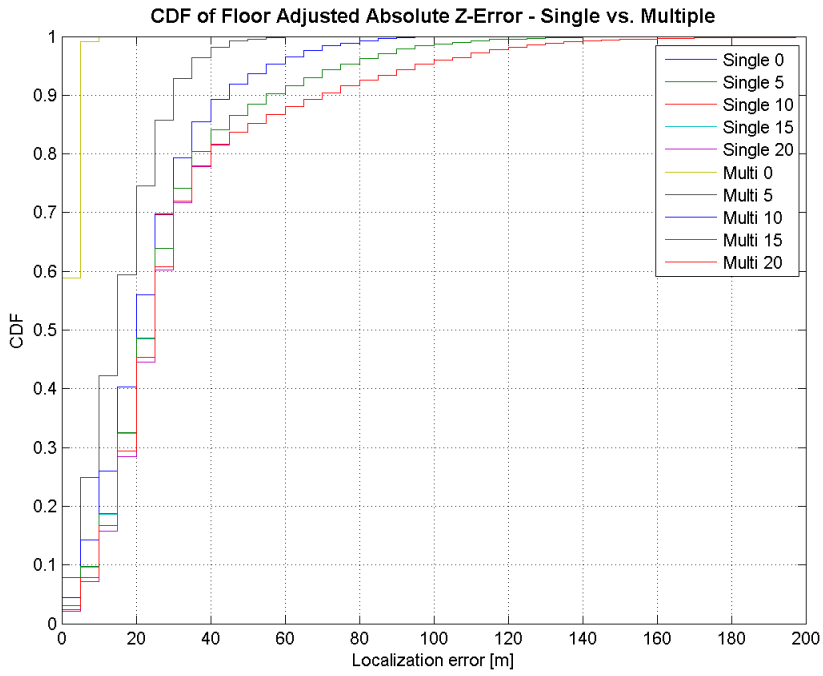

Figure 6.12: CDF of the Single and Multiple Building Experiments for Floor Corrected Analysis. The comparison between single and multiple building analysis shows a small reduction in performance in the multiple building experiments. This degradation does not drastically change the reduction in error for correcting the position of the target to a floor.

demonstrated that the single building experiment had larger error gains than the multiple building experiment in overall error, as is shown in Figure 6.20. The differences in error gain in the z-direction is largely unchanged, as is shown in Figure 6.21. This is due to the additional error introduced in the x- and y-directions in the multiple building experiments due to the wrong building being selected. Error in the z-direction is calculated the same regardless of which building the target has been placed in.

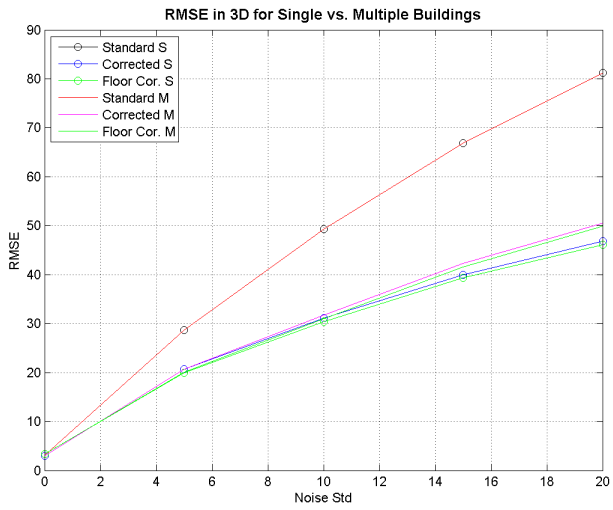

Figure 6.13: RMSE Comparison Between Multiple and Single Building Analysis in 3D. The comparison between single and multiple building RMSE analysis shows that the RMSE in 3D of the multiple building experiment is higher than that of the single building experiment. There is still a large reduction in RMSE between the corrected analyses and the uncorrected analysis for the multiple building experiment, showing that GIS data can aid in target location in scenarios when there are other buildings close by.

6.4 Conclusion

The single and multiple building experiments show that GIS data can aid in target location while the target is indoors. The improvement in performance in the z-component is significant in both the single and multiple building experiments. Additional z-component correction, though slight, aids in finding the target's z-coordinate when the target's location is translated to the nearest floor. The multiple building experiments have worse performance than the single building experiments, but there is still an improvement in performance over the uncorrected error analysis. The multiple building experiment shows that apriori knowledge of a building's size, location, shape, and number of floors, such as data provided by GIS, can aid in target location.

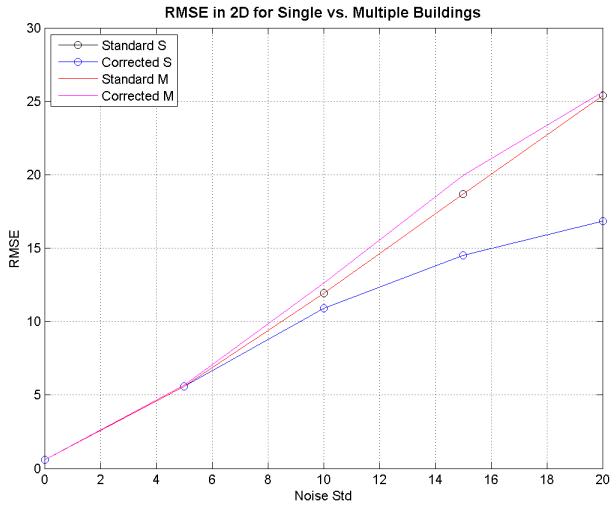

Figure 6.14: RMSE Comparison Between Multiple and Single Building Analysis in 2D

The 2D RMSE in the multiple building experiment is worse than the uncorrected or 'standard' 2D RMSE, which is expected due to the possibility for the target to be placed into the wrong building at high noise levels.

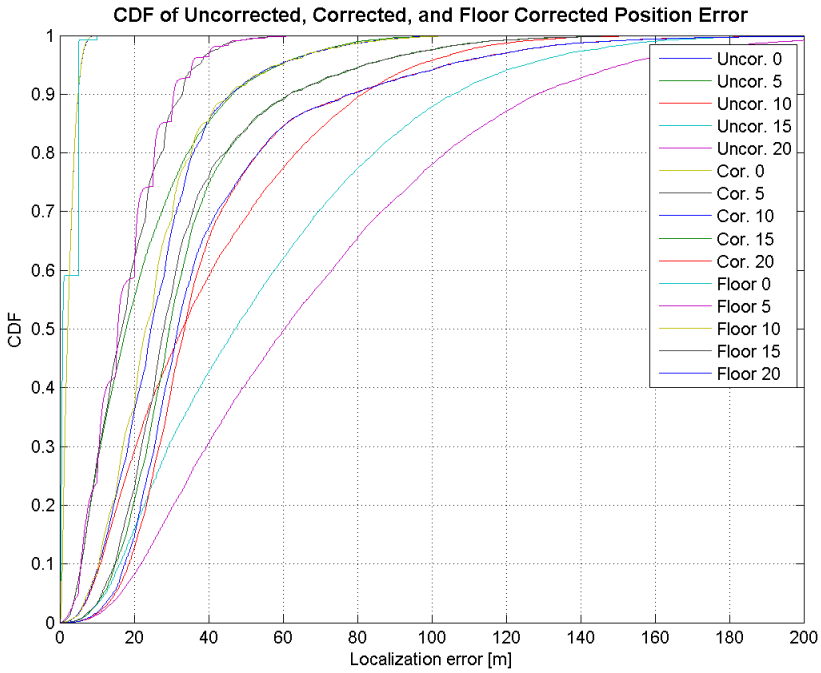

Figure 6.15: CDFs of 3D Error Analyses Together. The three error analyses (uncorrected, corrected, and floor corrected) are displayed on top of one another. The CDF improves with both corrected and floor corrected analysis. In the legend, the type of analysis is the abbreviated word, and the number represents the noise value in m^2.

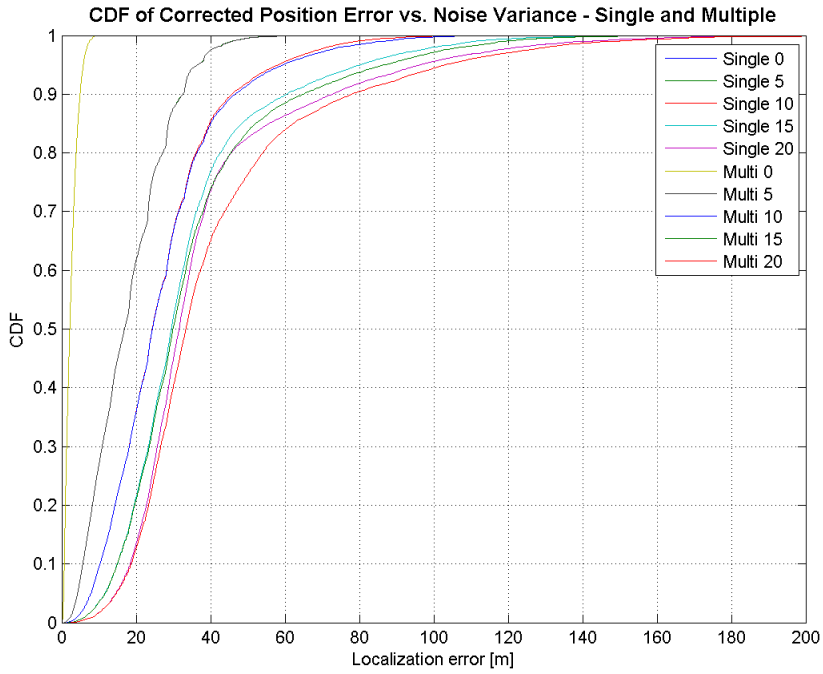

Figure 6.16: Comparison of Corrected Analysis CDF for Single and Multiple Building Experiments. The two experiments show similar performance for noise variances less than 10 m^2 and higher. At 10 m^2, the single building experiments performance becomes increasingly improved over the multiple building performance. This is expected due to the increase in error in the x and y coordinates.

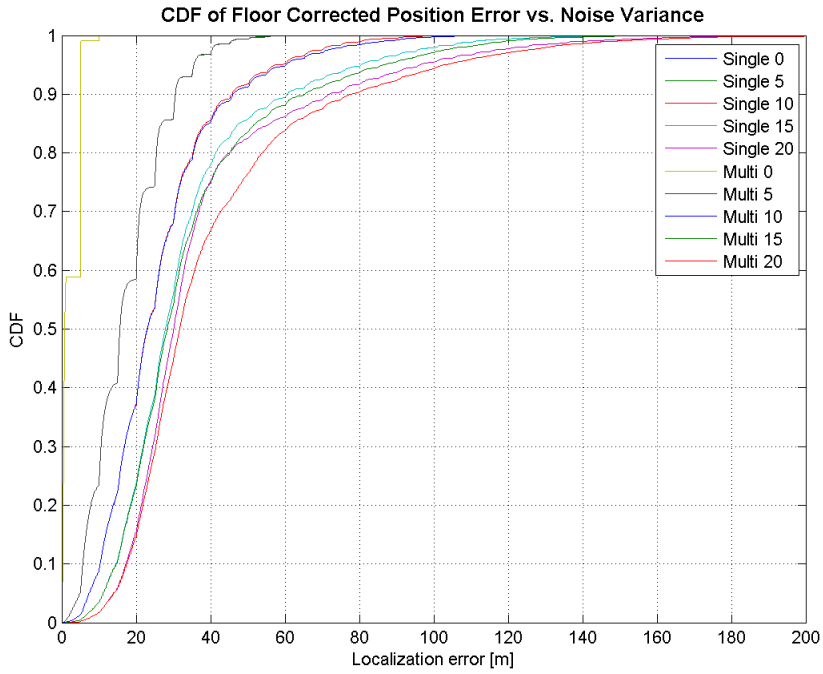

Figure 6.17: Comparison of Floor Corrected Analysis CDF for Single and Multiple Building Experiments. The two experiments show similar performance for noise variances less than 10 m^2 and higher. At 10 m^2, the single building experiments performance becomes increasingly improved over the multiple building performance. This is expected due to the increase in error in the x and y coordinates.

Noise Var.	Overall Error		
	Median	67th	90th
	Corrected		
5	1.23	3.17	13.45
10	7.84	16.92	35.8
15	17.94	30.55	45.49
20	26.9	40.65	51.01
	Floor Corrected		
5	2.33	4.82	15.9
10	9.21	18.19	35.78
15	19.39	31.98	45.26
20	28.67	41.94	51.2

Figure 6.18: Gains for the median, 67th percentile, and 90th percentile for the overall error in the multiple building experiments. Large gains are visible even in the multiple building experiments.

Noise Var.	Absolute Z-Error		
	Median	67th	90th
	Corrected		
5	1.68	3.21	13.51
10	7.1	17.51	35.77
15	20.06	32.71	47.19
20	30.01	45.2	54.57
	Floor Corrected		
5	2.3	4.81	16.14
10	10.1	20.51	34.86
15	19.04	33.83	49.2
20	30.61	48.2	55.2

Figure 6.19: Gains for the median, 67th percentile, and 90th percentile for the z-error in the multiple building experiments. Large gains slightly less than the overall error indicate the strong effect that the Z-error has on overall error.

Difference Between Single and Multi			
Noise Var.	**Median**	**67th**	**90th**
	Corrected		
5	-0.28	-0.2	0.2
10	0	0.15	-0.87
15	0.4	0.67	1.32
20	2.22	4.08	4.69
	Floor Corrected		
5	-0.13	0.05	0
10	0.11	0.51	-0.47
15	0.48	0.97	1.54
20	1.86	4.19	3.7

Figure 6.20: Comparison of gains for the median, 67th percentile, and 90th percentile for the overall error for both experiments. The values are the single building experiment gains minus the multiple building experiment gains, showing that the single building experiment gains are larger than the multiple building gains.

Zerror Diff. Between Single and Multi			
Noise Var.	**Median**	**67th**	**90th**
	Corrected		
5	-0.28	-0.13	0.88
10	0	0	-1.12
15	-0.24	-1.88	-0.38
20	-0.63	0	-0.98
	Floor Corrected		
5	0	0	0
10	0	0	0
15	0	0	-5
20	0	0	0

Figure 6.21: Comparison of gains for the median, 67th percentile, and 90th percentile for the z-error for both experiments. The values are the single building experiment gains minus the multiple building experiment gains, showing that gain values are mostly unchanged or are very similar.

Chapter 7

Uncertainty

Radio frequency propagation estimates are subject to dozens of variables, such as antenna height, terrain obstacles, climate, and frequency. The variables that are unaccounted for in the algorithm are a source of inaccuracy in most RF propagation algorithms available for use today. There is also a large source of error introduced with user inputs and terrain data. Errors in terrain data can cause translations of the propagation estimate, and user supplied data can have small errors in transmission antenna height, transmission power, etc. The small errors introduced by user supplied parameters will not substantially affect the estimate in general, but an estimate given more accurate parameters will always be better. This chapter explores the possible sources of uncertainty in the Large and Medium Scale RF Models. The largest source of uncertainty is the algorithms themselves.

7.1 GIS Based Uncertainty

One of the advantages to using geospatial software to model RF is also one of its disadvantages: terrain data is widely available. Numerous sources for terrain data provides a diverse selection of terrain options, such as resolution variations, surface models, and terrain models.

The terrain sources can come in a variety of geographic projections, resolutions, and level of detail. The DEM used for the Large Scale RF Model covers the entire state of Virginia at 30 meter resolution. The DEM used by Radio Mobile also uses a 30 meter resolution, but the data comes from a different source than the data used for the Large Scale model. This can account for errors when comparing the outputs of the Large Scale RF Model and Radio Mobile.

The DSM of Blacksburg used in the Medium Scale RF Model requires more detail, and has a resolution of 5 feet. Because the Virginia DEM used in the Large Scale RF Model has the terrain averaged over a larger area, the DEM will introduce more error than the DSM. Figure 7.1 shows the same area in the Blacksburg DSM and Virginia DEM. The DSM can also introduce error, as is seen in Figure 5.4 in Chapter 5 where the example building's rectangular shape is rounded due to the averaging of the DSM.

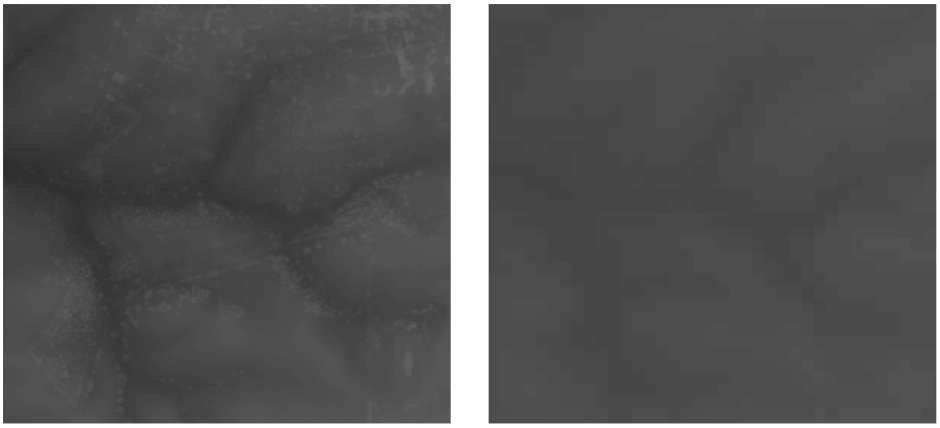

Figure 7.1: Illustration of Difference of Resolution. The two rasters show the same area of Blacksburg. The digital surface model in figure (a) shows details of buildings and trees at a higher resolution of 5 ft per pixel. The digital terrain model in figure (b) shows terrain data that does not have surface buildings at a resolution of 30 m per pixel.

Terrain is not the only source of uncertainty within GIS. Due to the ability to project rasters and feature classes into a different coordinate system, error is introduced when a

projection is performed. This can result in the geospatial object having its shape altered and its location translated. This can introduce error into future calculations. A common source of error is the misplacement of data due to a poor projection. This error was common when the comparison between the Large Scale RF Model and Radio Mobile was performed. Figure 7.2 (a) shows a polygon format of the Radio Mobile output over top of a polygon format of the Large Scale RF Model Output as it was originally created. Figure 7.2 (b) shows the two polygons after they have been aligned manually. Comparative analysis can only be performed when the data is aligned best.

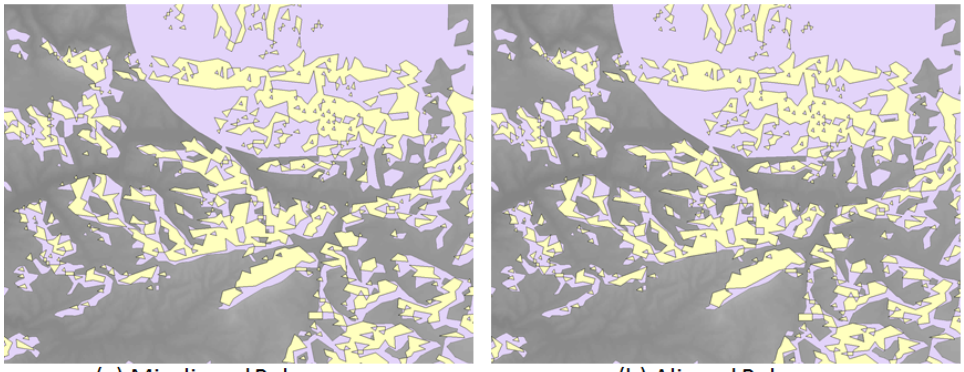

Figure 7.2: Illustration of Poor Alignment. The two polygons in (a) have been poorly placed due to differences in terrain data. The yellow polygon is an estimate created by Radio Mobile with USGS 30 meter resolution terrain data. The purple polygon is an estimate of the same tower generated by the Large Scale RF Model. In (b) the polygons have been translated so that they are aligned.

Building data can also be susceptible to uncertainty. New buildings are being constructed and old buildings are being removed at a rate that is nearly impossible to keep accurate within a database. Aschrafi et al. determined that certain RF propagation algorithms like the Dominant Path model are more robust to inaccuracies in building databases than others like a Ray Tracing model[64]. The Medium Scale RF Model is reasonably robust to building inaccuracies with its current algorithm. With some of the algorithm changes that can be

made, such as the algorithm where distance through a building is considered, will make database inaccuracies have a more significant effect.

7.2 Algorithm Uncertainty

There are multitudes of algorithms available to model RF propagation. Each algorithm has advantages and disadvantages. For example, the Irregular Terrain Model (ITM) provides a reasonable estimate for a large range of frequencies, but the algorithm can be quite complicated. The Okumura-Hata model provides an accurate empirical estimate for RF propagation in urban environments, but the model is only to be used for a small range of frequencies.

The Large Scale RF Model sacrifices much of its accuracy in exchange for simplicity and short computation time. It is based on the Friis free space path loss equation which is a very simplified propagation model. The path loss exponents and reference distance, d0, chosen for the model are chosen based on values found in sources and the algorithm's final output matching the Radio Mobile output most closely. Field Test analysis was not performed for the Large Scale RF Model.

The Medium Scale RF Model was altered slightly based on the gathered field test data. The alteration to the model brings the model's output closer to the field test data, but the results do not match field test data exactly. Both the Large Scale RF Model and the Medium Scale RF Model consider LOS as one of the most important factors in the algorithm. Since LOS is the most important factor in RF propagation, the Large Scale RF Model and the Medium Scale RF Model are accurate enough for planning purposes but are not detailed enough to provide an accurate representation of existing coverage.

7.3 User Based Uncertainty

Broadband providers and other wireless planners often have to record their RF system set up in order to provide the inputs required to generate an RF estimate. Those using RF models to estimate their coverage can introduce small amounts of error based on poor estimates of equipment location or position, or poor quality equipment. User provided data can introduce some error into the RF Propagation analysis. Common sources of error are:

- Latitude and Longitude
- Antenna Above Ground Level (AGL)
- Antenna Azimuth
- Antenna Elevation
- Transmission Power
- Antenna Pattern
- Antenna Gain
- Transmission Frequency
- Receiver Power Threshold

Many of these sources of error are due to inaccuracies in measuring equipment, such as latitude and longitude being estimated using a web map such as Google Maps. The errors introduced in this manner often do not have a significant role on the final estimate. When user provided data has errors in several of the above sources, this can create large errors in the final estimate.

7.4 Conclusion

There are multiple sources of uncertainty in the Large Scale and Medium Scale RF Models, the largest being the algorithm itself. The algorithms for both models are very simplified, similar to predicting tomorrows weather based on todays weather. Though both models will

not offer specific coverage estimates, they can give planners an idea of what the coverage of an antenna would look like. They can provide a reasonable estimate for broadband companies, GIS users, and city planners who are attempting to design a wireless broadband system.

Chapter 8

Conclusion and Future Work

In today's world, there is no shortage of algorithms for estimating RF coverage. Many of these algorithms do not consider specifics of terrain, or are too computationally or financially expensive to be considered by small WISPs to estimate their coverage. GIS provides access to the latest terrain data available and the geoprocessing tools that are designed to work with this data. ArcGIS is a common program used by city planners and government officials to maintain a wide variety of maps, including the Virginia statewide broadband map [8]. In this thesis, two RF models were developed to be used within ArcGIS to capitalize on the high quality terrain data and prevalence of ArcGIS users that are planning wireless systems.

The Large Scale RF Model is designed for use up to a 20 km scale. It is based on the Friis' free-space path loss algorithm and will provide a reasonable RF estimate for frequencies ranging from 500 MHz to 5 GHz. The Large Scale RF Model uses ArcGIS's Viewshed tool to calculate LOS connections to each location on the terrain map. The script will return an estimate in one of three formats within one minute's worth of computation time.

The Medium Scale RF Model is designed to use multipatch building data to estimate RF propagation through buildings at a WiFi access point's range of 300 m. The Model is currently designed for frequencies of 2400 MHz, which is a common WiFi system carrier

frequency. The Model is based on Friis' free-space path loss equation modified with additional attenuation for each building wall that the signal propagates through. The Intersect 3D Line with Multipatch tool is used in ArcGIS to determine the number of building walls the signal passes through, and attenuation is added to the free space path loss for each building wall. The script will return a raster containing received signal strength in three minutes of computation time.

The Large Scale RF Model and the Medium Scale RF Model will be available at `https://github.com/vtcgit` upon the completion of CGIT's State Broadband Initiative project. The goal of this thesis was to create open source scripts to model RF within ArcGIS so that those using them will be able to see the algorithms being used. They are also free to download and use for anyone with ArcGIS software.

This thesis also explores the possibility of GIS data aiding indoor geolocation. Simulations are performed in MATLAB to see if known building location, size, and shape will reduce the position error of RF location algorithms. Two experiments are conducted: one in which there is only one building (the 'single building experiment') and one in which there are other buildings surrounding the building of interest (the 'multiple building experiment'). In both experiments, the buildings' locations and boundaries are known, and a target in the central building is placed at random. Time difference of arrival (TDOA) calculations are performed to estimate the position of the target when noise and bias are added. After the position of the target is estimated, it is corrected to within the nearest building's boundaries.

The single building experiment shows the greatest improvement over an uncorrected location estimate. The multiple building experiment revealed an increase in the RMSE in the x- and y-coordinates, but the same reduction in error in the z-coordinate experienced in the single building experiment. Further analysis in which the target's location was corrected to a known floor of the building showed an increased reduction in the average z-coordinate error. The experiments demonstrate that GIS data can aid RF geolocation estimates, and open the way for further research.

8.1 Future Improvement

There are many areas of further study for the Large Scale RF Model, Medium Scale RF Model, and Indoor Positioning experiments. This section outlines some of the ways that these experiments can be improved.

Large Scale RF Model

The Large Scale RF Model uses a basic algorithm that is based on the Friis free-space path loss algorithm. There are other models, such as the Okumura-Hata model, that can be altered so that they can be used in Large Scale RF Model. These models can be modified to change the signal's decay rate depending on whether the receiver has a LOS or NLOS connection with the transmitter. Numerous models can be adapted, and the results can be compared to other existing RF propagation software for accuracy.

There is also the potential to test the algorithm in the field. With the proper equipment, data can be collected over a wide area and be compared to experimental results. The path loss exponents used in the algorithm can be altered to reflect the field test data.

Many available RF estimation tools today also offer the ability to estimate RF coverage using antenna patterns. There is the possibility that antenna patterns can be simulated in ArcGIS. There was not time to explore this additional feature to the Large Scale RF Model during the creation of this thesis, but the ability to simulate antenna patterns would greatly increase the applications of the Large Scale RF Model. The model will then be able to be used for estimating RF coverage of currently existing systems.

Medium Scale RF Model

There are a few ways of improving the Medium Scale RF Model developed in Chapter 5, such as the incorporation of a signal's path length through a building into the algorithm. The algorithm currently does not consider the effects of diffraction, so building data creates a larger shadow of reduced signal strength than would be seen in practice. By including the signal's path length through a building, we can simulate the effects of diffraction by reducing the attenuation experienced based on the length of time that the signal is within the building. For example, when a signal passes through the edge of a corner of a building, the signal is more likely to diffract over that edge and have a smaller signal strength reduction as a result. Diffraction estimation would also be pertinent analysis to add to the Medium Scale RF Model.

Incorporation of foliage and more detailed building parameters can add to the depth of the algorithm. Foliage data is potentially available for the state of Virginia, and can be as detailed as describing the breed of tree. There is also more detailed building information available that will allow for distinction of building materials.

A small field test of the algorithm was conducted, but a larger field test would vastly improve the algorithm. The Medium Scale RF Model can also be tested in areas where foliage attenuation will be prevalent to test the foliage expansion of the algorithm as well.

Indoor Positioning

The indoor positioning experiments conducted in Chapter 6 showed plausibility for GIS data to improve indoor RF geolocation. Due to the large amount of building data provided by GIS, such as building material and floor plans, further analysis can be conducted to determine if these additional factors can improve indoor geolocation. The experiment can also be introduced into the WiFi or ultra wide band frequencies that are being explored for Indoor Positioning currently.

Bibliography

[1] Internet World Stats. Internet usage and population in north america. Web, 2012.

[2] Protalinski, E. Over 70% of US Households now have Broadband Internet Access, with Cable Powering over 50% of the Market, Dec 9 2013. http://thenextweb.com/insider/2013/12/09/70-us-households-now-broadband-internet-access-cable-powering-50-market/.

[3] Fung, B. The FCC may consider a stricter definition of broadband in the Netflix age. Web, 2014. http://www.washingtonpost.com/blogs/the-switch/wp/2014/05/30/the-fcc-may-consider-a-stricter-definition-of-broadband-in-the-netflix-age/.

[4] Rappaport, T. S. *Wireless Communications: Principles and Practice*. Prentice Hall, 2 edition, January 2002.

[5] State Broadband Initiative. Web, May 2014. http://www2.ntia.doc.gov/SBDD.

[6] Liu, H., H. Darabi, P. Banerjee and J. Liu. Survey of Wireless Indoor Positioning Techniques and Systems. *IEEE Transactions on Systems, Man, and Cybernetics*, November 2007.

[7] Nemec, Z. and P. Bezousek. The Time Difference of Arrival Estimation of Wi-Fi Signals. *Radio Engineering*, 17(4):51–54, December.

[8] Virginia Information Technologies Agency. Web, Mar 2014. http://gismaps.vita.virginia.gov/broadband/.

[9] Softwright. TAP Software. Web, 2014. `http://www.softwright.com/products/tap-software/`.

[10] Okumura, Y. *et al.* Field strength and its variability in uhf and vhf land-mobile radio service. *Rev. Elec. Commun. Lab.*, 16, 1968.

[11] Hata, M. Empirical Fomula for Propagation Loss in Land Mobile Radio Services. *IEEE Transactions on Vehicular Technology*, VT-29(3):317–325, August 1980.

[12] Zekavat, R. and R. M. Buehrer. *Handbook of Position Location: Theory, Practice and Advances.* Wiley-IEEE Press, November 2011.

[13] ESRI Staff. Multipatches. Web, 2012. `http://help.arcgis.com/en/arcgisdesktop/10.0/help/index.html#//00q8000000mv000000`.

[14] ESRI Staff. *ArcGIS 9: What is ArcGIS?* ESRI, 2004.

[15] National Telecommunications and Information Administration. About FirstNet. Web, 2014. `http://www.ntia.doc.gov/page/about-firstnet/`.

[16] Federal Communications Commission. FCC Acts To Help Emergency Responders Locate Wireless 911 Callers. Web, 2014. `http://www.fcc.gov/document/fcc-acts-help-emergency-responders-locate-wireless-911-callers`.

[17] Federal Communications Commission. Proposes new indoor requirements and revisions to existing E911 rules. Web, 2014. `http://www.fcc.gov/document/proposes-new-indoor-requirements-and-revisions-existing-e911-rules`.

[18] Henderson, B. J. Radio Mobile Program Operating Guide, Jul 2013. Version 4.0.

[19] PE1MEW. Radio Coverage Probablility. Web, Mar 2014. `http://radiomobile.pe1mew.nl/?Calculations:Propagation_calculation:Radio_coverage_probability`.

[20] Rice, P. L., A. G. Longley, K. A. Norton and A. P. Barsis. *Transmission Loss Predictions for Tropospheric Communication Circuits.* National Bureau of Standards, May 1967. 101.

[21] Hufford, G. The ITS Irregular Terrain Model, version 1.2.2: The Algorithm. *National Telecommunications and Information Administration*, 2002.

[22] Hufford, G. A., A. G. Longley and W. A. Kissick. A Guide to the Use of the ITS Irregular Terrain Model in the Area Prediction Mode. Technical Report 82-100, NTIA, April 1982.

[23] Coudé, R. Radio Mobile Home Page. Web, Mar 2014. `http://www.cplus.org/rmw/english1.html`.

[24] Brown, I. D. An Introduction to Radio Mobile. RadCom, Oct 2006. `http://www.g3tvu.co.uk/Introduction_to_Radio_Mobile_RadCom_Oct06.pdf`.

[25] Brown, I. D. Radio Mobile: What can it do for you? *AntenneX*, Jul 2009. Issue No. 147.

[26] Softwright. Price Lists. Web, 2014. `http://www.softwright.com/products/price-list/`.

[27] Wikipedia. List of WLAN channels — Wikipedia, The Free Encyclopedia, 2014. [Online; accessed 29-April-2014].

[28] Durgin, G., T. S. Rappaport and H. Xu. 5.85-GHz Radio Path Loss and Penetration Loss Measurements In and Around Homes and Trees. *IEEE Personal Communications*, 2(3):70–72, March 1998.

[29] Durgin, G., T. S. Rappaport and H. Xu. Measurements and Models for Radio Path Loss and Penetration Loss In and Around Homes and Trees at 5.85-GHz. *IEEE Transactions on Communications*, 46(11):1484–1496, November 1998.

[30] Aguirre, S., L. H. Loew and Y. Lo. Radio Propagation Into Buildings at 912, 1920, and 5990 MHz Using Microcells. *Universal Personal Communications*, pages 129–134, September 1994.

[31] De Toledo, A. F., A. M. D. Turkmani and J. D. Parsons. Estimating Coverage of Radio Trasnmission into and within Buildings at 900, 1800, and 2300 MHz. *IEEE Communications Letters*, pages 40–47, April 1998.

[32] ESRI Staff. ArcInfo 8: A New Architecture for GIS. *ESRI ArcNews*, 2000.

[33] ESRI Staff. ARC/INFO: Computer Mapping and Geographic Information Management System, 1982.

[34] ESRI Staff. ESRI Company History, 2014.

[35] ESRI Staff. ArcView MDI Interface. Web, 2014. `http://surveying-mapping-gis.blogspot.com/2009/03/blast-from-past.html`.

[36] ESRI Staff. Software. Web, 2014. `http://sal.ocean.washington.edu/tutorials/arcgis/vector/vector_ov.html`.

[37] Elroi, D. Straight Talk From the Top. *Directions Magazine*, May 2000.

[38] GeoCommunity Staff. Here Comes ArcView 8.1. *GeoComm*, 2001.

[39] ESRI Staff. Defining Feature Class Properties. Web, 2010. `http://webhelp.esri.com/arcgisserver/9.3/java/index.htmgeodatabases/definin-643225741.htm`.

[40] ESRI Staff. What is ArcPy? Web, 2012. `http://help.arcgis.com/en/arcgisdesktop/10.0/help/index.html#//000v000000v7000000`.

[41] Federal Communications Commission. Web, Mar 2014. `http://www.broadband.gov/qualitytest/deadzone/`.

[42] Siedel, S. Y., Rappaport, T. S. and R. Singh. Path Loss and Multipath Delay Statistics in Four European Cities for 900 MHz Cellular and Microcellular Communications. *Electronics Letters*, 26(20):1713–1715, September 1990.

[43] ESRI Staff. Viewshed. Web, 2012. http://resources.arcgis.com/en/help/main/10.1/index.html#//009z000000v3000000.

[44] ESRI Staff. Using Viewshed and Observer Points for Visibility Analysis. Web, 2012. http://resources.arcgis.com/en/help/main/10.1/index.html#/Performing_visibility_analysis_with_Viewshed_and_Observer_Points/009z000000v8000000/.

[45] Ingram, M. A. Log-normal Shadowing. Web, 2014. http://www.ece.gatech.edu/research/labs/sarl/tutorials/ECE4606/20-Log-normalShadowing.pdf.

[46] ESRI Staff. How Band Collection Statistics Works. Web, 2012. http://help.arcgis.com/en/arcgisdesktop/10.0/help/index.html#//009z000000q3000000.htm.

[47] ESRI Staff. Construct Sight Lines (3D Analyst) . Web, 2012. http://resources.arcgis.com/en/help/main/10.2/index.html#//00q90000002p000000.

[48] ESRI Staff. Intersect 3D Line With Multipatch (3D Analyst). Web, 2012. http://resources.arcgis.com/en/help/main/10.2/index.htm#//00q90000004m0000000.

[49] ESRI Staff. Intersect 3D Line With Surface (3D Analyst). Web, 2012. http://resources.arcgis.com/en/help/main/10.2/index.html#//00q9000000mq000000.

[50] ESRI Staff. Feature Class Basics. Web, 2014. http://resources.arcgis.com/en/help/main/10.1/index.html#//003n00000005000000.

[51] ESRI Staff. An Overview of the Interpolation Toolset. Web, 2012. http://resources.arcgis.com/en/help/main/10.1/index.html#/An_overview_of_the_Interpolation_tools/009z00000069000000/.

[52] ESRI Staff. How Natural Neighbor Works. Web, 2012. http://help.arcgis.com/en/arcgisdesktop/10.0/help/index.html#/How_Natural_Neighbor_works/009z00000077000000/.

[53] ESRI Staff. How Kringing Works. Web, 2012. http://help.arcgis.com/en/arcgisdesktop/10.0/help/index.html#/How_Kriging_works/009z00000076000000/.

[54] ESRI Staff. How IDW Works. Web, 2012.

[55] ESRI Staff. IDW (Spatial Analyst). Web, 2012. http://resources.arcgis.com/en/help/main/10.1/index.html#/IDW/009z0000006m000000/.

[56] Meraki. N-Type Omni Antennas. Web, 2014. https://meraki.cisco.com/products/wireless/antennas-power#n-type-omini-antennas.

[57] Meraki. Meraki Range Calculator. Web, 2011. www.voipmonster.com/files/meraki_range_calculator.xls.

[58] Muza, M. WiFi Signal Mapping, 2011. Virginia Tech - Center for Geospatial Information Technology.

[59] Rolfe, B., S. W. Ekanayake, P. N. Pathirana and M. Palaniswami. Localization with Orientation using RSSI Measurements: RF Map Based Approach. *IEEE*, pages 311–316, 2007.

[60] Progri, I. F. Wireless-enabled GPS Indoor Geolocation System. *IEEE*, pages 526–538, 2010.

[61] Alavi, B., N. Alsindi, and K. Pahlavan. UWB Channel Measurements for Accurate Indoor Localization. *IEEE*, pages 1–7, 2006.

[62] Reliability The Communications Security and Interoperability Council III. Indoor Location Test Bed Report, March 2013.

[63] Chan, Y. T. and K. C. Ho. A Simple and Efficient Estimator for Hyperbolic Location. *IEEE Transactions on Signal Processing*, 42(8):1905–1915, August 1994.

[64] Aschrafi,A. et al. Impact of Building Database Accuracy on Predictions with Wave Propagation Models in Urban Scenarios. *IEEE*, pages 2681–2685, 2006.

Appendix A

Radio Mobile Analysis Instructions

The following is a walkthrough of modeling RF using Radio Mobile:

1. Click 'File' - 'Save Network As...' and save the network according to the WISP it represents.
2. Click 'File' - 'Unit Properties' to open the 'Units' window
   (a) Click a unit in the left portion of the window, change its name and enter its latitude and longitude information.
   (b) After entering in all of the towers, enter in a final unit called 'mobile' which will serve as our mobile unit for all of our propagation estimates. The mobile unit is also where the minimum required received power for that data rate will be entered.
3. Click 'File' - 'Network Properties' to open the 'Networks' window
   (a) For each data rate that the WISP offers, select a network and label it according to the data speed it represents
   (b) Under the 'Parameters' tab, set the minimum and maximum frequency given by the WISP. Change the other default parameters as needed.
   (c) Under the 'Systems' tab, create a system for each transmission power and antenna gain scenario, and create a system for each minimum required receive threshold

(d) Click the 'Membership' tab and select all of the towers that belong in the currently selected network. Select the desired system that the unit will use, and set the appropriate height for the antenna (in meters). You can also select the desired antenna pattern and set the azimuth and elevation angles.

4. Once the parameters have been entered in correctly, it is time to generate the map by clicking 'File' - 'Map Properties' to open the Map Properties window. Under the 'Centre' box, select a unit using the 'Select a unit' drop down box. Set the size of the radius being examined (25 km is what was typically used), and select the pixel height and width desired. Once you have selected all of these attributes, click 'Extract'.
   - Note 1: Radio Mobile may download map data from the USGS database during this time if a map has never been generated in this area before, or if this is your first time generating a map. This takes longer than it normally would to generate the map.
   - Note 2: Sometimes, the units created will not be calibrated correctly unless you generate a map to provide elevation data. If this is the case, generate a map, open the 'Units' window, and, for each tower, select it, open the LAT LONG window, and select 'Ok' without changing anything. The elevation of the tower (to the right of the Unit Name) should change from '0' to some number.
5. To prepare the resulting map for assimilation into ArcGIS for final processing, the image generated from the map must be a Boolean representation of coverage. Select 'File' - 'Picture Properties' and set the default terrain to a plain, white background.
6. Click on the 'Single Polar Radio Coverage' button (a yellow circle with a single '+' symbol) to bring up the Polar Coverage Window.
   (a) For the 'Centre unit,' select your desired tower. For the 'Mobile unit, select the unit created labeled 'mobile'. Then, select the desired Network.
   (b) To ensure a Boolean image, under 'Plot', select the 'Fill area' and 'Solid' check-boxes. For color, select something dark, like red.
   (c) Under 'Radial Range,' change the range so that its maximum is a reasonable

distance from the antenna on the tower (either specified by the WISP or set to 25 km).

(d) The 'Single Polar Radio Coverage' tool allows for last minute changes in antenna pattern. For towers that have multiple antennas, the 'Antenna pattern' section can be used to alter the antenna pattern without changing the settings in the 'Network Properties' menu.

7. When the settings within the 'Single Polar Radio Coverage menu are complete, click 'Draw' and the coverage estimate will be created in the blank map. Repeat Step 6 for all antennas on this tower, having the estimate drawn on top of the previous estimates.
8. Once the estimate for the tower is complete, save the image by selecting 'File' - 'Save Picture As...'. Name the file in a way that describes the tower it represents.
    - Note 1: This will result in 5 files being created, among which is the .png file and a .kml file which will be used to convert the .png file into a raster with geographical data. This raster can then be brought into ArcGIS to be changed into a format that is acceptable for the Statewide Broadband Map.
9. Repeat steps 6-8 for all towers.

Appendix B

Individual CDFs of Single Building Positioning Analysis

This Section contains Figures 1 and 2 representing the CDFs of the Error and Z-Error for the Single Building experiments.

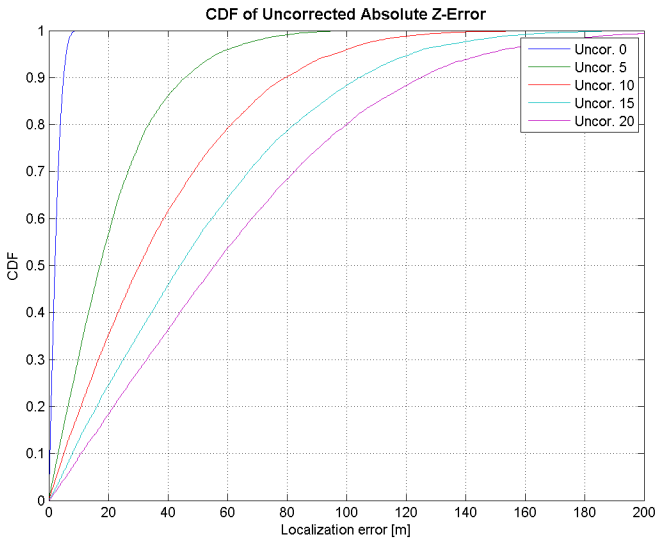

Figure B.1: CDF of 3D Z-Error Analyses: Uncorrected

The z-error analysis for the uncorrected target

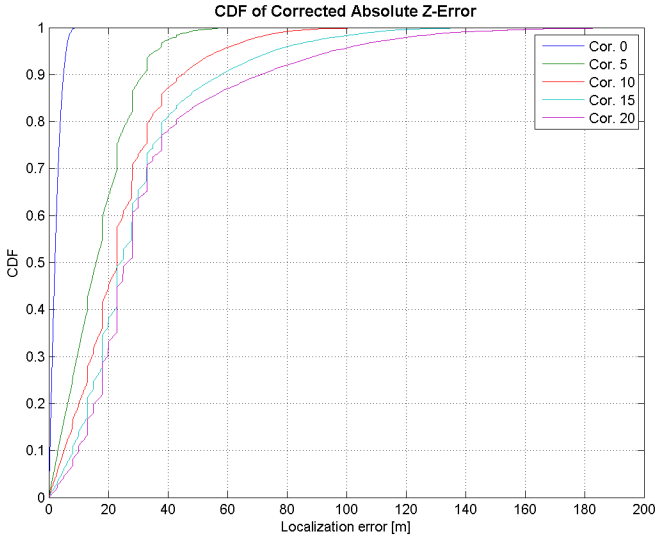

Figure B.2: CDF of 3D Z-Error Analyses: Corrected

The 'stair stepping' shape of the CDF becomes more pronounced due to an increase in the number of error values that are a multiple of 5.

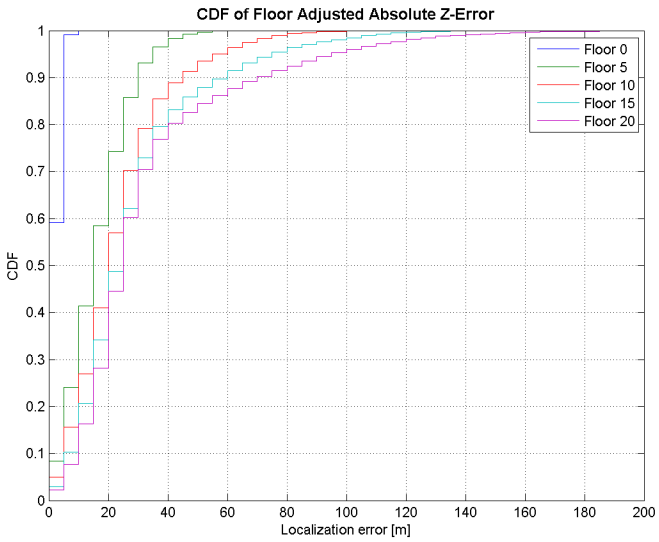

Figure B.3: CDF of 3D Z-Error Analyses: Floor Corrected

The 'stair stepping' shape of the CDF becomes more pronounced due to all of the error values being a multiple of 5.

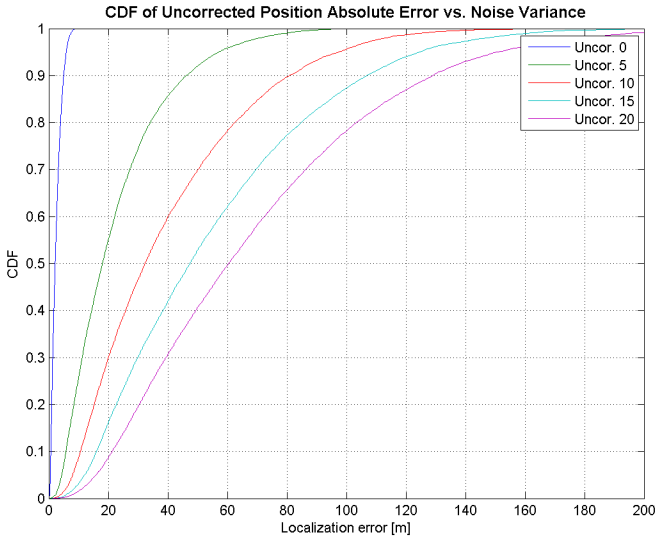

Figure B.4: CDF of 3D Error Analyses: Uncorrected

The error analysis for the uncorrected target

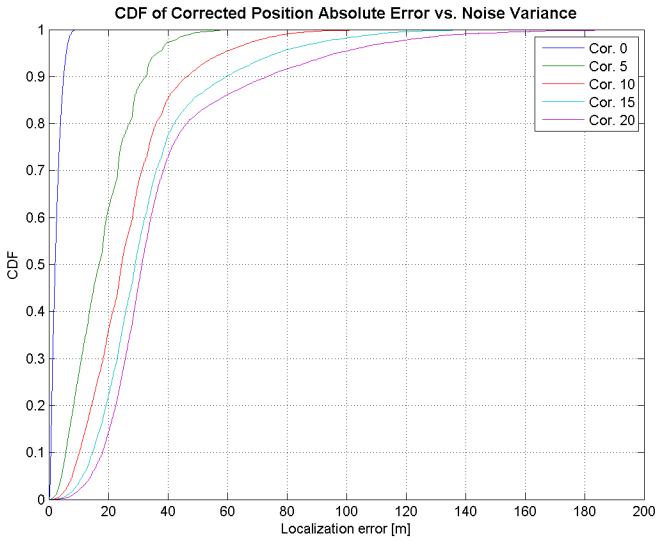

Figure B.5: CDF of 3D Error Analyses: Corrected

The 'small bumps' can be noticed on the variance = 5 line. This is due to an increase in the number of z-errors being a multiple of 5. In higher noise, the graphs become more smooth due to the larger variance in the z-errors that are multiples of 5.

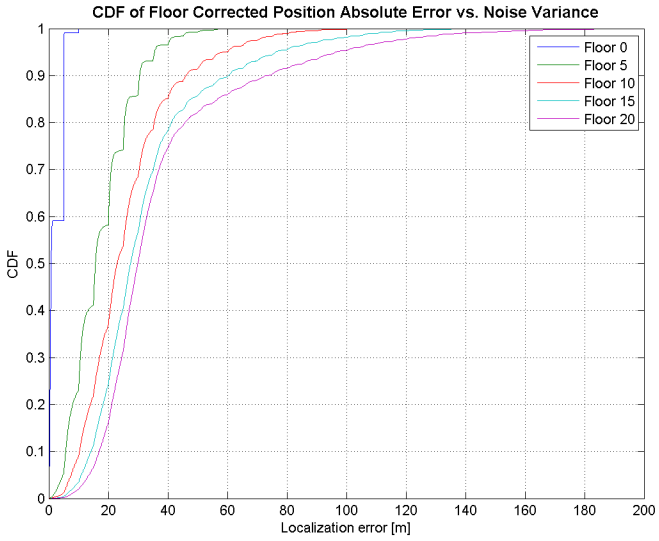

Figure B.6: CDF of 3D Error Analyses: Floor Corrected

The CDF shows more pronounced bumps due to the additional correction to a floor resulting in all z-errors being multiples of 5.

Appendix C

Individual CDFs of Multiple Building Positioning Analysis

This Section contains Figures 1 and 2 representing the CDFs of the Error and Z-Error for the Multiple Building experiments.

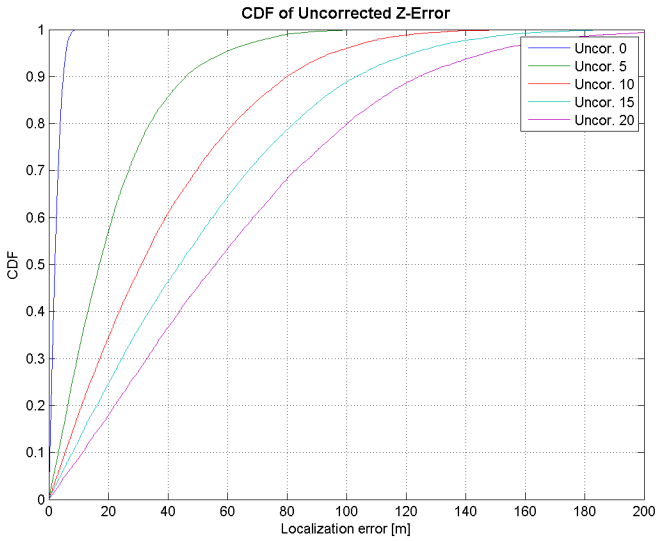

Figure C.1: CDF of 3D Z-Error Analyses: Uncorrected

The z-error analysis for the uncorrected target

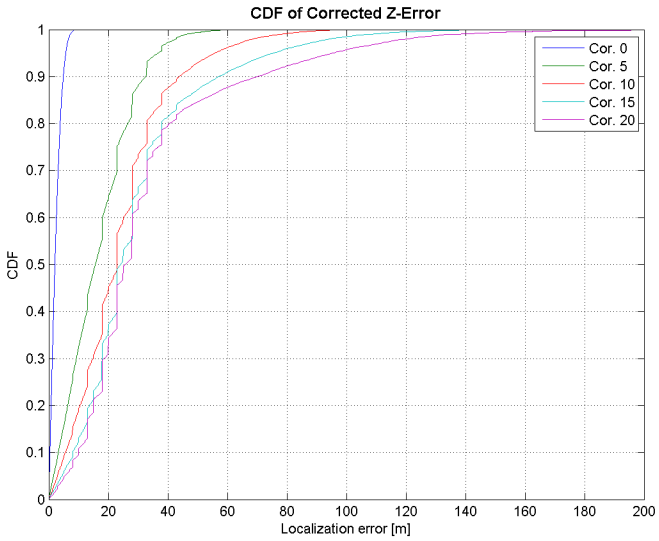

Figure C.2: CDF of 3D Z-Error Analyses: Corrected

The CDF is not smooth for noise variances of 5 m^2 and above. This is due to the correction algorithm translating the estimated target to within the building, resulting in values that are a multiple of 5. The CDF of the floor corrected z-error in Figure

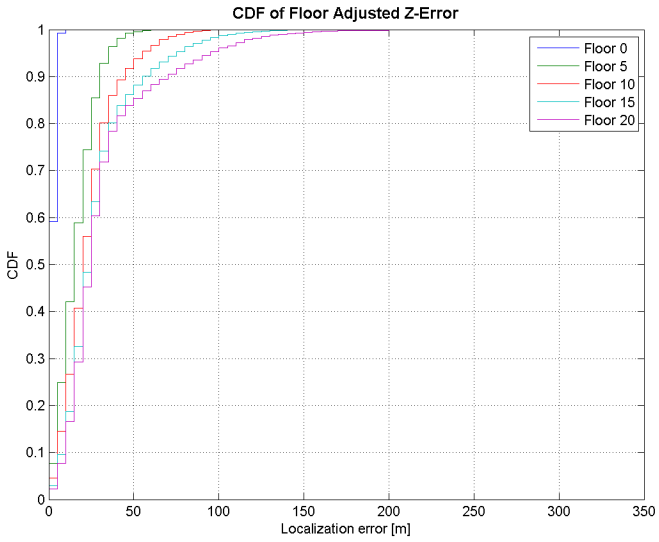

Figure C.3: CDF of 3D Z-Error Analyses: Floor Corrected

The 'stair stepping' shape of the CDF becomes more pronounced due to all of the error values being a multiple of 5.

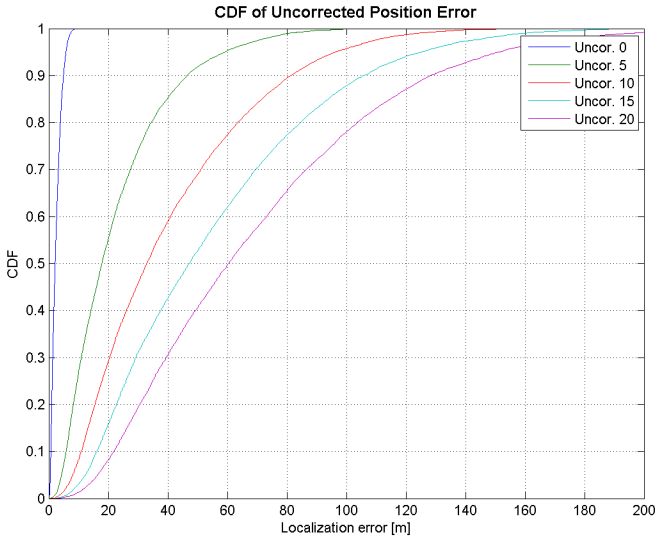

Figure C.4: CDF of 3D Error Analyses: Uncorrected

The error analysis for the uncorrected target

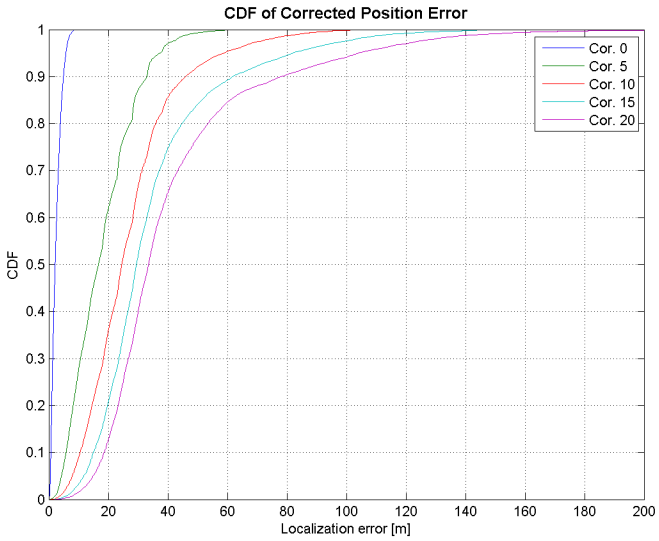

Figure C.5: CDF of 3D Error Analyses: Corrected

The 'small bumps' can be noticed on the variance = 5 line. This is due to an increase in the number of z-errors being a multiple of 5. In higher noise, the graphs become more smooth due to the larger variance in the z-errors that are multiples of 5.

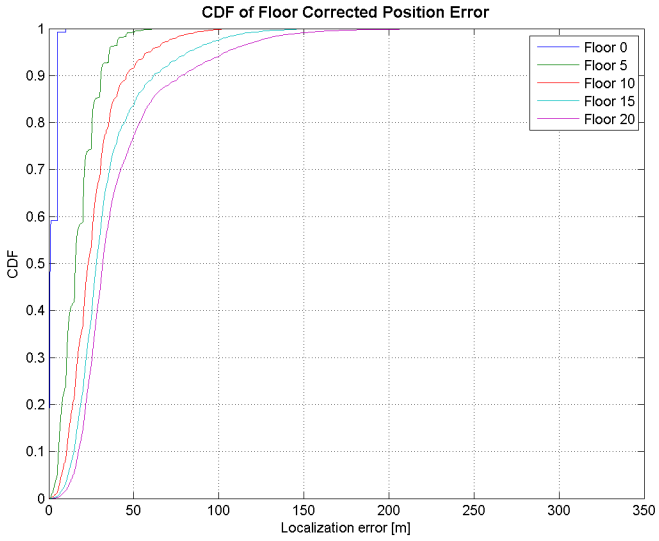

Figure C.6: CDF of 3D Error Analyses: Floor Corrected

The CDF shows more pronounced bumps due to the additional correction to a floor resulting in all z-errors being multiples of 5.